ARF6 IS A TARGETABLE NODE THAT ORCHESTRATES SIGNALING OF MULTIPLE ONCOGENIC PATHWAYS IN CUTANEOUS AND UVEAL MELANOMA

by

Jae Hyuk Yoo

A dissertation submitted to the faculty of
The University of Utah
in partial fulfillment of the requirements for the degree of

Doctor of Philosophy

Department of Oncological Sciences

The University of Utah

August 2015

The University of Utah Graduate School

STATEMENT OF DISSERTATION APPROVAL

The dissertation of **Jae Hyuk Yoo**

has been approved by the following supervisory committee members:

Dean Y. Li	, Chair	**06/03/2015** Date Approved
Sheri L. Holmen	, Member	**06/03/2015** Date Approved
Trudy G. Oliver	, Member	**06/03/2015** Date Approved
Jan L. Christian	, Member	**06/03/2015** Date Approved
Charles Murtaugh	, Member	**06/03/2015** Date Approved

and by **Bradley R. Cairns** , Chair/Dean of

the Department/College/School of **Oncological Sciences**

and by David B. Kieda, Dean of The Graduate School.

ABSTRACT

Melanoma is a malignant tumor that develops from melanocytes, which are pigmented cells primarily found in the epidermis, eye, and mucosal epithelia. Melanomas can occur in any tissue containing melanocytes. Although both cutaneous and uveal melanomas are derived from melanocytes, they have significant differences in terms of genetic alterations, metastatic pattern, tumorigenesis, and therapeutic response.

In this dissertation, I present the results of studies that explore the role of the small GTPase ARF6 in cutaneous and uveal melanoma. These studies show that ARF6 is required both for invasion and metastasis in cutaneous melanoma and for orchestrating oncogenic Gα protein-mediated signaling pathways that promote uveal melanoma cell proliferation. In cutaneous melanoma cells, WNT5A-FZD4-LRP6 signaling activates ARF6 via the guanine nucleotide exchange factor (GEF) GEP100. ARF6 activation promotes the release of β-catenin from cell-surface N-cadherin, thereby increasing the pool of cytoplasmic and nuclear β-catenin with a subsequent induction of transcription, invasion, and metastasis. As WNT signaling is implicated in many cancers, these findings suggest that a WNT-ARFGEF-ARF signaling module may play an important role in the metastasis of multiple cancers.

Uveal melanoma is the most common primary intraocular tumor. Activating mutations in *GNAQ* and *GNA11*, which encode members of the q class of the G-protein alpha subunit (Gαq), are the primary drivers of uveal melanoma tumorigenesis. I show

that oncogenic GNAQ forms a complex with GEP100 to activate ARF6, which in turn induces all known GNAQ-mediated signaling pathways as well as the relocalization of β-catenin from the cell surface to the nucleus. These findings indicate that ARF6 is the primary immediate effector of an oncogenic GNAQ/GEP100 complex that regulates multiple signaling pathways shown to be important in the control of uveal melanoma tumorigenesis and growth. These results not only provide an improved understanding of the molecular mechanism underlying Gαq-mediated tumorigenesis but also suggest a new target for therapeutic intervention in uveal melanoma.

TABLE OF CONTENTS

ACKNOWLEDGEMENTS

I am grateful to the many people who contributed to the success of the work described within this dissertation. This includes: Dean Li, Shannon Odelberg, Kirk Thomas, Allie Grossmann, Dallas Shi, Lise Sorensen, Aaron Rogers, Weiquan Zhu, Tara Mleynek, Zongzhong Tong, Kirill Ostanin, Alan Mueller, and Jake Winter.

CHAPTER 1

INTRODUCTION

The Role of WNT5A in Inducing Canonical WNT Signaling in Melanoma

Canonical WNT signaling has been largely attributed to the stabilization of the cytoplasmic pool of β-catenin, leading to nuclear translocation and activation of transcription[1]. In addition to transcription, β-catenin has a distinct structural role at the plasma membrane in stabilizing adherens junctions (AJs) and cell-cell contacts by linking cadherins to the actin cytoskeleton[2]. Although adhesion and transcription share the same intracellular pool of β-catenin, the mechanism that controls β-catenin movement between intracellular compartments[3] and how junctional β-catenin might contribute to canonical signaling is unknown. The release of β-catenin from cadherin potentially has dual roles in promoting tumor cell invasion. First, it weakens cell-cell contacts by destabilizing AJs, thus allowing cells to move more freely. Second, by increasing the pool of free cytoplasmic β-catenin, more β-catenin is available for translocation into the nucleus where it can promote transcription of genes involved in invasion and metastasis[2,3].

Although WNT5A has emerged as a key mediator of tumor cell invasion, its role in invasion has primarily been attributed to β-catenin-independent (noncanonical) signaling[4]. Several studies have demonstrated that WNT5A can stimulate canonical

signaling in *Xenopus* and in mammalian cells[5-10]. It has been shown that WNT5A induces β-catenin transactivation when the WNT receptor Frizzled 4 (FZD4) and its coreceptor LRP5 are overexpressed in HEK293T cells[10], which suggests that WNT5A can activate canonical WNT signaling depending on receptor context. However, it is unknown whether this occurs in an endogenous mammalian system or in the setting of cancer.

Previously, it has been shown that the WNT/β-catenin signaling pathway is necessary for melanocyte development[11] and that nuclear β-catenin promotes the proliferation and growth of melanoma cells through interactions with certain transcription factors[12]. However, the function of β-catenin in melanoma metastasis remains controversial. Some studies suggest that β-catenin suppresses invasion of melanoma cells[13], and the loss of β-catenin is correlated with a poor survival rate in melanoma patients[14,15]. However, other studies have shown that ectopic expression of wild type or stabilized β-catenin promotes melanoma invasion and metastasis[16-18]. Because melanoma is a heterogeneous disease, β-catenin function may be variable between cell lines and model systems. During the process of melanoma progression, tumor cells may need to switch between a proliferative versus invasive phenotype. Although the function of β-catenin during progression is unclear, it has been shown that the expression of LEF1 or TCF4, which are transcription factors that bind β-catenin to activate transcription, determined the proliferative or invasive phenotypes of melanoma cells[19]. In this study, we have found that nuclear β-catenin promotes invasion in the subpopulation of melanoma cells expressing WNT5A. Noncanonical WNT5A signaling is clearly important, but our data indicate that β-catenin signaling is also active downstream of WNT5A.

GPCR/Gαq Signaling in Cancer

The stimulation of G-protein-coupled receptors (GPCRs) by various extracellular signals induces several different intracellular signaling pathways that control many cellular biological functions. Ligand-induced stimulation of GPCRs causes a conformational change in the receptor, which stimulates it to act as a guanine nucleotide exchange factor (GEF) activity to activate heterotrimeric G-protein complexes consisting of Gα, Gβ, and Gγ subunits. The GEF activity of GPCRs induce the exchange of a GDP for a GTP on Gα subunits, causing a dissolution of the heterotrimeric G-protein complex and allowing the GTP-bound Gα subunit to modulate a diverse repertoire of effector molecules[20-23].

Emerging experimental results and intensive genomic approaches have identified activating mutations in GPCRs and G proteins in multiple human cancers[22]. For example, genomic analyses of many human cancers have recently identified a high frequency of activating somatic mutations in *Gα* subunits. The frequency of *GNAS* (encoding Gαs), *GNAQ* (encoding Gαq), and *GNA11* (encoding $G\alpha_{11}$) mutations is approximately 4.5%, 3.4%, and 2.5%, respectively, over all tumor types. The mutation hotspots are R201 or Q227 for GNAS and Q209 or R183 for GNAQ/GNA11. These mutations result in constitutively active Gα-mediated signaling by reducing the rate of GTP hydrolysis of the active GTP-bound Gα subunits[22]. These activating Gα mutations have thus far proved challenging for direct pharmacologic inhibition. Instead, most studies have focused on potential downstream therapeutic targets such as protein kinase C (PKC), a downstream component of GNAQ/GNA11 signaling[24,25]. Phospholipase C (PLC) cleaves phosphatidylinositol (4,5)-bisphosphate (PIP2) to produce diacylglycerol (DAG) and

inositol triphosphate (IP3), which then activate PKC-MAPK signaling[26]. A previous study showed that the combined inhibition of PKC and MAPK signaling reduces the proliferation of tumor cells and tumorigenesis in uveal melanoma xenograft models[25]. Moreover, the small GTPase proteins, RhoA and Rac1, have been also shown to be downstream components of oncogenic GNAQ/GNA11. Activation of RhoA and Rac1 by GNAQ initiates the activation of multiple MAPKs such as ERK, p38, and JNK, all of which regulate the activity of AP-1 transcriptional factors[27]. Recently, it has been demonstrated that oncogenic GNAQ-mediated activation of RhoA and Rac1 also promotes the translocation of YAP to the nucleus where it can associate with TEAD and promote transcription[28]. Although these findings identify promising candidates for therapeutic targeting, it would be unlikely to achieve complete inhibition of GNAQ/GNA11 oncogenic signaling by targeting each of these downstream targets individually. A similar situation occurs in RAS signaling. Somatic activating mutations in *RAS* are the most common mutations in human cancers. Although much effort has been expended to understand and inhibit the downstream components of oncogenic RAS, there is currently no effective therapeutic approach for targeting all of the oncogenic RAS-mediated signaling pathways[29].

Uveal melanoma is the most common ocular malignancy and there is currently no effective treatment for metastatic uveal melanoma largely because of the lack of an understanding of the molecular mechanisms underlying this cancer[30]. However, several recent major advances have been made in elucidating the signaling pathways that control uveal melanoma oncogenesis. Mutations in one of two different Gα subunits (GNAQ and GNA11) are found in over 80% of uveal melanomas[31,32]. Although it has been

demonstrated that activating mutations in GNAQ/GNA11 trigger multiple downstream effectors and pathways including PLC/PKC, ERK, p38, JNK, and YAP and that inhibition of any one of these downstream effectors reduces tumorigenesis in uveal melanoma xenograft models[24,25,27,28,33], the molecular mechanisms by which these activating Gα mutations orchestrate all of these signaling pathways remain unknown.

The Role of ARF Proteins in Endocytosis, Cytoskeletal Remodeling, and Cancer

ARF proteins are part of the Ras-superfamily of GTPases and mainly control membrane trafficking and cytoskeletal remodeling. In mammals, the ARF superfamily includes six ARF proteins and several ARF-like proteins. ARF proteins can be placed into three classes by their structural similarities: class I (ARF1-3), class II (ARF4 and 5), and class III (ARF6). It has been shown that ARF1 functions to regulate membrane trafficking at multiple intracellular sites. ARF6 is also involved in membrane trafficking and remodeling and functions mainly in membrane endocytosis and recycling at the cell periphery through its GTPase activity[34-36].

ARF6 Q67L is a constitutively active form of the protein due to its defect in GTP hydrolysis. It is primarily localized to invagination pits at plasma membrane or intracellular vacuoles and plays a role in blocking the endocytosis of several cell surface molecules. ARF6 T27N, which acts as a dominant negative due to its inability to bind guanine nucleotides, mainly localizes to intracellular tubulovesicular (TV) structures and can block cell surface molecules from recycling back to the cell surface. The endogenous ARF6 is usually found at the plasma membrane and intracellular compartments in the

pericentriolar region[37-39]. Therefore, it has been suggested that ARF6 GTPase activity controls the direction of membrane trafficking to regulate cell motility[40]. However, ARF6 may have different functions in different cellular contexts. The expression of ARF6 is ubiquitous and has been shown to function in a variety of biological events, including actin cytoskeletal remodeling and activation of phosphatidylinositol 5-kinase[35,41]. In endothelial cells, it has been shown that the SLIT-ROBO ligand-receptor system induces GTPase activating proteins (GAPs) to convert ARF6 to the inactive, GDP-bound state, enhancing VE-cadherin localization to the cell surface and promoting stability of cell-cell interactions[42,43]. In epithelial cells, ARF6 activated by hepatocyte growth factor (HGF) promotes internalization of E-cadherin and cell motility[44]. In breast cancer cells, the epidermal growth factor receptor (EGFR) activates ARF6 through GEP100, thus reducing E-cadherin at the cell surface and promoting an invasive phenotype[45]. Therefore, ARF6 is thought to be at the center of multiple signals that influence cellular motility by regulating AJs. ARF6 was initially found as a cofactor necessary for the cholera toxin-catalyzed ADP ribosylation of the Gαs subunit[46]. Several studies have demonstrated that ARF6 both regulates the internalization of GPCRs and is itself activated by Gα proteins following GPCR stimulation or through activating Gα mutations[47-51]. However, it is unknown whether ARF6 is necessary for the Gα protein-mediated signaling pathways that control multiple cellular biological functions.

Summary

In this dissertation, I show that ARF6 acts as a molecular switch to control the shuttling of β-catenin between the plasma membrane and the cytoplasm in cutaneous

melanoma. This switch is controlled by two competing signals, WNT5A and SLIT2. WNT5A activates ARF6, leading to the release of β-catenin from N-cadherin, accumulation of cytoplasmic and nuclear β-catenin, increased transcription, and tumor cell invasion. In contrast, SLIT2 inactivates ARF6, thus stabilizing the interaction between N-cadherin and β-catenin and reducing transcription and invasion. These results indicate that WNT5A can induce the disruption of cadherin-catenin interactions and WNT5A signaling contributes to canonical WNT/β-catenin signaling via ARF6.

In uveal melanoma, I demonstrate that ARF6 is both necessary and sufficient for oncogenic GNAQ signaling and that ARF6 acts an immediate downstream effector of a GNAQ/GEP100 complex by orchestrating multiple signaling pathways, including PLC/PKC, Rac/Rho, ERK/p38/JNK, YAP, and β-catenin. ARF6 controls these signaling pathways by regulating the intracellular trafficking of oncogenic GNAQ. Therefore, this work describes an upstream protein complex that controls all of the previously known GNAQ-mediated oncogenic pathways as well as the newly identified β-catenin signaling pathway. These results provide a new mechanistic framework for studying other cancers harboring activating Gα protein mutations and suggest a possible therapeutic approach for inhibiting multiple oncogenic pathways by targeting a single immediate effector of activated GNAQ that lies upstream of all the known oncogenic pathways.

References

1. van Amerongen, R. & Nusse, R. Towards an integrated view of Wnt signaling in development. *Development* **136**, 3205-3214 (2009).

2. Heuberger, J. & Birchmeier, W. Interplay of cadherin-mediated cell adhesion and canonical Wnt signaling. *Cold Spring Harbor Perspectives in Biology* **2**, a002915 (2010).

3. Nelson, W.J. & Nusse, R. Convergence of Wnt, beta-catenin, and cadherin pathways. *Science* **303**, 1483-1487 (2004).

4. Kikuchi, A., Yamamoto, H., Sato, A. & Matsumoto, S. Wnt5a: its signalling, functions and implication in diseases. *Acta Physiol (Oxf)* **204**, 17-33 (2012).

5. He, X., *et al.* A member of the Frizzled protein family mediating axis induction by Wnt-5A. *Science* **275**, 1652-1654 (1997).

6. Umbhauer, M., *et al.* The C-terminal cytoplasmic Lys-thr-X-X-X-Trp motif in frizzled receptors mediates Wnt/beta-catenin signalling. *The EMBO Journal* **19**, 4944-4954 (2000).

7. Tao, Q., *et al.* Maternal wnt11 activates the canonical wnt signaling pathway required for axis formation in Xenopus embryos. *Cell* **120**, 857-871 (2005).

8. Cha, S.W., Tadjuidje, E., Tao, Q., Wylie, C. & Heasman, J. Wnt5a and Wnt11 interact in a maternal Dkk1-regulated fashion to activate both canonical and non-canonical signaling in Xenopus axis formation. *Development* **135**, 3719-3729 (2008).

9. Cha, S.W., *et al.* Wnt11/5a complex formation caused by tyrosine sulfation increases canonical signaling activity. *Curr Biol* **19**, 1573-1580 (2009).

10. Mikels, A.J. & Nusse, R. Purified Wnt5a protein activates or inhibits beta-catenin-TCF signaling depending on receptor context. *PLoS Biology* **4**, e115 (2006).

11. Delmas, V., *et al.* Beta-catenin induces immortalization of melanocytes by suppressing p16INK4a expression and cooperates with N-Ras in melanoma development. *Genes & Development* **21**, 2923-2935 (2007).

12. Goodall, J., *et al.* Brn-2 expression controls melanoma proliferation and is directly regulated by beta-catenin. *Molecular and Cellular Biology* **24**, 2915-2922 (2004).

13. Arozarena, I., *et al.* In melanoma, beta-catenin is a suppressor of invasion. *Oncogene* **30**, 4531-4543 (2011).

14. Chien, A.J., *et al.* Activated Wnt/beta-catenin signaling in melanoma is associated with decreased proliferation in patient tumors and a murine melanoma model. *Proceedings of the National Academy of Sciences of the United States of America* **106**, 1193-1198 (2009).

15. Kageshita, T., *et al.* Loss of beta-catenin expression associated with disease progression in malignant melanoma. *The British Journal of Dermatology* **145**, 210-216 (2001).

16. Damsky, W.E., *et al.* beta-catenin signaling controls metastasis in Braf-activated Pten-deficient melanomas. *Cancer Cell* **20**, 741-754 (2011).

17. Murakami, T., *et al.* Constitutive activation of Wnt/beta-catenin signaling pathway in migration-active melanoma cells: role of LEF-1 in melanoma with increased metastatic potential. *Biochemical and Biophysical Research Communications* **288**, 8-15 (2001).

18. Zuidervaart, W., *et al.* Expression of Wnt5a and its downstream effector beta-catenin in uveal melanoma. *Melanoma Research* **17**, 380-386 (2007).

19. Eichhoff, O.M., *et al.* Differential LEF1 and TCF4 expression is involved in melanoma cell phenotype switching. *Pigment Cell Melanoma Res* **24**, 631-642 (2011).

20. Marinissen, M.J. & Gutkind, J.S. G-protein-coupled receptors and signaling networks: emerging paradigms. *Trends in Pharmacological Sciences* **22**, 368-376 (2001).

21. Dorsam, R.T. & Gutkind, J.S. G-protein-coupled receptors and cancer. *Nature Reviews. Cancer* **7**, 79-94 (2007).

22. O'Hayre, M., *et al.* The emerging mutational landscape of G proteins and G-protein-coupled receptors in cancer. *Nature Reviews. Cancer* **13**, 412-424 (2013).

23. O'Hayre, M., Degese, M.S. & Gutkind, J.S. Novel insights into G protein and G protein-coupled receptor signaling in cancer. *Current Opinion in Cell Biology* **27**, 126-135 (2014).

24. Sagoo, M.S., Harbour, J.W., Stebbing, J. & Bowcock, A.M. Combined PKC and MEK inhibition for treating metastatic uveal melanoma. *Oncogene* **33**, 4722-4723 (2014).

25. Chen, X., *et al.* Combined PKC and MEK inhibition in uveal melanoma with GNAQ and GNA11 mutations. *Oncogene* **33**, 4724-4734 (2014).

26. Nawaz, S., *et al.* Phosphatidylinositol 4,5-bisphosphate-dependent interaction of myelin basic protein with the plasma membrane in oligodendroglial cells and its rapid perturbation by elevated calcium. *The Journal of Neuroscience : The Official Journal of the Society for Neuroscience* **29**, 4794-4807 (2009).

27. Vaque, J.P., *et al.* A genome-wide RNAi screen reveals a Trio-regulated Rho GTPase circuitry transducing mitogenic signals initiated by G protein-coupled receptors. *Molecular Cell* **49**, 94-108 (2013).

28. Feng, X., *et al.* Hippo-independent activation of YAP by the GNAQ uveal melanoma oncogene through a trio-regulated rho GTPase signaling circuitry. *Cancer Cell* **25**, 831-845 (2014).

29. Stephen, A.G., Esposito, D., Bagni, R.K. & McCormick, F. Dragging ras back in the ring. *Cancer Cell* **25**, 272-281 (2014).

30. Wu, J., Brunner, G. & Celebi, J.T. A melanoma subtype: uveal melanoma. *Journal of the American Academy of Dermatology* **64**, 1185-1186 (2011).

31. Van Raamsdonk, C.D., *et al.* Frequent somatic mutations of GNAQ in uveal melanoma and blue naevi. *Nature* **457**, 599-602 (2009).

32. Van Raamsdonk, C.D., *et al.* Mutations in GNA11 in uveal melanoma. *The New England Journal of Medicine* **363**, 2191-2199 (2010).

33. Yu, F.X., *et al.* Mutant Gq/11 promote uveal melanoma tumorigenesis by activating YAP. *Cancer Cell* **25**, 822-830 (2014).

34. Schweitzer, J.K., Sedgwick, A.E. & D'Souza-Schorey, C. ARF6-mediated endocytic recycling impacts cell movement, cell division and lipid homeostasis. *Semin Cell Dev Biol* **22**, 39-47 (2011).

35. Donaldson, J.G. & Honda, A. Localization and function of Arf family GTPases. *Biochem Soc Trans* **33**, 639-642 (2005).

36. D'Souza-Schorey, C. & Chavrier, P. ARF proteins: roles in membrane traffic and beyond. *Nature reviews. Molecular Cell Biology* **7**, 347-358 (2006).

37. Klein, S., Franco, M., Chardin, P. & Luton, F. Role of the Arf6 GDP/GTP cycle and Arf6 GTPase-activating proteins in actin remodeling and intracellular transport. *The Journal of Biological Chemistry* **281**, 12352-12361 (2006).

38. Svensson, H.G., *et al.* A role for ARF6 in dendritic cell podosome formation and migration. *European Journal of Immunology* **38**, 818-828 (2008).

39. Luo, Y., Zhan, Y. & Keen, J.H. Arf6 regulation of Gyrating-clathrin. *Traffic* **14**, 97-106 (2013).

40. Palacios, F., Price, L., Schweitzer, J., Collard, J.G. & D'Souza-Schorey, C. An essential role for ARF6-regulated membrane traffic in adherens junction turnover and epithelial cell migration. *The EMBO Journal* **20**, 4973-4986 (2001).

41. Funakoshi, Y., Hasegawa, H. & Kanaho, Y. Regulation of PIP5K activity by Arf6 and its physiological significance. *Journal of Cellular Physiology* **226**, 888-895 (2011).

42. Jones, C.A., *et al.* Slit2-Robo4 signalling promotes vascular stability by blocking Arf6 activity. *Nature Cell Biology* **11**, 1325-1331 (2009).

43. London, N.R. & Li, D.Y. Robo4-dependent Slit signaling stabilizes the vasculature during pathologic angiogenesis and cytokine storm. *Curr Opin Hematol* **18**, 186-190 (2011).

44. Clague, M.J. Met receptor: a moving target. *Science Signaling* **4**, pe40 (2011).

45. Morishige, M., *et al.* GEP100 links epidermal growth factor receptor signalling to Arf6 activation to induce breast cancer invasion. *Nature Cell Biology* **10**, 85-92 (2008).

46. O'Neal, C.J., Jobling, M.G., Holmes, R.K. & Hol, W.G. Structural basis for the activation of cholera toxin by human ARF6-GTP. *Science* **309**, 1093-1096 (2005).

47. Hunzicker-Dunn, M., Gurevich, V.V., Casanova, J.E. & Mukherjee, S. ARF6: a newly appreciated player in G protein-coupled receptor desensitization. *FEBS Letters* **521**, 3-8 (2002).

48. Giguere, P., *et al.* ARF6 activation by Galpha q signaling: Galpha q forms molecular complexes with ARNO and ARF6. *Cellular Signalling* **18**, 1988-1994 (2006).

49. Lavezzari, G. & Roche, K.W. Constitutive endocytosis of the metabotropic glutamate receptor mGluR7 is clathrin-independent. *Neuropharmacology* **52**, 100-107 (2007).

50. Bouschet, T., Martin, S., Kanamarlapudi, V., Mundell, S. & Henley, J.M. The calcium-sensing receptor changes cell shape via a beta-arrestin-1 ARNO ARF6 ELMO protein network. *Journal of Cell Science* **120**, 2489-2497 (2007).

51. Kanamarlapudi, V., Thompson, A., Kelly, E. & Lopez Bernal, A. ARF6 activated by the LHCG receptor through the cytohesin family of guanine nucleotide exchange factors mediates the receptor internalization and signaling. *The Journal of Biological Chemistry* **287**, 20443-20455 (2012).

CHAPTER 2

THE SMALL GTPASE ARF6 STIMULATES BETA-CATENIN TRANSCRIPTIONAL ACIVITY DURING WNT5A-MEDIATED MELANOMA INVASION AND METASTASIS

The following chapter is a reprint of a manuscript published in Science Signaling. It was published March 5, 2013, volume 6 (265): ra14, doi: 10.1126/scisignal.2003398. In addition to myself, the other authors were Allie Grossmann, James Clancy, Lise Sorensen, Alanna Sedgwick, Zongzhong Tong, Kirill Ostanin, Aaron Rogers, Kenneth Grossmann, Sheryl Tripp, Kirk Thomas, Crislyn D'Souza-Schorey, Shannon Odelberg, and Dean Li. I participated in the design, execution, interpretation of data, and preparation of the manuscript.

Science Signaling
AAAS

` The Small GTPase ARF6 Stimulates {beta}-Catenin Transcriptional Activity During WNT5A-Mediated Melanoma Invasion and Metastasis

Allie H. Grossmann, Jae Hyuk Yoo, James Clancy, Lise K. Sorensen, Alanna Sedgwick, Zongzhong Tong, Kirill Ostanin, Aaron Rogers, Kenneth F. Grossmann, Sheryl R. Tripp, Kirk R. Thomas, Crislyn D'Souza-Schorey, Shannon J. Odelberg and Dean Y. Li (5 March 2013)
Science Signaling **6** (265), ra14. [DOI: 10.1126/scisignal.2003398]

Science Signaling (ISSN 1937-9145) is published weekly, except the last week in December, by the American Association for the Advancement of Science, 1200 New York Avenue, NW, Washington, DC 20005.

RESEARCH ARTICLE

CANCER

The Small GTPase ARF6 Stimulates β-Catenin Transcriptional Activity During WNT5A-Mediated Melanoma Invasion and Metastasis

Allie H. Grossmann,[1,2,3*] Jae Hyuk Yoo,[3,4*] James Clancy,[5] Lise K. Sorensen,[3] Alanna Sedgwick,[5] Zongzhong Tong,[6] Kirill Ostanin,[6] Aaron Rogers,[1] Kenneth F. Grossmann,[7,8] Sheryl R. Tripp,[9] Kirk R. Thomas,[3,7] Crislyn D'Souza-Schorey,[5] Shannon J. Odelberg,[3,6,7†] Dean Y. Li[3,4,7,10,11†]

β-Catenin has a dual function in cells: fortifying cadherin-based adhesion at the plasma membrane and activating transcription in the nucleus. We found that in melanoma cells, WNT5A stimulated the disruption of N-cadherin and β-catenin complexes by activating the guanosine triphosphatase adenosine diphosphate ribosylation factor 6 (ARF6). Binding of WNT5A to the Frizzled 4–LRP6 (low-density lipoprotein receptor–related protein 6) receptor complex activated ARF6, which liberated β-catenin from N-cadherin, thus increasing the pool of free β-catenin, enhancing β-catenin–mediated transcription, and stimulating invasion. In contrast to WNT5A, the guidance cue SLIT2 and its receptor ROBO1 inhibited ARF6 activation and, accordingly, stabilized the interaction of N-cadherin with β-catenin and reduced transcription and invasion. Thus, ARF6 integrated competing signals in melanoma cells, thereby enabling plasticity in the response to external cues. Moreover, small-molecule inhibition of ARF6 stabilized adherens junctions, blocked β-catenin signaling and invasiveness of melanoma cells in culture, and reduced spontaneous pulmonary metastasis in mice, suggesting that targeting ARF6 may provide a means of inhibiting WNT/β-catenin signaling in cancer.

INTRODUCTION

The canonical function of WNTs has been largely attributed to the stabilization of the cytoplasmic pool of β-catenin, leading to nuclear translocation and activation of transcription (*1*). In addition to transcription, β-catenin has a distinct structural role at the plasma membrane in adherens junctions in linking cadherins to the actin cytoskeleton and stabilizing cell-cell contacts (*2*). Although adhesion and transcription can share the same pool of β-catenin, our understanding of the mechanisms by which junctional β-catenin feeds into canonical signaling is limited (*2*, *3*). The release of β-catenin from cadherin potentially has dual roles in promoting tumor cell invasion: (i) weakening cell-cell contacts by destabilizing adherens junctions and (ii) enhancing transcription by augmenting the nuclear pool of β-catenin. Among the WNTs, WNT5A has emerged as a key mediator of tumor cell invasion (*4*), yet its role has been attributed to β-catenin independent, noncanonical signaling mechanisms. WNT5A can stimulate β-catenin signaling, depending on receptor context (*5*–*10*), but whether this occurs naturally in mammalian cells or in the setting of cancer is unknown.

[1]Department of Pathology, University of Utah, Salt Lake City, UT 84112, USA. [2]ARUP Laboratories, University of Utah, Salt Lake City, UT 84108, USA. [3]Program in Molecular Medicine, University of Utah, Salt Lake City, UT 84112, USA. [4]Department of Oncological Sciences, University of Utah, Salt Lake City, UT 84112, USA. [5]Department of Biological Sciences, University of Notre Dame, Notre Dame, IN 46556, USA. [6]Navigen Inc., Salt Lake City, UT 84108, USA. [7]Department of Medicine, University of Utah, Salt Lake City, UT 84132, USA. [8]Division of Medical Oncology, Huntsman Cancer Institute, University of Utah, Salt Lake City, UT 84132, USA. [9]ARUP Institute for Clinical and Experimental Pathology, Salt Lake City, UT 84112, USA. [10]Cardiology Section, VA Salt Lake City Health Care System, Salt Lake City, UT 84112, USA. [11]The Key Laboratory for Human Disease Gene Study of Sichuan Province, Institute of Laboratory Medicine, Sichuan Academy of Medical Sciences & Sichuan Provincial People's Hospital, Chengdu, Sichuan 610072, China.
*These authors contributed equally to this work.
†To whom correspondence should be addressed. E-mail: dean.li@u2m2.utah.edu (D.Y.L.); sodelber@genetics.utah.edu (S.J.O.)

Adenosine diphosphate (ADP) ribosylation factor 6 (ARF6) is a small guanosine triphosphatase (GTPase) that is a critical mediator of endocytosis and recycling of cadherin-catenin complexes at the cell surface (*11*). In the endothelium, we have shown that the ligand SLIT and its receptor ROBO induce GTPase-activating proteins (GAPs) to convert ARF6 to the inactive, guanosine diphosphate (GDP) bound state (*12*), enhancing the localization of vascular endothelial cadherin to the cell surface and promoting stability of cell-cell interactions (*13*). In epithelial cells, hepatocyte growth factor activates ARF6 to promote internalization of E-cadherin and cell motility (*11*). Likewise, in breast cancer, the epidermal growth factor receptor induces guanine exchange proteins (GEFs) to induce guanosine 5′-triphosphate (GTP) loading and activation of ARF6 (ARF6-GTP), reducing E-cadherin at the cell surface and promoting an invasive phenotype (*14*). Thus, ARF6 is at the center of opposing signals that influence cellular motility by regulating adherens junctions. Whether ARF6 is also central to the mechanism controlling the relationship between junctional and nuclear pools of β-catenin has not been explored.

Here, we showed in melanoma cells that ARF6 acts as a molecular switch to control the shuttling of β-catenin between the plasma membrane and the cytoplasm. This switch is controlled by two competing signals, WNT5A and SLIT2. WNT5A activates ARF6, leading to the disruption of N-cadherin β-catenin complexes, accumulation of cytoplasmic and nuclear β-catenin, increased transcription, and tumor cell invasion. In contrast, SLIT2 inactivates ARF6, thus stabilizing N-cadherin β-catenin interactions and reducing transcription and invasion. Hence, the activation state of ARF6 controls the intracellular location of β-catenin, which directly stimulates tumor cell invasion. Our work indicates that a WNT can induce the disruption of cadherin-catenin interactions and that endogenous WNT5A signaling augments canonical signaling. Our data support a mechanism in which ARF6 is critical in the WNT5A signaling cascade and explain how junctional and nuclear β-catenin pools are related.

Furthermore, we show that inhibition of this ARF6 mechanism impedes spontaneous melanoma metastasis in vivo.

RESULTS

ARF6 controls the release of β-catenin from N-cadherin, affecting β-catenin transactivation

Because activated ARF6 increases endothelial and epithelial cell motility by decreasing the surface localization of cadherins (*11 14*), we hypothesized that ARF6 might promote tumor cell invasion by a similar mechanism. To this end, we evaluated the role of ARF6 in invasion of melanoma cells. Both N-cadherin (*15 20*) and ARF6 (*21 23*) have been implicated in melanoma invasion, but a relationship between the two has not been investigated. N-cadherin abundance in plasma membrane fractions was unchanged after small interfering RNA (siRNA) mediated knockdown of ARF6 in LOX melanoma cells (fig. S1). In contrast, ARF6 knockdown in LOX cells increased both the association of β-catenin with N-cadherin (Fig. 1A and figs. S2A and S3A) and the membrane fraction of β-catenin (Fig. 1B and figs. S2B and S3B), with a concomitant decrease in cytoplasmic and nuclear β-catenin (Fig. 1B and figs. S2B and S3B). Immunofluorescence staining of LOX cells showed that N-cadherin localization was relatively unchanged in ARF6 knockdown cells (fig. S3C), whereas membrane localization of β-catenin increased (fig. S3D) and active β-catenin in the nucleus decreased (fig. S3E). ARF6 silencing did not alter total β-catenin or the amount of unphosphorylated, stabilized, active β-catenin (fig. S4A), suggesting that the ARF6-dependent increase in cytoplasmic and nuclear β-catenin was unrelated to mechanisms controlling β-catenin protein stability. In support of this, silencing of ARF6 did not affect the phosphorylation of low-density lipoprotein receptor related protein 6 (LRP6) (fig. S4A), a marker for the sequestration of the β-catenin degradation complex by Dishevelled (*24*). In addition, ARF6 activation was not altered by chemical manipulation of the β-catenin degradation complex. Specifically, the amount of ARF6-GTP was constant in LOX cells exposed to the AXIN stabilizer *endo*-IWR 1, the tankyrase inhibitor XAV-939, or the glycogen synthase kinase 3β (GSK3β) inhibitor BIO (fig. S4B). In addition, the amount of β-catenin bound to N-cadherin was not altered by AXIN stabilization or inhibition of GSK3β (fig. S4C), suggesting that the N-cadherin associated pool of β-catenin was distinct from the canonical, WNT-generated pool of β-catenin. These data suggest that ARF6 controls the disassembly of cadherin and β-catenin, converting junctional β-catenin into cytoplasmic pools available for nuclear translocation.

To determine whether the activated form of ARF6 is necessary for the release of β-catenin from N-cadherin, we inhibited ARF6 activation in LOX cells by either activating ARF6 GAPs or inhibiting ARF6 GEFs. SLIT2, which is a ligand for ROBO receptors, inhibits ARF6 activation in endothelial cells by stimulating ARF6 GAP activity in a ROBO4-dependent manner (*12*). Similarly, ROBO1 was necessary for the inhibitory effects of SLIT2 on ARF6 activation in LOX cells (fig. S5, A and B). ARF6 GEFs, such as cytohesins and IQSECs (for example, GEP100, which is also known as IQSEC1), and the PSD families convert inactive ARF6-GDP to active ARF6-GTP, and some ARF6 GEFs can be inhibited with the small-molecule SecinH3 (*25*). SecinH3 inhibited ARF6 activation in LOX cells (fig. S5C). Treatment of LOX cells with either SLIT2 (Fig. 1, C and D, and fig. S2, C and D) or SecinH3 (Fig. 1, E and F, and fig. S2, E and F) mimicked the effects of ARF6 knockdown on β-catenin localization, causing an increase in N-cadherin bound β-catenin at the plasma membrane and a decrease in cytoplasmic and nuclear β-catenin. This shift in β-catenin from the nucleus to the membrane in response to SLIT2 or SecinH3 was observed after 3 hours and persisted up to 24 hours (fig. S6, A and B). These data suggested that ARF6-GTP switched β-catenin localization from the cell surface to the cytoplasm where it could then translocate to the nucleus. Consistent with this interpretation, ectopic expression of the constitutively active mutant of ARF6 (Q67L) reduced N-cadherin bound β-catenin and the membrane fraction of β-catenin and increased both cytoplasmic and nuclear β-catenin (Fig. 1, G and H, and fig. S2, G and H). Together, these data indicate that ARF6-GTP induces the release of β-catenin from N-cadherin, thus increasing the pool of free β-catenin that is available for nuclear translocation.

Given that changes in the activation state of ARF6 altered the amount of nuclear β-catenin, we reasoned that ARF6 may also affect β-catenin mediated transcription. Indeed, ARF6 knockdown (Fig. 1I and fig. S7, A and B) or inhibition of ARF6 activation by SLIT2-ROBO1 (Fig. 1J) or SecinH3 (Fig. 1K) significantly blunted both the activity of a reporter gene for β-catenin mediated transcriptional activity (7TFP-luciferase) and the expression of *AXIN2*, a β-catenin target. In contrast, ectopic expression of ARF6 Q67L increased luciferase activity and *AXIN2* expression (Fig. 1L). Together, these data demonstrated that activated ARF6 could activate β-catenin mediated transcription. This study demonstrates that ARF6 controls the cadherin-bound pool of β-catenin and that, when released, this source of β-catenin can activate transcription.

WNT5A activates ARF6 through Frizzled 4 and LRP6

Because SLIT2-ROBO1 inactivates ARF6 and opposes β-catenin signaling in melanoma cells, we reasoned that there must be a source of ARF6 activation in these cells. The ability of ARF6 to affect β-catenin transactivation suggests that WNTs may activate ARF6. LOX melanoma cells produce generous amounts of WNT5A (fig. S7C), consistent with their invasive and metastatic behavior (*21*, *26*). WNT5A is a key mediator of tumor cell invasion (*4*), and thus far, its role in invasion has been attributed only to β-catenin independent (noncanonical) signaling mechanisms (*27 30*). In LOX cells, silencing WNT5A reduced the amount of ARF6-GTP (Fig. 2A and fig. S2I). In contrast, after serum starvation and cell washing to remove endogenous WNT5A, treatment with recombinant WNT5A increased ARF6-GTP (Fig. 2B and fig. S2J). Among the nine human melanoma cell lines we evaluated, four produced endogenous WNT5A (fig. S7C). In A2058 and Yusac-2 melanoma cells, WNT5A was present in relatively low amounts. Treatment of these cells with recombinant WNT5A resulted in an increase in ARF6-GTP (Fig. 2B and fig. S2I). A375 melanoma cells produced the highest amounts of WNT5A among the cell lines we tested (fig. S7C). Regardless of the relative amounts of endogenous WNT5A, knockdown of WNT5A reduced ARF6-GTP abundance (Fig. 2C and fig. S2K). LOX cells also produced low amounts of WNT2, but WNT3A and WNT7A were not detected (fig. S7D). WNT5A knockdown did not reduce *WNT2* expression (fig. S7E). ARF6 activation was reduced by WNT2 knockdown (fig. S8A), but knockdown of WNT2 did not affect *WNT5A* expression (fig. S8B). Together, these data demonstrate that ARF6 is activated by endogenous WNT5A in multiple melanoma cell lines but that other WNTs may be upstream of ARF6.

Because the repertoire of Frizzled receptors present at the cell surface can influence whether WNT5A activates β-catenin signaling (*5*), we sought to determine which WNT5A receptors were responsible for ARF6 activation. Among the Frizzled (FZD) proteins, FZD2 (*31*), FZD4 (*32*), FZD5 (*33*), and FZD7 (*9*) have been reported to be WNT5A receptors, but only FZD4 and the co-receptor LRP5 allow WNT5A to activate β-catenin mediated transcription when ectopically expressed in human embryonic kidney (HEK) 293 cells (*5*). Although LOX cells

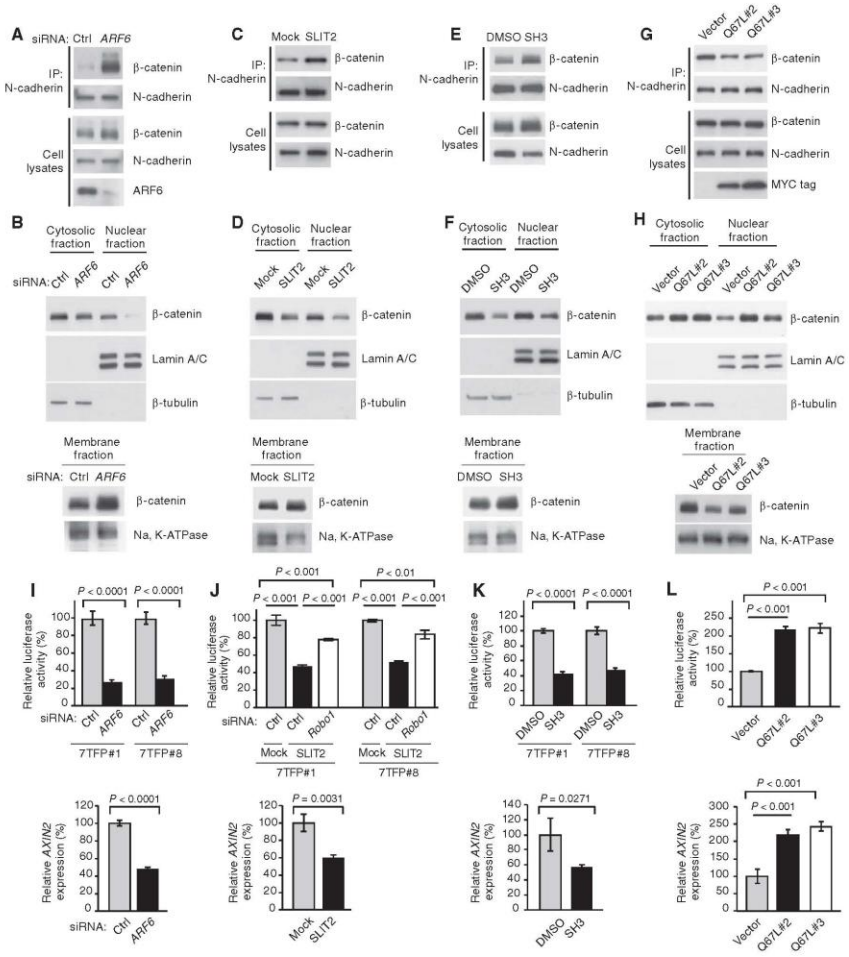

Fig. 1. ARF6-GTP induces release of β-catenin from N-cadherin and augments β-catenin transactivation. (**A**) Coimmunoprecipitation of N-cadherin and β-catenin in LOX cells treated with control (Ctrl) or *ARF6* siRNAs. (**B**) Subcellular fractionation of β-catenin in LOX cells treated with Ctrl or *ARF6* siRNAs. (**C**) Coimmunoprecipitation of N-cadherin and β-catenin in LOX cells treated with Mock or SLIT2. (**D**) Subcellular fractionation of β-catenin in LOX cells treated with control Mock or SLIT2. (**E**) Coimmunoprecipitation of N-cadherin and β-catenin in LOX cells treated with dimethyl sulfoxide (DMSO) or SecinH3 (SH3). (**F**) Subcellular fractionation of β-catenin in LOX cells treated with DMSO or SH3. (**G**) Coimmunoprecipitation of N-cadherin and β-catenin in LOX cells stably transformed with empty vector or Myc-tagged ARF6-GTP (Q67L, stable clones #2 and #3). (**H**) Subcellular fractionation of β-catenin in LOX cells stably transformed with vector or Q67L #2 or #3. (**I**) β-Catenin transactivation in LOX cells treated with Ctrl or *ARF6* siRNAs (two-tailed *t* test). (**J**) β-Catenin transactivation in LOX cells treated with Mock or SLIT2. Upper panel: Rescue of β-catenin–mediated luciferase activity with Ctrl or *ROBO1* siRNA–transfected LOX cells treated with Mock or SLIT2 [upper panel, one-way analysis of variance (ANOVA) and Tukey's post hoc test; lower panel, two-tailed *t* test]. (**K**) β-Catenin transactivation in LOX cells treated with DMSO or SH3 (upper panel, one-way ANOVA and Tukey's post hoc test; lower panel, two-tailed *t* test). (**L**) β-Catenin transactivation in LOX cells stably transformed with vector or Q67L #2 or #3. Stable 7TFP-luciferase clones, 7TFP#1 and 7TFP#8 (I to K), were used for all luciferase assays except in (L). For (L), stable Q67L clones were infected with 7TFP lentivirus before the luciferase assay (one-way ANOVA and Dunnett's post hoc test). For all, error bars represent SD and $n \geq 3$ independent experiments. See fig. S2 (A to H) for quantification of blots. See related experiments in figs. S3 to S7.

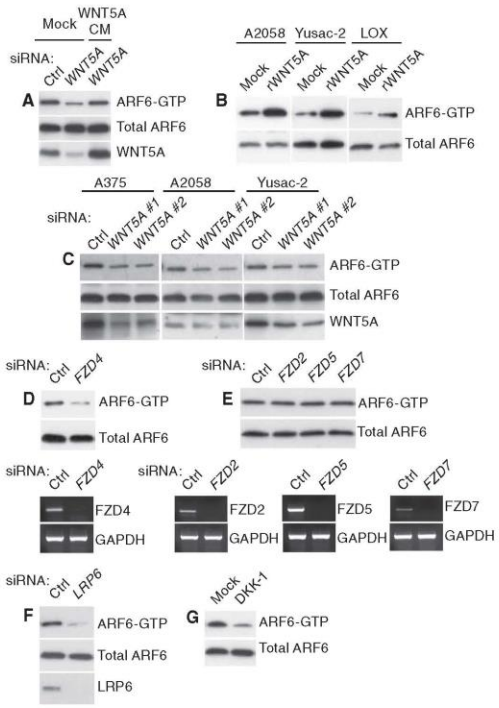

Fig. 2. WNT5A activates ARF6 through FZD4 and LRP6. (**A**) ARF6-GTP amounts in LOX melanoma cells treated with control (Ctrl) or *WNT5A* siRNAs and rescue of ARF6-GTP amounts with WNT5A conditioned medium (CM). (**B**) ARF6-GTP in A2058, Yusac-2, or LOX melanoma cells treated with Mock or recombinant WNT5A (rWNT5A). (**C**) ARF6-GTP amounts in A375, A2058, or Yusac-2 cells treated with Ctrl or *WNT5A* #1 or #2 siRNAs. (**D**) ARF6-GTP amounts in LOX cells treated with Ctrl or *FZD4* siRNAs. Lower panel, reverse transcription polymerase chain reaction (RT-PCR) for *FZD4* mRNA. (**E**) ARF6-GTP amounts in LOX cells treated with Ctrl, *FZD2*, *FZD5*, or *FZD7* siRNAs. Lower panels, RT-PCR for *FZD* mRNAs. (**F**) ARF6-GTP amounts in LOX cells treated with Ctrl or *LRP6* siRNAs. (**G**) ARF6-GTP amounts in LOX cells treated with Mock or DKK-1. For all, $n = 3$ independent experiments. See fig. S2 (I to O) for quantification of blots. See related experiments in figs. S9 and S10.

express FZD1 to FZD10 (fig. S8C), silencing of FZD4 (Fig. 2D and figs. S2L and S9), but not FZD2, FZD5, or FZD7 (Fig. 2E and fig. S2M), reduced the accumulation of ARF6-GTP in LOX cells. Silencing of the WNT co-receptor LRP6 (Fig. 2F and fig. S2N) or inhibition of LRP6 with DKK-1 (Fig. 2G and fig. S2O) also prevented ARF6 activation. These data indicate that ARF6 activation by WNT5A requires FZD4 and LRP6.

WNT5A-FZD4-LRP6 stimulate the release of β-catenin from N-cadherin, augmenting β-catenin signaling

We next tested whether knockdown of WNT5A, FZD4, and LRP6 increased the pool of junctional β-catenin. Silencing of WNT5A, FZD4, or LRP6 in LOX cells caused a redistribution of β-catenin, with an increase in β-catenin associated with N-cadherin and a simultaneous decrease in cytosolic and nuclear β-catenin (Fig. 3, A to E, and fig. S2, P to S), a result that mirrors knockdown or inhibition of ARF6 (Fig. 1 and fig. S3). Silencing of WNT5A caused a significant decrease in both the activity of 7TFP-luciferase and *AXIN2* expression (Fig. 3F). Luciferase activity was partially rescued and *AXIN2* expression was completely rescued by treatment with recombinant WNT5A in WNT5A knockdown cells (Fig. 3G), demonstrating that β-catenin–mediated transcription was specifically activated by WNT5A. Endogenous WNT5A also activated β-catenin in other melanoma cells (fig. S10). Specifically, knockdown of ARF6 or WNT5A in A375, A2058, or Yusac-2 cells significantly reduced 7TFP-luciferase activity. WNT5A siRNA treatment had no effect on 7TFP-luciferase activity in MeWo melanoma cells (fig. S10), which do not produce WNT5A (fig. S7C). These data indicate that endogenous WNT5A–ARF6–β-catenin signaling is present in multiple human melanoma cell lines. In LOX cells, silencing of FZD4 or LRP6 reduced luciferase activity and *AXIN2* expression (Fig. 3H). These data confirm that WNT5A, FZD4, and LRP6 stimulate β-catenin signaling in melanoma cells, similar to activated ARF6. Thus, these results implicate WNT5A in disrupting adherens junctions and driving junctional β-catenin into the canonical pathway.

Activated ARF6 restores β-catenin signaling and invasion when WNT5A is silenced

Because ARF6 was necessary for WNT5A-meditated β-catenin signaling, we asked whether activated ARF6 was sufficient to rescue β-catenin signaling when WNT5A is silenced. In WNT5A-depleted LOX cells, expression of ARF6 Q67L disrupted the N-cadherin–β-catenin interaction (Fig. 4A and fig. S2T) and rescued cytoplasmic and nuclear accumulation of β-catenin (Fig. 4B and fig. S2U), as well as *AXIN2* expression (Fig. 4C). WNT5A stimulates motility (*27*) and invasion in several other melanoma cell lines (*28*, *29*). Silencing of WNT5A inhibited invasion of LOX cells, a result that was reversed by ectopic expression of ARF6 Q67L (Fig. 4D). Although β-catenin–independent WNT5A pathways have been described in melanoma (*27*–*30*), our data indicate that WNT5A stimulates ARF6 to release cadherin-bound β-catenin, increasing the pool of β-catenin available for nuclear translocation, transactivation, and tumor cell invasion.

ARF6 and stabilized β-catenin promote invasion and facilitate invadopodia activity

To determine the requirement of ARF6 for melanoma invasion, we silenced ARF6 in eight melanoma cell lines. ARF6 knockdown consistently inhibited invasion (Fig. 5A), a result that is consistent with studies showing that overexpression of an inactive mutant ARF6 inhibited invasion, whereas a constitutively active mutant ARF6 enhanced invasion of LOX cells (*21*–*23*).

Expression profiling of uveal melanomas indicates that reduced *ROBO1* expression is among the 12 expression markers that predict progression to metastatic disease (*34*). As indicated above, in LOX cells, SLIT2 inhibited ARF6 activation in a ROBO1-dependent manner (fig. S5A). SLIT2 also reduced invasion of LOX cells in a ROBO1-dependent manner (Fig. 5B). Furthermore, invadopodia activity was abrogated by SLIT2 (Fig. 5C). A similar phenotype was observed upon inhibition of

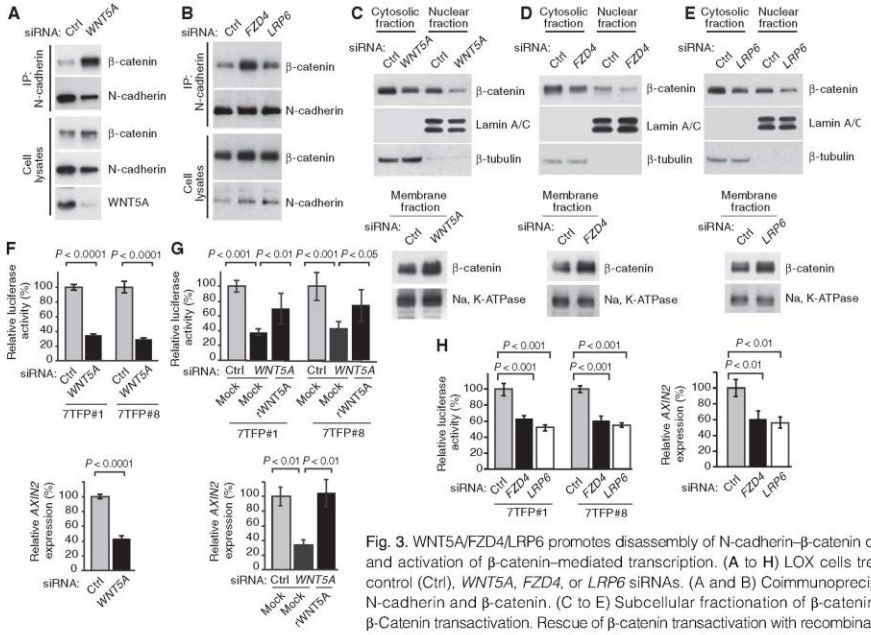

Fig. 3. WNT5A/FZD4/LRP6 promotes disassembly of N-cadherin–β-catenin complexes and activation of β-catenin–mediated transcription. (**A** to **H**) LOX cells treated with control (Ctrl), *WNT5A*, *FZD4*, or *LRP6* siRNAs. (A and B) Coimmunoprecipitation of N-cadherin and β-catenin. (C to E) Subcellular fractionation of β-catenin. (F to H) β-Catenin transactivation. Rescue of β-catenin transactivation with recombinant WNT5A (rWNT5A) in LOX cells treated with Ctrl or *WNT5A* siRNAs (G). 7TFP#1 and 7TFP#8: stable 7TFP luciferase clones. For all, error bars represent SD and $n \geq 3$ independent experiments. For (F), two-tailed *t* test. For (G) and (H), one-way ANOVA with Tukey's (G) or Dunnett's (H) post hoc test. See fig. S2 (P to S) for quantification of blots.

ARF6 activation with SecinH3 (Fig. 5, D and E), confirming that this small molecule phenocopied the effects of either ARF6 protein loss or inactivation.

Although the disruption of the cadherin–β-catenin complex is one mechanism by which WNT5A and ARF6-GTP can stimulate invasion, we sought to determine whether stabilized, active β-catenin also contributes to invasion. Ectopic expression of stabilized β-catenin (S33Y-β-catenin) increased the invasive properties of LOX cells (Fig. 5, F and G). The effect of S33Y-β-catenin had a greater effect on invasion than invadopodia activity, suggesting that β-catenin might control tumor motility to a greater extent than matrix degradation. Regardless, these data support a role for nuclear β-catenin in LOX melanoma cell invasion and are consistent with findings in vitro (*19*, *20*, *35*) and in vivo (*36*) whereby transcriptionally active β-catenin increases melanoma invasion and metastasis, respectively.

GEP100 is necessary for WNT5A-induced ARF6 activation, β-catenin transactivation, and invasion

To further understand the mechanism by which WNT5A activates ARF6 to release junctional β-catenin and promote invasion, we sought to identify the GEF responsible for activation of ARF6 downstream of WNT5A. Cytohesins are ARF GEFs that are targets of SecinH3 (*25*). Because SecinH3 inhibits ARF6 activation (fig. S5C) and the subsequent downstream effects on β-catenin signaling and invasion (Figs. 1, E, F, and K, and 5, D and E, and fig. S2, E and F), we reasoned that cytohesins were responsible for ARF6 activation in LOX cells. Silencing of cytohesin-1, cytohesin-2 (also called ARNO), or cytohesin-3 failed to reduce ARF6-GTP abundance in LOX cells (fig. S11). In contrast, GEP100 knockdown significantly reduced ARF6 activation (Fig. 6A and fig. S2V) and prevented recombinant WNT5A from activating ARF6 (Fig. 6B and fig. S2W) in LOX cells. Silencing of GEP100 mimicked WNT5A and ARF6 knockdown, fortifying N-cadherin–β-catenin interactions, reducing nuclear β-catenin and transcription, and melanoma invasion (Fig. 6, C to F, and fig. S2, X and Y). GEP100 catalyzed the activation of ARF6 in nucleotide exchange assays carried out in vitro (*37*), and SecinH3 exhibited comparable inhibitory potencies for ARF6 nucleotide exchange in the presence of GEP100 or ARNO (Fig. 6G). Together, these data identify GEP100 as a critical member of a signaling pathway consisting of WNT5A, ARF6, and β-catenin that leads to melanoma invasion.

Pharmacologic inhibition of ARF6 activation reduces spontaneous pulmonary metastasis

On the basis of the data presented thus far, we hypothesized that metastasis would be inhibited by blocking the signaling pathway consisting of WNT5A, FZD4, LRP6, GEP100, ARF6, and β-catenin. Because

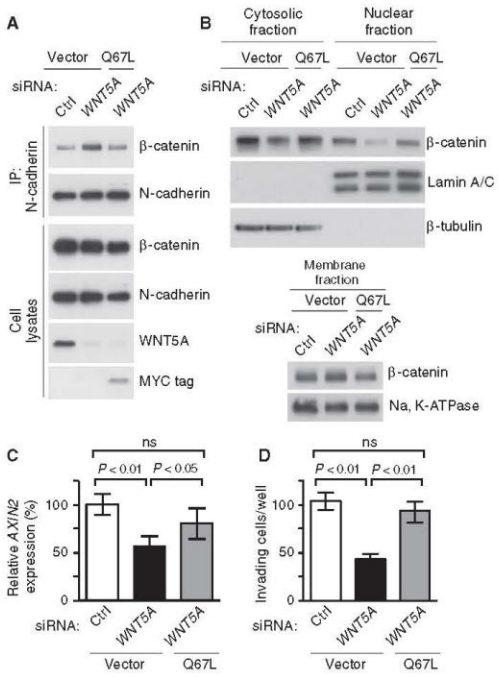

Fig. 4. Activated ARF6 restores β-catenin signaling and melanoma invasion when WNT5A is silenced. (A to D) LOX melanoma cells transfected with control (Ctrl) or *WNT5A* siRNAs in the presence or absence of stable expression of Myc-tagged ARF6 Q67L. (A) Coimmunoprecipitation of N-cadherin and β-catenin. (B) Subcellular fractionation of β-catenin. (C) Relative *AXIN2* expression. (D) Matrigel invasion (average number of invaded cells per well, counted at ×200 magnification). Error bars represent SD (C) or SEM (D). For all, $n \geq 3$ independent experiments. For (C) and (D), one-way ANOVA with Tukey's post hoc test. See fig. S2 (T and U) for quantification of blots.

pharmacologic inhibition of ARF6 activation with SecinH3 (fig. S5C) strengthened the N-cadherin β-catenin interaction (Fig. 1E and fig. S2E), reduced cytoplasmic and nuclear pools of β-catenin (Fig. 1F and fig. S2F), reduced β-catenin signaling (Fig. 1K), and suppressed invasion (Fig. 5, D and E), we sought to test whether SecinH3 had antimetastatic activity in vivo. Subcutaneous LOX xenograft tumors produce spontaneous pulmonary micrometastases that are identified grossly as discrete, round, hemorrhagic foci (*26*) (Fig. 7A). Systemic treatment with SecinH3 significantly reduced both the number of metastatic foci (Fig. 7B) and the number of mice with metastasis (Fig. 7C). There was no difference in overall primary tumor growth between the two groups (Fig. 7D). We frequently observed reduced nuclear β-catenin staining in primary tumors from SecinH3-treated mice but not in those from control mice (fig. S12). These data support a role for ARF6 in melanoma metastasis in vivo and suggest that ARF6 or ARF6 GEFs (or both) may be viable targets for systemic intervention in patients, particularly those with WNT/β-catenin driven cancers.

DISCUSSION

Here, we define a signaling cascade consisting of WNT5A, FZD4, LRP6, GEP100, ARF6, and β-catenin that promotes melanoma invasion and metastasis (Fig. 7E). GEP100 and ARF6 link WNT5A stimulation to the release of β-catenin from N-cadherin, ultimately increasing β-catenin transactivation. Thus, WNT5A and ARF6-GTP facilitate the switch in β-catenin function from adhesion to transcription. BCL9 (*38*) and FoxM1 (*39*) mediate β-catenin nuclear transport, but unlike these proteins, ARF6 localizes to the plasma membrane and endosomes (*40*) and may not be directly involved in nuclear translocation of β-catenin. Activated ARF6 mediates invasion of diverse malignant lineages, including melanoma, breast carcinoma, and glioma (*21 23*). In breast cancer cells, GEP100 facilitates ARF6 activation to promote invasion and metastasis (*14*). The proinvasive activities of ARF6 have been attributed to its role in vesicular transport and remodeling of the actin cytoskeleton (*40 42*) but have not been linked to β-catenin function. ARF6 may shuttle β-catenin between the plasma membrane and cytosol through endocytic mechanisms.

ARF6 as an integrative switch

Our data reveal the importance of ARF6 in the integration of competing signals that help drive plasticity in β-catenin function and the melanoma cell response. WNT5A activates ARF6 to shift the cadherin pool of β-catenin into the nucleus, whereas SLIT2 inactivates ARF6, fortifying the association of β-catenin and N-cadherin at the plasma membrane. SLIT2-ROBO1 inhibits canonical WNT signaling in mammary myoepithelial cells, affecting duct branching during maturation (*43*). Together with our data, it appears that SLIT-ROBO may be a natural antagonist of WNT signaling in multiple cell types. In melanoma, both WNT5A and SLIT2-ROBO1 appear to be clinically relevant pathways. Detection of WNT5A in patient tumors correlates with disease progression and reduced survival (*29*, *44*), and loss of *ROBO1* expression in uveal melanoma helps identify patients at high risk for metastasis (*34*). Somatic loss or mutations of the *SLIT2*, *ROBO1*, and *ROBO2* genes have been observed in pancreatic ductal adenocarcinoma (*45*), providing further evidence that these genes have a tumor suppressor role.

Our data show that both WNT5A and SLIT2-ROBO1 control invasion by regulating the activation state of ARF6 and, as a consequence, the integrity of adherens junctions and β-catenin signaling. This is analogous to the opposing effects of SLIT2-ROBO4 on inflammatory signals whereby SLIT2 promotes endothelial barrier function by inhibiting ARF6 activation and stabilizing cadherin-catenin interactions at the cell surface (*46*). Hence, SLIT-ROBO opposes the effects of distinct promigratory signals in inflammation and cancer by inactivating ARF6. In addition, we have demonstrated that the proinflammatory cytokines interleukin-1β and tumor necrosis factor α activate ARF6 and that inhibiting ARF6 activation in mouse models of rheumatoid arthritis and inflammation reduces vascular leak and inflammation (*47*). The present study shows that the activation state of ARF6 can control the intracellular location of β-catenin in melanoma cells, thereby influencing cancer cell invasion. Combined, these studies suggest

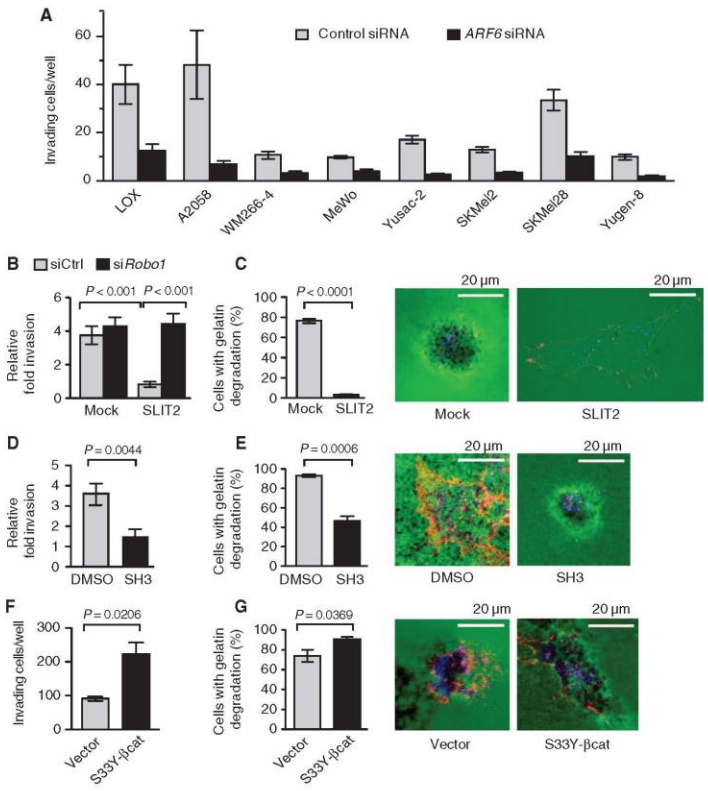

Fig. 5. Inhibition of ARF6 prevents invasion, whereas stabilized β-catenin promotes invasion of melanoma cells. (**A**) LOX, A2058, WM266-4, MeWo, Yusac-2, SKMel2, SKMel28, and Yugen-8 melanoma cells were transiently transfected with control (Ctrl) or *ARF6* siRNAs and assayed for Matrigel invasion. For LOX cells, $P = 0.0028$. For A2058 cells, $P = 0.0092$. For all other cells, $P < 0.0001$. Statistical significance was determined by a two-tailed *t* test. (**B**) Matrigel invasion of LOX cells transfected with Ctrl or *ROBO1* siRNAs and treated with Mock or SLIT2 (one-way ANOVA, Tukey's post hoc test). (**C**) Invadopodia assay in LOX cells treated with Mock or SLIT2. (**D** and **E**) Matrigel invasion (D) and invadopodia assay (E) of LOX cells treated with DMSO or SecinH3 (SH3). (**F** and **G**) Matrigel invasion (F) and invadopodia assay (G) of LOX cells stably expressing empty vector or S33Y-β-catenin (S33Y-β-cat). Invasion data are presented as the average number of invading cells per well (A and F) or the fold invasion relative to unstimulated cells (B and D), counted at 320× (A, B, and D) or 200× (F) magnification. (C, E, and G) Invadopodia activity is presented as the percent of cells demonstrating degradation (black) of gelatin (green). Individual cells were visualized with cortactin (blue) and actin (red) staining. For all, $n \geq 3$ experiments, and error bars represent SEM. For (C) to (G), two-tailed *t* test.

that ARF6 forms a molecular convergent point between inflammatory cytokine signaling cascades and cancer-promoting pathways such as WNT/β-catenin signaling. Future studies will need to explore whether inflammation disrupts surface cadherin-catenin complexes and increases intracellular pools of β-catenin in neoplastic cells, potentially rendering them more sensitive to perturbations of WNT/β-catenin signaling.

WNT5A and β-catenin signaling

Our study describes an endogenous WNT5A pathway in human melanoma cells that facilitates β-catenin signaling. Although previous investigations into the mechanism of WNT5A-mediated invasion have uncovered only noncanonical pathways (*27*–*30*), Wnt5a can stimulate canonical signaling in *Xenopus* (*6*–*10*) and in mammalian cells (*5*). Thus, the dichotomy between canonical and noncanonical pathways might be less distinct than had been appreciated. These data have been received with some caution, however, because of the use of overexpressed proteins (*1*). Wnt5a ectopic expression induces β-catenin transactivation in the developing mouse embryo (*48*). Our data provide evidence for a native WNT5A/β-catenin pathway in human cancer cells. We showed that WNT5A used the cadherin-bound pool of β-catenin for canonical signaling through ARF6. Whether ARF6 is also important for noncanonical signaling remains to be investigated. In the cell lines we studied, noncanonical mechanisms might be important for invasion, and our data do not rule out this possibility. Our data both support the model advocated by van Amerongen and Nusse (*1*), in which WNTs can initiate various interrelated signaling events, and provide information that explains how β-catenin signaling can be propagated by a prototypical noncanonical WNT.

The ability of ARF6 to facilitate WNT5A/β-catenin signaling raises the question whether ARF6 meditates other WNT/β-catenin pathways. On the basis of our observation that WNT2 also activates ARF6 (fig. S8), we suspect that ARF6 may be a general effector in WNT signaling. Previous reports indicate that QS11, an ARF GAP inhibitor that increases ARF6-GTP abundance, can boost WNT3A-dependent TOPFlash activity in HEK293 cells (*49*), and ARF1 and ARF6 are activated by WNT3A conditioned medium in HEK293T cells (*50*). Our data show the mechanism by which ARF6 mediates an endogenous WNT5A/β-catenin pathway that is biologically active in cancer invasion. These findings imply that ARF6 may impinge on various WNT-dependent processes in development and cancer, which will need to be addressed using in vivo genetic approaches.

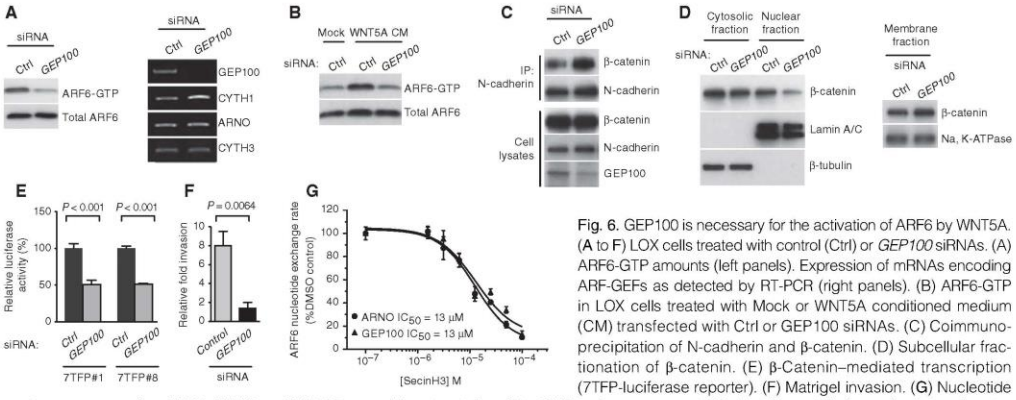

Fig. 6. GEP100 is necessary for the activation of ARF6 by WNT5A. (A to F) LOX cells treated with control (Ctrl) or *GEP100* siRNAs. (A) ARF6-GTP amounts (left panels). Expression of mRNAs encoding ARF-GEFs as detected by RT-PCR (right panels). (B) ARF6-GTP in LOX cells treated with Mock or WNT5A conditioned medium (CM) transfected with Ctrl or GEP100 siRNAs. (C) Coimmunoprecipitation of N-cadherin and β-catenin. (D) Subcellular fractionation of β-catenin. (E) β-Catenin–mediated transcription (7TFP-luciferase reporter). (F) Matrigel invasion. (G) Nucleotide exchange assay using ARF6, ARNO, or GEP100 recombinant proteins. (E to G) Error bars represent SD. For all, $n = 3$ independent experiments. (E and F) Two-tailed t test. See fig. S2 (V to Y) for quantification of blots.

β-Catenin in melanoma

In our system, stabilized, active β-catenin induced invasion of melanoma cells (Fig. 5, F and G), which agrees with a study demonstrating that stabilized β-catenin enhances melanoma metastasis in mice (*36*). In contrast, β-catenin may also suppress invasion of melanoma cells (*51*). In this latter study, silencing of β-catenin increased invasion in vitro. There are several possible explanations for these discordant results. First, melanoma is a heterogeneous disease. β-Catenin function may be context-dependent and, therefore, may vary between cell lines and model systems. Second, knockdown of β-catenin will decrease the abundance of β-catenin not only in the nucleus but also at the membrane. The loss of β-catenin could destabilize adherens junctions and increase cell motility. This is supported by reports showing that in melanoma cells, β-catenin interacts with N-cadherin during the initial contacts with endothelial cells but must be released from N-cadherin for transendothelial migration to occur (*19*, *20*). Once released from N-cadherin, β-catenin accumulates in the nucleus of melanoma cells and activates transcription, facilitating transendothelial migration (*19*). This study highlights the fact that invasion is a dynamic process and that β-catenin function alternates between the membrane and the nucleus as cells make and break contacts during this process. Thus, drawing conclusions about β-catenin cellular function based on subcellular localization requires an evaluation in migrating cells.

Given the dynamic nature of β-catenin localization during invasion, care must be exercised when interpreting β-catenin staining patterns at a single point in time, such as in patient samples. Correlative clinical studies suggest that nuclear β-catenin staining is a useful prognostic marker, predicting a more favorable outcome in melanoma (*52*–*54*). Although these studies do not establish causality, they may hint at a biphasic population of malignant cells within the tumors. Chien *et al.* (*52*) showed that proliferation is inversely related to nuclear β-catenin staining in both primary and metastatic lesions. Hence, nuclear β-catenin staining may be a surrogate for nonproliferating cells in these samples and may, in fact, be highlighting the nonproliferative, invasive population within these tumors.

During cancer progression, tumor cells may switch between invasive and proliferative states, and nuclear β-catenin may favor one phenotype over the other. Phenotype switching is a poorly understood process, and the role of β-catenin in melanoma is unclear. The presence of LEF1 or TCF4 has been shown by one study (*55*) to determine the proliferative or invasive phenotypes of melanoma cells, respectively. These data reveal that β-catenin function can be context-dependent. Future studies of phenotype switching may shed more light on β-catenin function. For now, we and others have observed that nuclear β-catenin promotes invasion. We recognize that activation of β-catenin signaling is not the only means of stimulating invasion downstream of WNT5A. Noncanonical WNT5A signaling is important, but our data indicate that β-catenin signaling is also active downstream of WNT5A and is dependent on activated ARF6.

Clinical implications

We have shown that pharmacologic inhibition of ARF6 activation fortifies adherens junctions, effectively inhibiting β-catenin signaling (Fig. 1, E, F, and K, and fig. S2, E and F), melanoma invasion (Fig. 5, D and E), and spontaneous pulmonary metastasis of melanoma (Fig. 7). In cancer, ARF6 is necessary for invasion of tumor cells originating from diverse cell lineages (*14*, *21*–*23*, *56*, *57*), indicating that migrating malignant cells readily recruit ARF6. As a molecular switch, ARF6 is ideally suited for controlling the dynamic changes in cell function that are required for invasion and metastasis. Clinically, inhibitors of the metastatic process are needed to improve therapeutic outcomes (*58*). This is particularly important for melanoma because, despite substantial progress in the development of immunotherapy and therapies that target activating mutations in the kinase BRAF, few patients achieve a sustainable response that affords long-term remission (*59*–*61*). We have exploited the aggressive nature of melanoma to elucidate a role for WNT5A, FZD4, LRP6, GEP100, and ARF6 in β-catenin function and show that this signaling pathway controls invasion and metastasis. It will be important to evaluate whether targeting ARF6 is an effective strategy in other WNT/β-catenin–driven cancers.

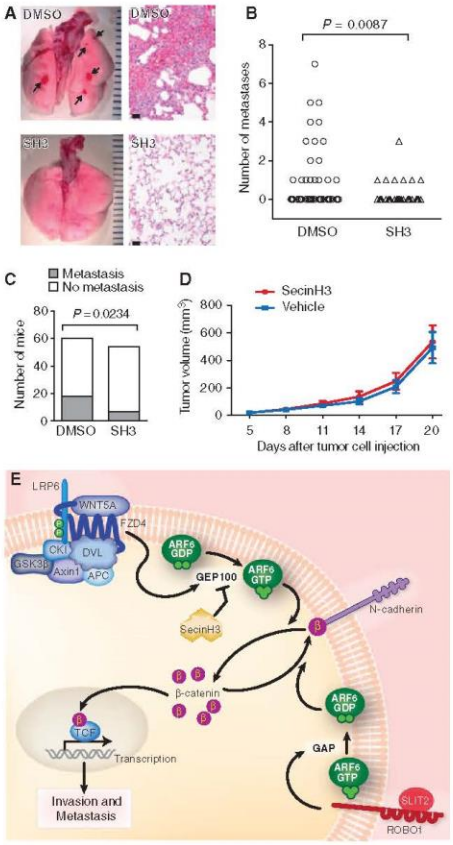

Fig. 7. Pharmacologic inhibition of ARF6-GTP with SecinH3 reduces spontaneous pulmonary metastasis of melanoma in vivo. (A) Gross and hematoxylin and eosin (H&E) images (400×) of lungs from mice with LOX xenograft tumors, treated with either vehicle or SecinH3 (SH3) daily. Ruler hatch marks (gross): 1 mm. Scale bars (microscopic): 20 μm. Arrows: hemorrhagic foci of micrometastases (upper left panel) with clusters of melanoma cells (upper right panel). (B) Number of lung metastases per mouse (Mann-Whitney test, one-tailed). (C) Total number of mice with lung metastasis (Fisher's exact test, one-tailed). (D) Primary tumor growth. Error bars = SEM. (E) Model of ARF6-dependent WNT5A/β-catenin signaling in melanoma invasion and metastasis. In the presence of WNTs, the degradation complex consisting of APC, Axin1, CK1, and GSK3β is sequestered by Dishevelled (DSH), allowing β-catenin stabilization. WNT5A activates ARF6 through FZD4 and LRP6 by stimulating GEP100, a GEF for ARF6. ARF6-GTP facilitates release of junctional β-catenin to augment transactivation of β-catenin, invasion, and metastasis. This process can be antagonized by SLIT2-ROBO1, which stimulates GAPs to convert ARF6-GTP to ARF6-GDP. Pharmacologic inhibition of ARF6 activation with SecinH3, an ARF6 GEF inhibitor, also prevents WNT5A/β-catenin signaling, invasion, and metastasis.

MATERIALS AND METHODS

Cell lines

LOX, SKMel28, Yugen-8, and Yusac-2 cells were provided by D. Grossman (Huntsman Cancer Institute, University of Utah), and A375 cells were a gift from S. Holmen (Huntsman Cancer Institute, University of Utah). HEK293T, A2058, MeWo, SKMel2, and WM266-4 cells were purchased from the American Type Culture Collection (ATCC). All cells except SKMel28 and A375 were maintained in Dulbecco's modified Eagle's medium + GlutaMAX supplemented with 1 mM sodium pyruvate. SKMel28 cells were maintained in modified Eagle's medium + GlutaMAX and 1 mM sodium pyruvate. A375 cells were maintained in RPMI 1640 medium including GlutaMAX and 1 mM sodium pyruvate. LOX, Yugen-8, and Yusac-2 were maintained with 5% fetal bovine serum (FBS), whereas the other cells received 10% FBS.

Plasmids and transfections

FLAG-tagged S33Y-β-catenin in pcDNA3.1 was provided by C. Murtaugh (Department of Human Genetics, University of Utah). Murine *Wnt2*, *Wnt5a*, and *Wnt7a*, and human *WNT3A* coding sequences were individually cloned into the pCI vector under the control of the cytomegalovirus promoter. HEK293T cells were transiently transfected with 10 μg of plasmid using Lipofectamine 2000 (Invitrogen) according to the manufacturer's instructions. For establishing stable cell lines, LOX cells were transfected with 2 μg of pcDNA3.1 (Invitrogen) vector, *ARF6 Q67L*, or *S33Y β-catenin* using Metafectene (Biontex Laboratories) according to the manufacturer's instructions and selected and maintained with G418 (800 μg/ml; Gibco) for 2 weeks. Myc-tagged ARF6 Q67L in pcDNA3.1 was generated by PCR-based mutagenesis from the full-length coding sequence of human *ARF6*. Briefly, two fragments of overlapping *ARF6* sequence were amplified. The first fragment was amplified with primers hARF6-F-Kpn I (5′-cggGGTACCgccaccatggggaaggtgctatcca-3′) and hARF6-Q67L-R (5′-gagcggccggatcttgtccaggccgcccacatcccatac-3′) and contained base pairs 1 to 219. The second fragment was amplified with primers hARF6-Q67L-F (5′-gtatgggatgtgggcggcctggacaagatccggccgctc-3′) and hARF6-R-Not I (5′-ataagaatGCGGCCGCcaagatttgtagttagagg-3′) and contained base pairs 181 to 526. The two DNA fragments were mixed in equal amounts for fusion PCR. The full-length human ARF6 Q67L coding sequence was amplified from the fusion template with primers hARF6-F-Kpn I and hARF6-R-Not I and sequenced for verification.

Lentiviral transduction

For lentiviral transduction, LOX, MeWo, A375, A2058, and Yusac-2 cells were plated at 10,000 cells per well on a 96-well plate in growth medium and incubated at 37°C/5% CO_2 overnight. Cells were then treated with lentiviral particles at a multiplicity of infection of 3 to 5 in growth medium containing hexadimethrine bromide (8 μg/ml) and incubated for 20 hours at 37°C/CO_2. Medium was replaced with fresh growth medium, and the cells were incubated overnight and then split into 24-well plates. Forty-eight hours after removal of the lentivirus-containing medium, selection for cells containing stable integration of the lentiviral construct was begun using growth medium containing puromycin (0.5 μg/ml; Invitrogen) for LOX cells and puromycin (1 μg/ml) for MeWo, A375, A2058, and Yusac-2. Selection was complete by 3 days of treatment. However, cells were expanded for 2 weeks on selection medium before being used for cellular assays.

RNA interference, recombinant proteins, and SecinH3

All siRNA and short hairpin RNA (shRNA) sequences are listed in table S1. siRNA duplexes (20 nM) were transfected into LOX cells using

HiPerFect (Qiagen) according to the manufacturer's instructions. Forty-eight hours after transfection, cells were split to 50% confluency, retransfected, and grown for another 24 hours before cellular assays. Recombinant WNT5A was obtained from R&D Systems and PeproTech. Control (Mock) and WNT5A conditioned media were collected from L cells (mouse fibroblasts) (ATCC) grown according to ATCC instructions. For ARF6-GTP pull-downs, cells were serum-starved overnight, washed in phosphate-buffered saline (PBS) to remove endogenous WNT5A, and then treated with recombinant WNT5A (100 ng/ml) or WNT5A conditioned medium for 3 hours. For luciferase assays, recombinant WNT5A (10 ng/ml) was given in complete medium for 6 hours in WNT5A knockdown LOX cells. Human DKK-1 was purchased from R&D Systems, and cells were treated with 300 ng/ml in complete medium for 3 hours. For recombinant SLIT2 generation, LOX cells were infected with either empty adenovirus (Mock) or adenovirus containing a *SLIT2* expression construct, and either SLIT2 was salt-extracted from the conditioned medium as previously described (*62*) or the conditioned medium was directly used without salt extraction. For ARF6-GTP pull-downs, cells were treated with 20 nM SLIT2 for 3 hours. For fractionation, 7TFP-luciferase, and *AXIN2* experiments, cells were treated with 20 nM SLIT2 for 24 hours. For Matrigel invasion and invadopodia activity, cells were treated with 10 nM SLIT2 conditioned medium, or a single dose (20 nM) of salt-extracted SLIT2 was added to the medium. SecinH3 was purchased from Calbiochem and Albany Molecular Research Inc. For ARF6-GTP pull-downs, cells were treated with 30 μM SecinH3 for 3 hours in complete medium. For fractionation, luciferase, and *AXIN2* experiments, cells were treated with 30 μM SecinH3 for 24 hours. For Matrigel invasion and invadopodia activity, cells were treated with one dose of 30 μM SecinH3 over the entire course of the experiment. *endo*-IWR 1 and XAV-939 were purchased from Calbiochem. BIO was obtained from Tocris Bioscience. For ARF6-GTP pull-downs, LOX cells were treated with *endo*-IWR 1 (25 μM), XAV-939 (2 μM), or BIO (5 μM) for 3 hours in complete medium. For immunoprecipitation with β-catenin and N-cadherin, cells were treated with 25 μM *endo*-IWR 1, 2 μM XAV-939, or 5 μM BIO for 18 hours.

Western blots, immunoprecipitation, cell fractionation, and ARF6-GTP pull-downs

With the exception of the GGA3 ARF6-GTP pull-downs and cell fractionations, all cell lysates were prepared with 25 mM Hepes (pH 7.4), 150 mM NaCl, 1% Triton X-100, and 1% sodium deoxycholate, plus phosphatase and protease inhibitors. For immunoprecipitation, lysates were centrifuged at 12,000*g* for 10 min, precleared with protein A/G (GE Healthcare) coupled to agarose beads for 2 hours, and then incubated for 1 hour at 4°C with N-cadherin antibody and protein A/G agarose beads. For immunoblotting, primary antibodies were diluted in 5% nonfat dry milk in PBS + 0.1% Tween 20 and incubated overnight at 4°C. For cell fractionation, whole-cell lysates were prepared in radioimmunoprecipitation assay buffer [50 mM tris-Cl (pH 7.4), 150 mM NaCl, 1% NP-40, 0.5% sodium deoxycholate, 0.1% SDS] plus protease and phosphatase inhibitors. Quantification was by scanning densitometry whereby changes were normalized to loading controls or input and represents an amalgamation of all independent experiment replicates ($n > 3$ each).

Antibodies against ARF6, active β-catenin (Millipore), WNT5A, WNT3A, LRP6, phospho-LRP6, lamin A/C, β-actin, Na,K-ATPase (Cell Signaling), WNT2, WNT7A, β-tubulin, Myc (Santa Cruz Biotechnology), N-cadherin, and β-catenin (BD Biosciences) were used for immunoblotting and/or immunoprecipitation. GGA3 ARF6-GTP pull-downs were performed with Arf6 Activation Assay Kit (Cell Biolabs) according to the manufacturer's instructions. Cytoplasmic and nuclear fractions were prepared with NE-PER Nuclear and Cytoplasmic Extraction Reagents (Thermo Scientific). Membrane and plasma membrane fractions were isolated with Plasma Membrane Protein Extraction Kit (Abcam) according to the manufacturer's instructions.

Quantification of immunoblots and statistical analysis

Quantitative values were obtained by scanning densitometry. Each band on the immunoblots was normalized to its paired internal control protein. After normalization, the ratio of each experimental treatment to its paired control treatment was obtained, and the geometric means and 95% confidence intervals were calculated.

RNA extraction and quantitative RT-PCR

RNA was prepared with NucleoSpin RNA II (Macherey-Nagel). Complementary DNA was synthesized from 5 μg of total RNA with Oligo(dT) primers and Superscript III reverse transcriptase (Invitrogen). Quantitative RT-PCR was performed with the Applied Biosystems 7900HT and QuantiTect SYBR Green PCR Kits (Qiagen) with the primers listed in table S2. All samples were run in triplicate and normalized to *GAPDH*. *AXIN2* and *GAPDH* primers were validated for equal amplification efficiencies, and the relative expression of these genes was determined with the $\Delta\Delta C_T$ method. All primer sequences are listed in table S2.

Luciferase assay

Luciferase activity was assayed with lentivirally transduced cells that stably express the TOPFlash-based 7TFP reporter (Addgene) (*63*). Twenty micrograms of lysate was assayed for firefly luciferase with Promega's Luciferase Assay System according to the manufacturer's instructions. Twelve replicates (wells) were assayed for each experimental condition. Stable Q67L clones were infected with 7TFP lentivirus 48 hours before the luciferase assay.

Matrigel invasion

BD Biocoat Matrigel Invasion Chambers (24-well plates) were purchased from BD Biosciences, and cells were assayed according to the manufacturer's instructions, with minor modifications. Briefly, cells were pretreated with mitomycin C (10 μg/ml) for 2 hours to prevent cell division, washed, and resuspended in medium with 0.2% serum. For most assays, cells were plated at a density of 5×10^4 cells per well. Cells stably expressing ARF6 Q67L were plated at 2.5×10^4 cells per well. Invasion was induced with complete medium in the lower chamber. Cells were fixed with 5% glutaraldehyde for 20 min and stained with 0.5% toluidine blue in 3% $NaHCO_3$ for 40 min. Five separate fields were counted per well (four wells per experimental variable).

Invadopodia assay

LOX cells were evaluated for invadopodia activity as previously described (*21*). Invadopodia activity was scored by counting the percentage of total cells that show pericellular gelatin degradation.

Immunofluorescence staining

LOX cells were plated for 24 hours at a density of 8×10^4 cells per well in complete medium on collagen-coated eight-well cover glasses, washed twice in PBS, and fixed. For intracellular staining, monolayers were fixed in 1:1 methanol/acetone at −20°C and permeabilized in 0.5% Triton X-100 for 10 min. For cell surface staining of N-cadherin, monolayers were fixed in 4% paraformaldehyde for 10 min at room temperature, followed by 10 min in 100% methanol at −20°C. Both fixation conditions were blocked in 5% bovine serum albumin for 1 hour at room temperature. Primary antibodies against active β-catenin (Millipore), β-catenin (Invitrogen), and N-cadherin (BD Transduction Laboratories) were diluted according

to the manufacturer's specifications and applied overnight at 4°C. Signals were detected by Alexa Fluor conjugated anti immunoglobulin G (IgG) diluted to 10 μg/ml. Fields for imaging were randomly selected in the 4′,6-diamidino-2-phenylindole channel and imaged at 600× on an Olympus FV1000 confocal microscope.

Four-micrometer sections of formalin-fixed, paraffin-embedded LOX xenograft tumors were subjected to heat-induced epitope retrieval in citrate buffer (pH 6.0) before immunostaining. The β-catenin primary antibody (clone 14, BD Transduction Laboratories; 1:50) was preincubated with secondary antibody (rabbit anti-mouse Fab2, Dako; 1:100) for 30 min. To reduce background staining of mouse tissue, 5 μl of mouse serum was added and incubated for 30 min, creating a primary/secondary cocktail. Sections were incubated with this cocktail for 2 hours at 37°C. A biotinylated tertiary antibody (goat anti-rabbit IgG, Sigma, 1:100) was applied for 32 min. Development of the alkaline phosphate red signal was performed with the Ventana XT detection kit. Levamisole was applied for 8 min as a blocker, and slides were counterstained with hematoxylin for 4 min. Using a BioView Duet imaging system, we chose three random 400× fields per tumor on bright field and then imaged them on a fluorescence microscope. Investigators were blinded to the treatment groups when evaluating β-catenin staining.

Xenograft melanoma model

Athymic nude and nonobese diabetic/severe combined immunodeficient mice were purchased from Jackson Laboratories. Mice were injected subcutaneously with 2×10^6 to 3×10^6 LOX cells in 0.1 ml of Dulbecco's PBS. Tumors were allowed to establish for 5 days before initiating daily intraperitoneal injections of 0.1 ml of 5 mM SecinH3 or vehicle (25% DMSO + 3.75% dextrose). Investigators were blinded to treatment groups for evaluation of primary tumor size and scoring of metastasis. Primary subcutaneous tumors were measured every 3 days. Tumor volume was calculated using the ellipsoid formula: $V = 4/3 \times \pi \times \text{length}/2 \times \text{width}/2 \times \text{depth}/2$. On day 21 after tumor cell injection, mice were sacrificed by isoflurane inhalation and evaluated for spontaneous pulmonary metastasis. Lungs were removed and rinsed thoroughly in PBS. Discrete, round, and red metastatic foci were identified and counted. Primary tumors were evaluated histologically by H&E staining.

Biochemical nucleotide exchange assay

Nucleotide exchange was assayed in vitro using ARF6 (amino acids 14 to 175, which lacks the N-terminal autoinhibitory region), as well as ARNO (also known as cytohesin2) (amino acids 50 to 255), or GEP100 (amino acids 391 to 602) protein fragments that include Sec7 domains. All recombinant proteins were expressed as N-terminally His-tagged fusions in *Escherichia coli* system using pET28a vector and purified to apparent homogeneity by immobilized metal affinity chromatography. The nucleotide exchange reaction was carried out with 50 mM tris-HCl (pH 7.5), 1 mM $MgCl_2$, 0.001% Triton X-100, 2 mM β-mercaptoethanol, 1% DMSO, and 50 nM GTP-BODIPY FL supplemented with 50 nM GEF protein and 200 nM GDP-bound form of ARF6 in the absence or presence of SecinH3. Replacement of ARF6-bound GDP with GTP-BODIPY FL was monitored by measuring increases in fluorescence intensity that result from the relief of intramolecular fluorescence quenching of the latter fluorogenic nucleotide upon binding to the GTPase (*64*). Specifically, fluorescence intensities were determined in real-time mode with a Synergy 4 plate reader (BioTek) at excitation and emission wavelengths of 490 and 520 nm, respectively.

Statistical analysis

Excel or Prism was used to assess statistical significance. When two groups were compared, a Student's *t* test was performed. When more than two groups were compared, one-way ANOVA followed by either Tukey's or Dunnett's post hoc test was performed. When one-way ANOVA was performed, *P* values shown in figures represent results from the post hoc test. When data were not normally distributed, nonparametric Mann-Whitney test was used. Fisher's exact test was performed to analyze data from contingency tables.

SUPPLEMENTARY MATERIALS

www.sciencesignaling.org/cgi/content/full/6/265/ra14/DC1

Fig. S1. ARF6 knockdown does not alter total N-cadherin protein at the plasma membrane.
Fig. S2. Quantification of immunoblots.
Fig. S3. ARF6 knockdown drives β-catenin from the nucleus to N-cadherin.
Fig. S4. ARF6, junctional β-catenin, and the canonical destruction complex.
Fig. S5. SLIT2-ROBO1 and SecinH3 inhibit ARF6 activation.
Fig. S6. Time course of β-catenin relocalization after ARF6 inhibition.
Fig. S7. ARF6-dependent β-catenin transactivation and relative WNT production in melanoma cell lines.
Fig. S8. WNT2 knockdown reduces ARF6 activation.
Fig. S9. FZD4 knockdown reduces ARF6 activation.
Fig. S10. WNT5A, ARF6, and β-catenin signaling in multiple human melanoma cell lines.
Fig. S11. Cytohesin knockdown does not reduce ARF6 activation.
Fig. S12. β-Catenin immunostaining of LOX melanoma xenograft tumors.
Table S1. siRNA and shRNA sequences.
Table S2. Primer sequences for RT-PCR.

REFERENCES AND NOTES

1. R. van Amerongen, R. Nusse, Towards an integrated view of Wnt signaling in development. *Development* **136**, 3205–3214 (2009).
2. J. Heuberger, W. Birchmeier, Interplay of cadherin-mediated cell adhesion and canonical Wnt signaling. *Cold Spring Harb. Perspect. Biol.* **2**, a002915 (2010).
3. W. J. Nelson, R. Nusse, Convergence of Wnt, β-catenin, and cadherin pathways. *Science* **303**, 1483–1487 (2004).
4. A. Kikuchi, H. Yamamoto, A. Sato, S. Matsumoto, Wnt5a: Its signalling, functions and implication in diseases. *Acta Physiol.* **204**, 17–33 (2012).
5. A. J. Mikels, R. Nusse, Purified Wnt5a protein activates or inhibits β-catenin–TCF signaling depending on receptor context. *PLoS Biol.* **4**, e115 (2006).
6. S. W. Cha, E. Tadjuidje, Q. Tao, C. Wylie, J. Heasman, Wnt5a and Wnt11 interact in a maternal Dkk1-regulated fashion to activate both canonical and non-canonical signaling in *Xenopus* axis formation. *Development* **135**, 3719–3729 (2008).
7. S. W. Cha, E. Tadjuidje, J. White, J. Wells, C. Mayhew, C. Wylie, J. Heasman, Wnt11/5a complex formation caused by tyrosine sulfation increases canonical signaling activity. *Curr. Biol.* **19**, 1573–1580 (2009).
8. Q. Tao, C. Yokota, H. Puck, M. Kofron, B. Birsoy, D. Yan, M. Asashima, C. C. Wylie, X. Lin, J. Heasman, Maternal wnt11 activates the canonical wnt signaling pathway required for axis formation in *Xenopus* embryos. *Cell* **120**, 857–871 (2005).
9. M. Umbhauer, A. Djiane, C. Goisset, A. Penzo-Méndez, J. F. Riou, J. C. Boucaut, D. L. Shi, The C-terminal cytoplasmic Lys-thr-X-X-X-Trp motif in frizzled receptors mediates Wnt/β-catenin signalling. *EMBO J.* **19**, 4944–4954 (2000).
10. X. He, J. P. Saint-Jeannet, Y. Wang, J. Nathans, I. Dawid, H. Varmus, A member of the Frizzled protein family mediating axis induction by Wnt-5A. *Science* **275**, 1652–1654 (1997).
11. F. Palacios, L. Price, J. Schweitzer, J. G. Collard, C. D'Souza-Schorey, An essential role for ARF6-regulated membrane traffic in adherens junction turnover and epithelial cell migration. *EMBO J.* **20**, 4973–4986 (2001).
12. C. A. Jones, N. Nishiya, N. R. London, W. Zhu, L. K. Sorensen, A. C. Chan, C. J. Lim, H. Chen, Q. Zhang, P. G. Schultz, A. M. Hayallah, K. R. Thomas, M. Famulok, K. Zhang, M. H. Ginsberg, D. Y. Li, Slit2–Robo4 signalling promotes vascular stability by blocking Arf6 activity. *Nat. Cell Biol.* **11**, 1325–1331 (2009).
13. N. R. London, W. Zhu, F. A. Bozza, M. C. Smith, D. M. Greif, L. K. Sorensen, L. Chen, Y. Kaminoh, A. C. Chan, S. F. Passi, C. W. Day, D. L. Barnard, G. A. Zimmerman, M. A. Krasnow, D. Y. Li, Targeting Robo4-dependent Slit signaling to survive the cytokine storm in sepsis and influenza. *Sci. Transl. Med.* **2**, 23ra19 (2010).
14. M. Morishige, S. Hashimoto, E. Ogawa, Y. Toda, H. Kotani, M. Hirose, S. Wei, A. Hashimoto, A. Yamada, H. Yano, Y. Mazaki, H. Kodama, Y. Nio, T. Manabe, H. Wada, H. Kobayashi, H. Sabe, GEP100 links epidermal growth factor receptor signalling to Arf6 activation to induce breast cancer invasion. *Nat. Cell Biol.* **10**, 85–92 (2008).
15. M. Y. Hsu, F. E. Meier, M. Nesbit, J. Y. Hsu, P. Van Belle, D. E. Elder, M. Herlyn, E-cadherin expression in melanoma cells restores keratinocyte-mediated growth control and down-regulates expression of invasion-related adhesion receptors. *Am. J. Pathol.* **156**, 1515–1525 (2000).

16. M. Y. Hsu, M. J. Wheelock, K. R. Johnson, M. Herlyn, Shifts in cadherin profiles between human normal melanocytes and melanomas. *J. Investig. Dermatol. Symp. Proc.* **1**, 188–194 (1996).
17. G. Li, K. Satyamoorthy, M. Herlyn, N-cadherin-mediated intercellular interactions promote survival and migration of melanoma cells. *Cancer Res.* **61**, 3819–3825 (2001).
18. C. K. Augustine, Y. Yoshimoto, M. Gupta, P. A. Zipfel, M. A. Selim, P. Febbo, A. M. Pendergast, W. P. Peters, D. S. Tyler, Targeting N-cadherin enhances antitumor activity of cytotoxic therapies in melanoma treatment. *Cancer Res.* **68**, 3777–3784 (2008).
19. J. Qi, N. Chen, J. Wang, C. H. Siu, Transendothelial migration of melanoma cells involves N-cadherin-mediated adhesion and activation of the β-catenin signaling pathway. *Mol. Biol. Cell* **16**, 4386–4397 (2005).
20. J. Qi, J. Wang, O. Romanyuk, C. H. Siu, Involvement of Src family kinases in N-cadherin phosphorylation and β-catenin dissociation during transendothelial migration of melanoma cells. *Mol. Biol. Cell* **17**, 1261–1272 (2006).
21. S. E. Tague, V. Muralidharan, C. D'Souza-Schorey, ADP-ribosylation factor 6 regulates tumor cell invasion through the activation of the MEK/ERK signaling pathway. *Proc. Natl. Acad. Sci. U.S.A.* **101**, 9671–9676 (2004).
22. V. Muralidharan-Chari, J. Clancy, C. Plou, M. Romao, P. Chavrier, G. Raposo, C. D'Souza-Schorey, ARF6-regulated shedding of tumor cell-derived plasma membrane microvesicles. *Curr. Biol.* **19**, 1875–1885 (2009).
23. V. Muralidharan-Chari, H. Hoover, J. Clancy, J. Schweitzer, M. A. Suckow, V. Schroeder, F. J. Castellino, J. S. Schorey, C. D'Souza-Schorey, ADP-ribosylation factor 6 regulates tumorigenic and invasive properties in vivo. *Cancer Res.* **69**, 2201–2209 (2009).
24. J. Bilic, Y. L. Huang, G. Davidson, T. Zimmermann, C. M. Cruciat, M. Bienz, C. Niehrs, Wnt induces LRP6 signalosomes and promotes dishevelled-dependent LRP6 phosphorylation. *Science* **316**, 1619–1622 (2007).
25. M. Hafner, A. Schmitz, I. Grüne, S. G. Srivatsan, B. Paul, W. Kolanus, T. Quast, E. Kremmer, I. Bauer, M. Famulok, Inhibition of cytohesins by SecinH3 leads to hepatic insulin resistance. *Nature* **444**, 941–944 (2006).
26. R. H. Shoemaker, D. J. Dykes, J. Plowman, S. D. Harrison Jr., D. P. Griswold Jr., B. J. Abbott, J. G. Mayo, O. Fodstad, M. R. Boyd, Practical spontaneous metastasis model for in vivo therapeutic studies using a human melanoma. *Cancer Res.* **51**, 2837–2841 (1991).
27. E. S. Witze, E. S. Litman, G. M. Argast, R. T. Moon, N. G. Ahn, Wnt5a control of cell polarity and directional movement by polarized redistribution of adhesion receptors. *Science* **320**, 365–369 (2008).
28. M. P. O'Connell, J. L. Fiori, M. Xu, A. D. Carter, B. P. Frank, T. C. Camilli, A. D. French, S. K. Dissanayake, F. E. Indig, M. Bernier, D. D. Taub, S. M. Hewitt, A. T. Weeraratna, The orphan tyrosine kinase receptor, ROR2, mediates Wnt5A signaling in metastatic melanoma. *Oncogene* **29**, 34–44 (2010).
29. A. T. Weeraratna, Y. Jiang, G. Hostetter, K. Rosenblatt, P. Duray, M. Bittner, J. M. Trent, Wnt5a signaling directly affects cell motility and invasion of metastatic melanoma. *Cancer Cell* **1**, 279–288 (2002).
30. S. K. Dissanayake, M. Wade, C. E. Johnson, M. P. O'Connell, P. D. Leotlela, A. D. French, K. V. Shah, K. J. Hewitt, D. T. Rosenthal, F. E. Indig, Y. Jiang, B. J. Nickoloff, D. D. Taub, J. M. Trent, R. T. Moon, M. Bittner, A. T. Weeraratna, The Wnt5A/protein kinase C pathway mediates motility in melanoma cells via the inhibition of metastasis suppressors and initiation of an epithelial to mesenchymal transition. *J. Biol. Chem.* **282**, 17259–17271 (2007).
31. D. C. Slusarski, V. G. Corces, R. T. Moon, Interaction of Wnt and a Frizzled homologue triggers G-protein-linked phosphatidylinositol signalling. *Nature* **390**, 410–413 (1997).
32. W. Chen, D. ten Berge, J. Brown, S. Ahn, L. A. Hu, W. E. Miller, M. G. Caron, L. S. Barak, R. Nusse, R. J. Lefkowitz, Dishevelled 2 recruits β-arrestin 2 to mediate Wnt5A-stimulated endocytosis of Frizzled 4. *Science* **301**, 1391–1394 (2003).
33. M. Sen, M. Chamorro, J. Reifert, M. Corr, D. A. Carson, Blockade of Wnt-5A/frizzled 5 signaling inhibits rheumatoid synoviocyte activation. *Arthritis Rheum.* **44**, 772–781 (2001).
34. M. D. Onken, L. A. Worley, M. D. Tuscan, J. W. Harbour, An accurate, clinically feasible multi-gene expression assay for predicting metastasis in uveal melanoma. *J. Mol. Diagn.* **12**, 461–468 (2010).
35. T. Sinnberg, M. Menzel, D. Ewerth, B. Sauer, M. Schwarz, M. Schaller, C. Garbe, B. Schittek, β-Catenin signaling increases during melanoma progression and promotes tumor cell survival and chemoresistance. *PLoS One* **6**, e23429 (2011).
36. W. E. Damsky, D. P. Curley, M. Santhanakrishnan, L. E. Rosenbaum, J. T. Platt, B. E. Gould Rothberg, M. M. Taketo, D. Dankort, D. L. Rimm, M. McMahon, M. Bosenberg, β-Catenin signaling controls metastasis in Braf-activated Pten-deficient melanomas. *Cancer Cell* **20**, 741–754 (2011).
37. A. Someya, M. Sata, K. Takeda, G. Pacheco-Rodriguez, V. J. Ferrans, J. Moss, M. Vaughan, ARF-GEP$_{100}$, a guanine nucleotide-exchange protein for ADP-ribosylation factor 6. *Proc. Natl. Acad. Sci. U.S.A.* **98**, 2413–2418 (2001).
38. F. H. Brembeck, T. Schwarz-Romond, J. Bakkers, S. Wilhelm, M. Hammerschmidt, W. Birchmeier, Essential role of BCL9-2 in the switch between β-catenin's adhesive and transcriptional functions. *Genes Dev.* **18**, 2225–2230 (2004).
39. N. Zhang, P. Wei, A. Gong, W. T. Chiu, H. T. Lee, H. Colman, H. Huang, J. Xue, M. Liu, Y. Wang, R. Sawaya, K. Xie, W. K. Yung, R. H. Medema, X. He, S. Huang, FoxM1 promotes β-catenin nuclear localization and controls Wnt target-gene expression and glioma tumorigenesis. *Cancer Cell* **20**, 427–442 (2011).
40. C. D'Souza-Schorey, P. Chavrier, ARF proteins: Roles in membrane traffic and beyond. *Nat. Rev. Mol. Cell Biol.* **7**, 347–358 (2006).
41. J. K. Schweitzer, A. E. Sedgwick, C. D'Souza-Schorey, ARF6-mediated endocytic recycling impacts cell movement, cell division and lipid homeostasis. *Semin. Cell Dev. Biol.* **22**, 39–47 (2011).
42. V. Muralidharan-Chari, J. W. Clancy, A. Sedgwick, C. D'Souza-Schorey, Microvesicles: Mediators of extracellular communication during cancer progression. *J. Cell Sci.* **123**, 1603–1611 (2010).
43. H. Macias, A. Moran, Y. Samara, M. Moreno, J. E. Compton, G. Harburg, P. Strickland, L. Hinck, SLIT/ROBO1 signaling suppresses mammary branching morphogenesis by limiting basal cell number. *Dev. Cell* **20**, 827–840 (2011).
44. P. D. Da Forno, J. H. Pringle, P. Hutchinson, J. Osborn, Q. Huang, L. Potter, R. A. Hancox, A. Fletcher, G. S. Saldanha, WNT5A expression increases during melanoma progression and correlates with outcome. *Clin. Cancer Res.* **14**, 5825–5832 (2008).
45. A. V. Biankin, N. Waddell, K. S. Kassahn, M. C. Gingras, L. B. Muthuswamy, A. L. Johns, D. K. Miller, P. J. Wilson, A. M. Patch, J. Wu, D. K. Chang, M. J. Cowley, B. B. Gardiner, S. Song, I. Harliwong, S. Idrisoglu, C. Nourse, E. Nourbakhsh, S. Manning, S. Wani, M. Gongora, M. Pajic, C. J. Scarlett, A. J. Gill, A. V. Pinho, I. Rooman, M. Anderson, O. Holmes, C. Leonard, D. Taylor, S. Wood, Q. Xu, K. Nones, J. L. Fink, A. Christ, T. Bruxner, N. Cloonan, G. Kolle, F. Newell, M. Pinese, R. S. Mead, J. L. Humphris, W. Kaplan, M. D. Jones, E. K. Colvin, A. M. Nagrial, E. S. Humphrey, A. Chou, V. T. Chin, L. A. Chantrill, A. Mawson, J. S. Samra, J. G. Kench, J. A. Lovell, R. J. Daly, N. D. Merrett, C. Toon, K. Epari, N. Q. Nguyen, A. Barbour, N. Zeps, N. Kakkar, F. Zhao, Y. Q. Wu, M. Wang, D. M. Muzny, W. E. Fisher, F. C. Brunicardi, S. E. Hodges, J. G. Reid, J. Drummond, K. Chang, Y. Han, L. R. Lewis, H. Dinh, C. J. Buhay, T. Beck, L. Timms, M. Sam, K. Begley, A. Brown, D. Pai, A. Panchal, N. Buchner, R. De Borja, R. E. Denroche, C. K. Yung, S. Serra, N. Onetto, D. Mukhopadhyay, M. S. Tsao, P. A. Shaw, G. M. Petersen, S. Gallinger, R. H. Hruban, A. Maitra, C. A. Iacobuzio-Donahue, R. D. Schulick, C. L. Wolfgang, R. A. Morgan, R. T. Lawlor, P. Capelli, V. Corbo, M. Scardoni, G. Tortora, M. A. Tempero, K. M. Mann, N. A. Jenkins, P. A. Perez-Mancera, D. J. Adams, D. A. Largaespada, L. F. Wessels, A. G. Rust, L. D. Stein, D. A. Tuveson, N. G. Copeland, E. A. Musgrove, A. Scarpa, J. R. Eshleman, T. J. Hudson, R. L. Sutherland, D. A. Wheeler, J. V. Pearson, J. D. McPherson, R. A. Gibbs, S. M. Grimmond, Pancreatic cancer genomes reveal aberrations in axon guidance pathway genes. *Nature* **491**, 399–405 (2012).
46. N. R. London, D. Y. Li, Robo4-dependent Slit signaling stabilizes the vasculature during pathologic angiogenesis and cytokine storm. *Curr. Opin. Hematol.* **18**, 186–190 (2011).
47. W. Zhu, N. R. London, C. C. Gibson, C. T. Davis, Z. Tong, L. K. Sorensen, D. S. Shi, J. Guo, M. C. P. Smith, A. H. Grossmann, K. R. Thomas, D. Y. Li, Interleukin receptor activates a MyD88–ARNO–ARF6 cascade to disrupt vascular stability. *Nature* **492**, 252–255 (2012).
48. R. van Amerongen, C. Fuerer, M. Mizutani, R. Nusse, Wnt5a can both activate and repress Wnt/β-catenin signaling during mouse embryonic development. *Dev. Biol.* **369**, 101–114 (2012).
49. Q. Zhang, M. B. Major, S. Takanashi, N. D. Camp, N. Nishiya, E. C. Peters, M. H. Ginsberg, X. Jian, P. A. Randazzo, P. G. Schultz, R. T. Moon, S. Ding, Small-molecule synergist of the Wnt/β-catenin signaling pathway. *Proc. Natl. Acad. Sci. U.S.A.* **104**, 7444–7448 (2007).
50. W. Kim, S. Y. Kim, T. Kim, M. Kim, D. J. Bae, H. I. Choi, I. S. Kim, E. Jho, ADP-ribosylation factors 1 and 6 regulate Wnt/β-catenin signaling via control of LRP6 phosphorylation. *Oncogene* 10.1038/onc.2012.373 (2012).
51. I. Arozarena, H. Bischof, D. Gilby, B. Belloni, R. Dummer, C. Wellbrock, In melanoma, beta-catenin is a suppressor of invasion. *Oncogene* **30**, 4531–4543 (2011).
52. A. J. Chien, E. C. Moore, A. S. Lonsdorf, R. M. Kulikauskas, B. G. Rothberg, A. J. Berger, M. B. Major, S. T. Hwang, D. L. Rimm, R. T. Moon, Activated Wnt/β-catenin signaling in melanoma is associated with decreased proliferation in patient tumors and a murine melanoma model. *Proc. Natl. Acad. Sci. U.S.A.* **106**, 1193–1198 (2009).
53. T. Kageshita, C. V. Hamby, T. Ishihara, K. Matsumoto, T. Saida, T. Ono, Loss of β-catenin expression associated with disease progression in malignant melanoma. *Br. J. Dermatol.* **145**, 210–216 (2001).
54. I. M. Bachmann, O. Straume, H. E. Puntervoll, M. B. Kalvenes, L. A. Akslen, Importance of P-cadherin, β-catenin, and Wnt5a/frizzled for progression of melanocytic tumors and prognosis in cutaneous melanoma. *Clin. Cancer Res.* **11**, 8606–8614 (2005).
55. O. M. Eichhoff, A. Weeraratna, M. C. Zipser, L. Denat, D. S. Widmer, M. Xu, L. Kriegl, T. Kirchner, L. Larue, R. Dummer, K. S. Hoek, Differential LEF1 and TCF4 expression is involved in melanoma cell phenotype switching. *Pigment Cell Melanoma Res.* **24**, 631–642 (2011).
56. B. Hu, B. Shi, M. J. Jarzynka, J. J. Yiin, C. D'Souza-Schorey, S. Y. Cheng, ADP-ribosylation factor 6 regulates glioma cell invasion through the IQ-domain GTPase-activating protein 1-Rac1–mediated pathway. *Cancer Res.* **69**, 794–801 (2009).

57. S. Hashimoto, Y. Onodera, A. Hashimoto, M. Tanaka, M. Hamaguchi, A. Yamada, H. Sabe, Requirement for Arf6 in breast cancer invasive activities. *Proc. Natl. Acad. Sci. U.S.A.* **101**, 6647–6652 (2004).
58. L. A. Mina, G. W. Sledge Jr., Rethinking the metastatic cascade as a therapeutic target. *Nat. Rev. Clin. Oncol.* **8**, 325–332 (2011).
59. M. B. Atkins, M. T. Lotze, J. P. Dutcher, R. I. Fisher, G. Weiss, K. Margolin, J. Abrams, M. Sznol, D. Parkinson, M. Hawkins, C. Paradise, L. Kunkel, S. A. Rosenberg, High-dose recombinant interleukin 2 therapy for patients with metastatic melanoma: Analysis of 270 patients treated between 1985 and 1993. *J. Clin. Oncol.* **17**, 2105–2116 (1999).
60. F. S. Hodi, S. J. O'Day, D. F. McDermott, R. W. Weber, J. A. Sosman, J. B. Haanen, R. Gonzalez, C. Robert, D. Schadendorf, J. C. Hassel, W. Akerley, A. J. van den Eertwegh, J. Lutzky, P. Lorigan, J. M. Vaubel, G. P. Linette, D. Hogg, C. H. Ottensmeier, C. Lebbé, C. Peschel, I. Quirt, J. I. Clark, J. D. Wolchok, J. S. Weber, J. Tian, M. J. Yellin, G. M. Nichol, A. Hoos, W. J. Urba, Improved survival with ipilimumab in patients with metastatic melanoma. *N. Engl. J. Med.* **363**, 711–723 (2010).
61. P. B. Chapman, A. Hauschild, C. Robert, J. B. Haanen, P. Ascierto, J. Larkin, R. Dummer, C. Garbe, A. Testori, M. Maio, D. Hogg, P. Lorigan, C. Lebbe, T. Jouary, D. Schadendorf, A. Ribas, S. J. O'Day, J. A. Sosman, J. M. Kirkwood, A. M. Eggermont, B. Dreno, K. Nolop, J. Li, B. Nelson, J. Hou, R. J. Lee, K. T. Flaherty, G. A. McArthur; BRIM-3 Study Group, Improved survival with vemurafenib in melanoma with BRAF V600E mutation. *N. Engl. J. Med.* **364**, 2507–2516 (2011).
62. C. A. Jones, N. R. London, H. Chen, K. W. Park, D. Sauvaget, R. A. Stockton, J. D. Wythe, W. Suh, F. Larrieu-Lahargue, Y. S. Mukouyama, P. Lindblom, P. Seth, A. Frias, N. Nishiya, M. H. Ginsberg, H. Gerhardt, K. Zhang, D. Y. Li, Robo4 stabilizes the vascular network by inhibiting pathologic angiogenesis and endothelial hyperpermeability. *Nat. Med.* **14**, 448–453 (2008).
63. C. Fuerer, R. Nusse, Lentiviral vectors to probe and manipulate the Wnt signaling pathway. *PLoS One* **5**, e9370 (2010).
64. D. P. McEwen, K. R. Gee, H. C. Kang, R. R. Neubig, Fluorescent BODIPY-GTP analogs: Real-time measurement of nucleotide binding to G proteins. *Anal. Biochem.* **291**, 109–117 (2001).

Acknowledgments: We thank J. Christian, A. Welm, C. Murtaugh, R. Dorsky, D. Jones, S. Holmen, and R. Stewart for critical reading of the manuscript. We thank T. Greene (Study Design and Biostatistics Center, University of Utah) for support with statistical analyses. We thank C. Murtaugh and D. Grossman for reagents and technical advice, H. S. Kim for technical guidance, R. Zhang for technical support, and D. Lim for graphical assistance. **Funding:** D.Y.L. is supported by grants from the Huntsman Cancer Institute, University of Utah CRR Program, National Heart, Lung, and Blood Institute (NHLBI), Juvenile Diabetes Research Foundation, Rocky Mountain Regional Center for Excellence in Biodefense and Emerging Infectious Disease, American Asthma Foundation, and Department of Defense. A.H.G. was supported by the R. L. Kirschstein NRSA (2T32HL007576-26) from the NHLBI. Additional grants (C.D.S.-S.) are from the National Cancer Institute and the University of Notre Dame SAPC Program. J.C. is an Indiana-CTSI predoctoral fellow and A.S. is supported by a University of Notre Dame Graduate Assistantship. **Author contributions:** A.H.G., J.H.Y., S.J.O., and D.Y.L. were responsible for project conceptualization, experimental design, data analysis, and manuscript preparation. A.H.G. generated in vitro and in vivo data, provided pathology expertise, and was primarily responsible for writing the manuscript. J.H.Y. generated biochemical and in vitro data. J.C., A.S., and C.D.S.-S. provided in vitro data and helped in the critical reading of the manuscript. L.K.S. generated in vitro data and immunocytofluorescence images. Z.T. and K.R.T. provided several plasmid constructs and adenoviruses. K.R.T. provided critical review of the manuscript. K.O. provided data from GTP exchange assays. A.R. provided in vitro data. K.F.G. provided expert opinion in melanoma medical oncology and helped prepare the manuscript. S.R.T. performed immunofluorescence staining and image acquisition of tumors. S.J.O. generated in vivo data and performed statistical analyses. **Competing interests:** The authors declare competing financial interests. The University of Utah has filed intellectual property concerning targeting signaling pathways to treat cancer and licensed technology to Navigen, a biotechnology company owned in part by the University of Utah Research Foundation. D.Y.L. and K.R.T. have equity interest, management or advisory relationships, and paid consulting relationship with Navigen. Those relationships are related to patent applications surrounding small-molecule inhibition of Arf6 that predate this article and are licensed from the University of Utah by Navigen. Navigen is owned in part by the University of Utah Research Foundation.

Submitted 13 July 2012
Accepted 25 January 2013
Final Publication 5 March 2013
10.1126/scisignal.2003398
Citation: A. H. Grossmann, J. H. Yoo, J. Clancy, L. K. Sorensen, A. Sedgwick, Z. Tong, K. Ostanin, A. Rogers, K. F. Grossmann, S. R. Tripp, K. R. Thomas, C. D'Souza-Schorey, S. J. Odelberg, D. Y. Li, The small GTPase ARF6 stimulates β-catenin transcriptional activity during WNT5A-mediated melanoma invasion and metastasis. *Sci. Signal.* **6**, ra14 (2013).

Science Signaling
AAAS
www.sciencesignaling.org/cgi/content/full/6/265/ra14/DC1

Supplementary Materials for

The Small GTPase ARF6 Stimulates β-Catenin Transcriptional Activity During WNT5A-Mediated Melanoma Invasion and Metastasis

Allie H. Grossmann, Jae Hyuk Yoo, James Clancy, Lise K. Sorensen, Alanna Sedgwick, Zongzhong Tong, Kirill Ostanin, Aaron Rogers, Kenneth F. Grossmann, Sheryl R. Tripp, Kirk R. Thomas, Crislyn D'Souza-Schorey, Shannon J. Odelberg,* Dean Y. Li*

*To whom correspondence should be addressed. E-mail: dean.li@u2m2.utah.edu (D.Y.L.); sodelber@genetics.utah.edu (S.J.O.)

Published 5 March 2013, *Sci. Signal.* **6**, ra14 (2013)
DOI: 10.1126/scisignal.2003398

The PDF file includes:

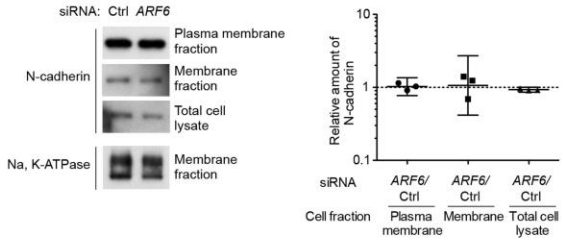

Figure S1: ARF6 knockdown does not alter total N-cadherin protein at the plasma membrane. N-cadherin immunoblots of plasma membrane fractions, membrane fractions, and total cell lysates from LOX cells treated with Control (Ctrl) or *ARF6* siRNAs. Scatter plot shows quantification of immunoblots. Data points = individual experiments (*n=3*). Solid line within data points = geometric mean. Error bars = 95% CI.

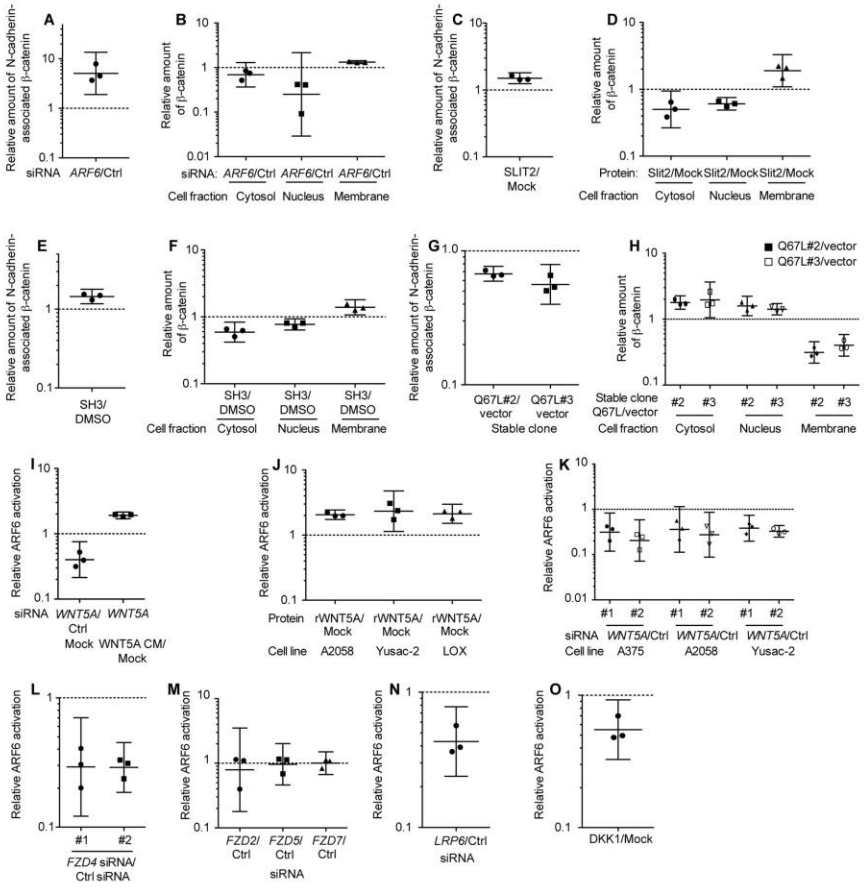
A
Relative amount of N-cadherin-associated β-catenin
siRNA ARF6/Ctrl
B
Relative amount of β-catenin
siRNA: ARF6/Ctrl ARF6/Ctrl ARF6/Ctrl
Cell fraction Cytosol Nucleus Membrane
C
Relative amount of N-cadherin-associated β-catenin
SLIT2/ Mock
D
Relative amount of β-catenin
Protein: Slit2/Mock Slit2/Mock Slit2/Mock
Cell fraction Cytosol Nucleus Membrane
E
Relative amount of N-cadherin-associated β-catenin
SH3/ DMSO
F
Relative amount of β-catenin
SH3/ DMSO SH3/ DMSO SH3/ DMSO
Cell fraction Cytosol Nucleus Membrane
G
Relative amount of N-cadherin-associated β-catenin
Q67L#2/ vector Q67L#3 vector
Stable clone
H
Q67L#2/vector
Q67L#3/vector
Relative amount of β-catenin
Stable clone #2 #3 #2 #3 #2 #3
Q67L/vector
Cell fraction Cytosol Nucleus Membrane
I
Relative ARF6 activation
siRNA WNT5A/ Ctrl WNT5A
Mock WNT5A CM/ Mock
J
Relative ARF6 activation
Protein rWNT5A/ Mock rWNT5A/ Mock rWNT5A/ Mock
Cell line A2058 Yusac-2 LOX
K
Relative ARF6 activation
#1 #2 #1 #2 #1 #2
siRNA WNT5A/Ctrl WNT5A/Ctrl WNT5A/Ctrl
Cell line A375 A2058 Yusac-2
L
Relative ARF6 activation
#1 #2
FZD4 siRNA/ Ctrl siRNA
M
Relative ARF6 activation
FZD2/ Ctrl FZD5/ Ctrl FZD7/ Ctrl
siRNA
N
Relative ARF6 activation
LRP6/Ctrl siRNA
O
Relative ARF6 activation
DKK1/Mock

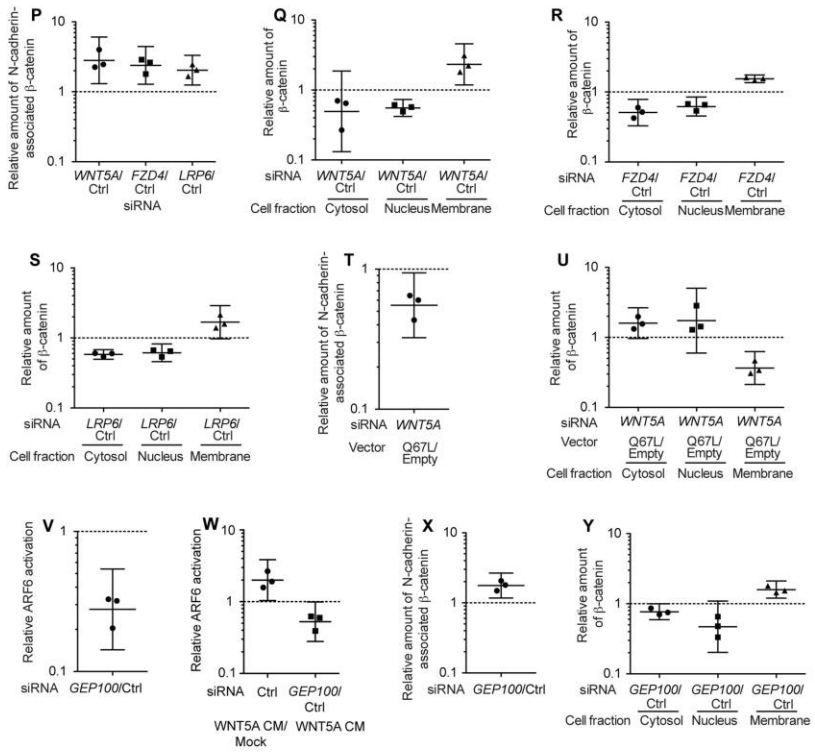

Figure S2: Quantification of immunoblots from main figures. Graphs relate to (A) Fig. 1A, (B) Fig. 1B, (C) Fig. 1C, (D) Fig. 1D, (E) Fig. 1E, (F) Fig. 1F, (G) Fig. 1G, (H) Fig. 1H, (I) Fig. 2A, (J) Fig. 2B, (K) Fig. 2C, (L) Fig. 2D and S9A, (M) Fig. 2E, (N) Fig. 2F, (O) Fig. 2G, (P) Figs. 3A and 3B, (Q) Fig. 3C, (R) Fig. 3D, (S) Fig. 3E, (T) Fig. 4A, (U) Fig. 4B, (V) Fig. 6A, (W) Fig. 6B, (X) Fig. 6C, (Y) Fig. 6D. (A) to (Y) Data points = individual experiments ($n=3$). Solid line within data points = geometric mean. Error bars = 95% CI.

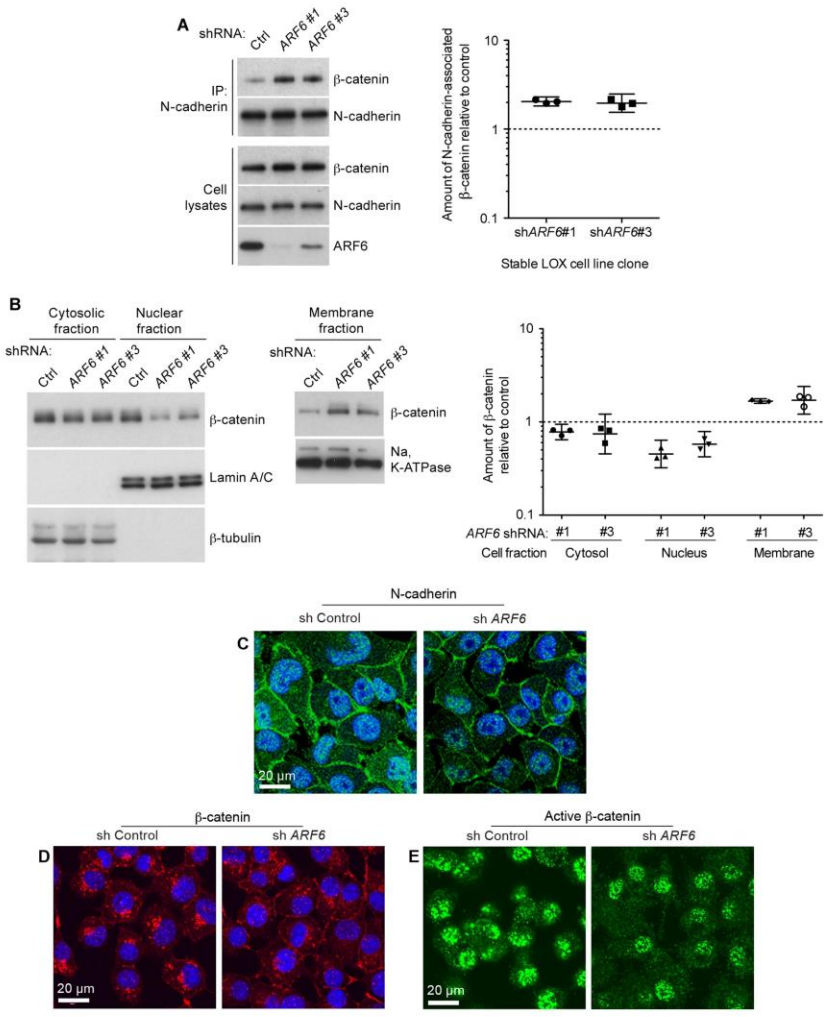
A
shRNA:
Ctrl
ARF6 #1
ARF6 #3
IP:
N-cadherin
β-catenin
N-cadherin
Cell lysates
β-catenin
N-cadherin
ARF6
Amount of N-cadherin-associated β-catenin relative to control
10
1
0.1
shARF6#1
shARF6#3
Stable LOX cell line clone
B
Cytosolic fraction
Nuclear fraction
Membrane fraction
shRNA:
Ctrl
ARF6 #1
ARF6 #3
β-catenin
Lamin A/C
β-tubulin
Na, K-ATPase
Amount of β-catenin relative to control
ARF6 shRNA:
#1
#3
Cell fraction
Cytosol
Nucleus
Membrane
C
N-cadherin
sh Control
sh ARF6
20 μm
D
β-catenin
sh Control
sh ARF6
20 μm
E
Active β-catenin
sh Control
sh ARF6
20 μm

Figure S3

Figure S3: ARF6 knockdown drives β-catenin from the nucleus to N-cadherin.(A) Coimmunoprecipitation of N-cadherin and β-catenin and (B) subcellular fractionation of β-catenin in LOX cells stably expressing Control (Ctrl) or *ARF6* (sh*ARF6* #1 and #3) shRNAs. Scatter plots show quantification of immunoblots. Data points = individual experiments (*n=3*). Solid line within data points = geometric mean. Error bars = 95% CI. (C) to (E) Immunofluorescent staining of (C) N-cadherin, (D) total β-catenin, and (E) active β-catenin in LOX cells stably expressing Ctrl or *ARF6* (sh*ARF6*) shRNAs. ARF6 silencing does not alter N-cadherin localization at the membrane (C) but results in more β-catenin at the cell surface (D) and less in the nucleus (E). (C) to (E) 600X magnification + 2X zoom. For all, *n=3* experiments.

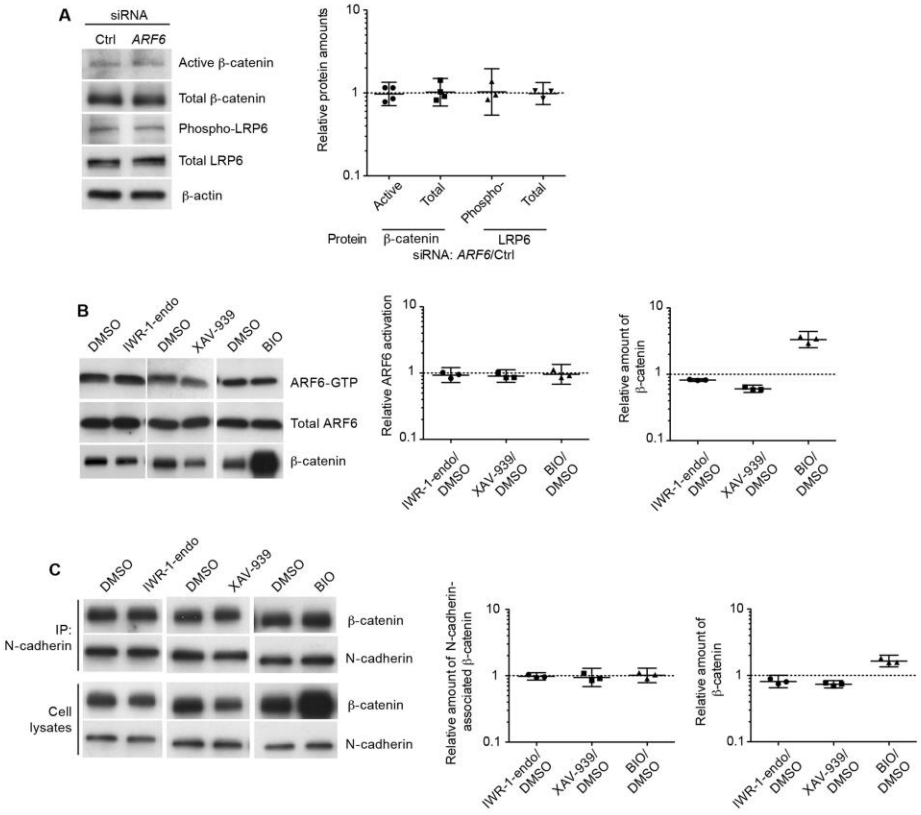

Figure S4: ARF6, junctional β-catenin, and the canonical destruction complex. (A) Immunoblots of active β-catenin, total β-catenin, phosphorylated LRP6, and total LRP6 from LOX cells treated with Control (Ctrl) or *ARF6* siRNAs. (B) GGA3-pulldown of ARF6-GTP in LOX cells treated with IWR-1-*endo*, XAV-939, or BIO. (C) Coimmunoprecipitation of N-cadherin and β-catenin in LOX cells treated with IWR-1-*endo* or XAV-939, or BIO. Scatter plot

shows quantification of immunoblots. Data points = individual experiments (*n=3*). Solid line within data points = geometric mean. Error bars = 95% CI.

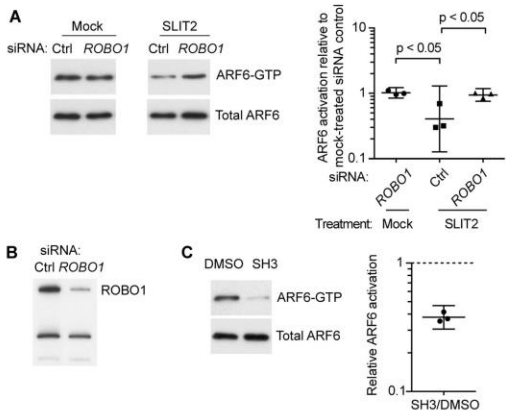

Figure S5: SLIT2-ROBO1 and SecinH3 inhibit ARF6 activation. (A) GGA3-pull down of ARF6-GTP in LOX cells transfected with Control (Ctrl) or *ROBO1* siRNAs and treated with Mock or SLIT2. For plotting purposes, geometric mean and 95% CI were estimated separately for each treatment (two-way ANOVA, Tukey's post hoc test with experiment factor treated as a blocking factor in the statistical analysis). (B) Immunoblot of ROBO1 in LOX cells transfected with Ctrl or *ROBO1* siRNAs. (C) GGA3-pull down of ARF6-GTP in LOX cells treated with DMSO or SecinH3 (SH3). (C) Scatter plot shows quantification of immunoblots. Data points = individual experiments ($n=3$). Solid line within data points = geometric mean. Error bars = 95% CI.

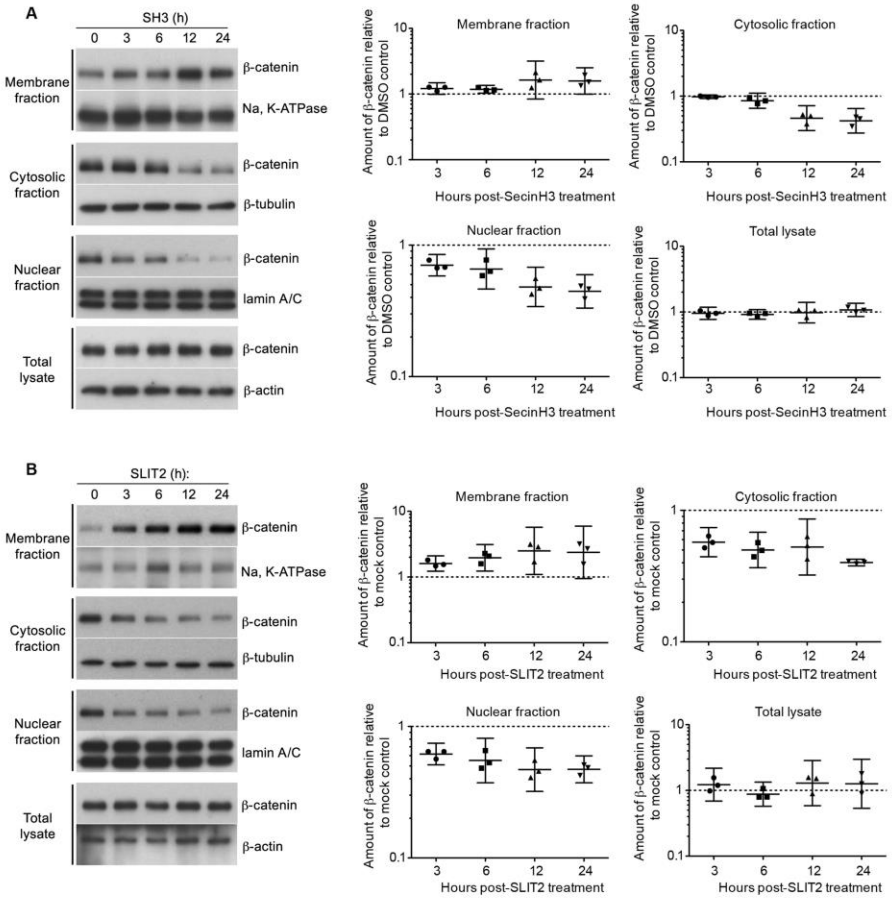

Figure S6: Time course of β-catenin relocalization after ARF6 inhibition. Subcellular fractionation of LOX cells after treatment with (A) SecinH3 (SH3) or (B) SLIT2 at 0, 3, 6, 12, or 24 hours (h). (A) and (B) A shift in β-catenin from the cytosol and nucleus to the membrane fraction was apparent after 3 hours and persisted at each subsequent interval. Scatter plots show

quantification of immunoblots. Data points = individual experiments (*n=3*). Solid line within data points = geometric mean. Error bars = 95% CI.

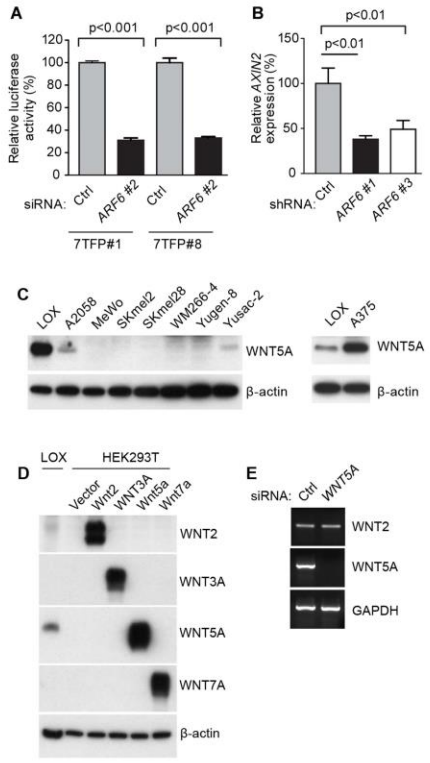

Figure S7: ARF6-dependent β-catenin transactivation and relative WNT production in melanoma cell lines. (A) 7TFP luciferase assay and (B) *Axin2* qRT-PCR in LOX cells stably expressing Control (Ctrl) or *ARF6* (shARF6 #1 and #3) shRNAs (related to Fig. 1I). (C) WNT5A is abundant in LOX and A375 cells and present in A2058 and Yusac2 cells. (D) LOX cells produce low amounts of WNT2, but WNT3A and WNT7A were not detected. (D) HEK293T cells with ectopic overexpression of WNT2, WNT3A, WNT5A, or WNT7A act as immunoblot positive controls. (E) *WNT2* expression is not altered following WNT5A knockdown (see also

Fig. S6A-B). (A) Two-tailed t test. (B) One-way ANOVA with Dunnett's post hoc test test.

For all, error bars = SD, *n=3* experiments.

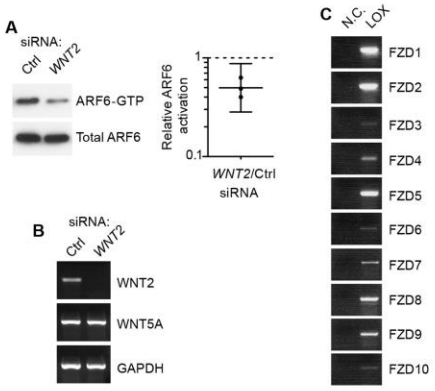

Figure S8: WNT2 knockdown reduces ARF6 activation. (A) GGA3 pulldown of ARF6-GTP and (B) confirmation of *WNT2* knockdown with RT-PCR in LOX cells transiently transfected with Control (Ctrl) or *WNT2* siRNAs. (A) Scatter plot shows quantification of immunoblots. Data points = individual experiments (*n=3*). Solid line within data points = geometric mean. Error bars = 95% CI. (B) *WNT5A* mRNA expression, as detected by RT-PCR, is not reduced by siRNA to *WNT2* (related to Fig. S5D). (**C**) Expression of Frizzled (*FZD*) family members in LOX cells, evaluated by RT-PCR. N.C. = no template control. *n=3* experiments.

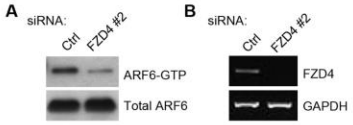

Figure S9: FZD4 knockdown reduces ARF6 activation. (A) GGA3 pulldown of ARF6-GTP and (B) confirmation of knockdown by RT-PCR in LOX cells transiently transfected with Control (Ctrl) or *Frizzled 4* sequence #2 (*FZD4 #2*) siRNAs. See also Fig. 2D and S2L.

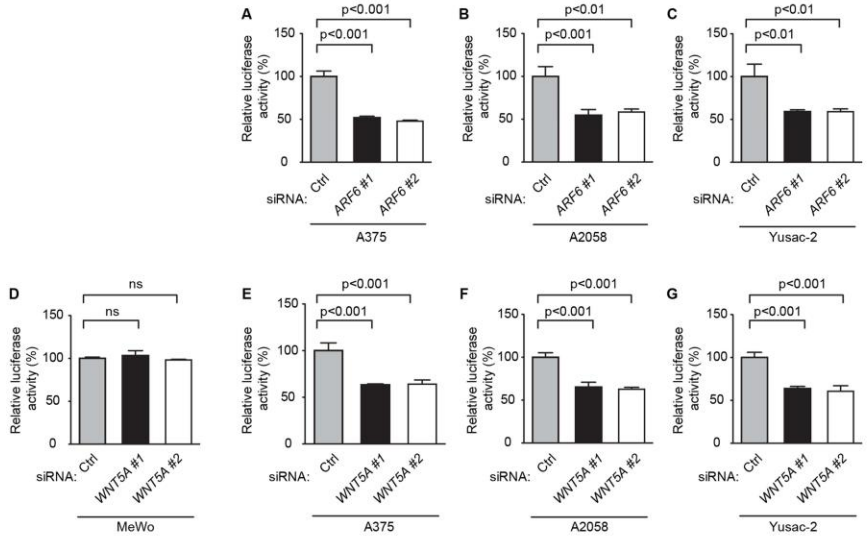

Figure S10: WNT5A, ARF6, and β-catenin signaling in multiple human melanoma cell lines. (A) to (G) 7TFP luciferase assay for β-catenin-mediated transcription in A375, A2058,Yusac-2, and MeWo melanoma cells. (A) to (C) Cells treated with Control (Ctrl) or *ARF6* (ARF6 #1 and #2) siRNAs. (D) to (G) Cells treated with Ctrl or *WNT5A* (WNT5A #1 and #2) siRNAs. (D) MeWo cells, which do not produce WNT5A (see Fig. S7C), were used as a negative control to show the specificity of the *WNT5A* siRNAs. For all, one-way ANOVA followed by Dunnett's post hoc test, error bars = SD, *n=3* experiments.

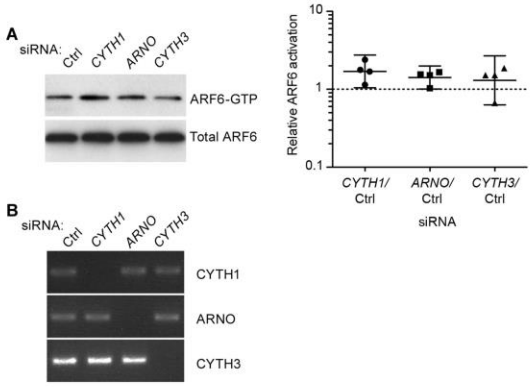

Figure S11: Cytohesin knockdown does not reduce ARF6 activation. (A) GGA3 pulldown of ARF6-GTP and (B) confirmation of knockdown by RT-PCR in LOX cells transiently transfected with Control (Ctrl) or *cytohesion 1* (*CYTH1*), *cytohesin-2* (also called *ARNO*), or *cytohesion 3* (*CYTH3*) siRNAs. (A) Scatter plot shows quantification of immunoblots. Data points = individual experiments (*n=4*). Solid line within data points = geometric mean. Error bars = 95% CI.

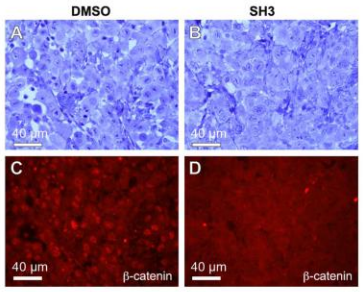

Figure S12: β-Catenin immunostaining of LOX melanoma xenograft tumors. (A) to (B) Representative bright field images of hematoxylin-counterstain and (C) to (D) fluorescent images of β-catenin staining (Alk Phos Red) of LOX melanoma xenograft tumors from mice treated with (A) and (C) DMSO vehicle or (B) and (D) SecinH3 (SH3). 400X magnification. *n=7* primary tumors from each treatment group.

Supplementary Table 1. siRNA and shRNA sequences.

Target Gene Symbol	siRNA ID	Sense Sequence 5'to 3'	Vendor
Control	AllStars Neg. Control siRNA		Qiagen
ARF6 #1	SI02757286	CAACGTGGAGACGGTGACTTA	Qiagen
ARF6 #2	S1565	GUCUCAUCUUCGUAGUGGATT	Ambion
WNT5a #1 (pooled)	J-003939-09	GCCAAGGGCUCCUACGAGA	Thermo
	J-003939-10	GUUCAGAUGUCAGAAGUAU	Thermo
	J-003939-11	CAUCAAAGAAUGCCAGUAU	Thermo
	J-003939-12	GAAACUGUGCCACUUGUAU	Thermo
WNT5a #2	S100051779	CCGGATAACCTTGTAACATAT	Qiagen
FZD4 #1	S15840	CAGUAUGUGCUAUAAUAUUTT	Ambion
FZD4 #2	S100097965	TAGGTGATCGATACTTGTCAA	Qiagen
FZD2	S10275743	CACGGTCTACATGATCAAATA	Qiagen
FZD5	S102757650	TAAGGTTGGCGTTGTAATGAA	Qiagen
FZD7	SI02631237	TCACCTACCTGGTGGACATGC	Qiagen
LRP6 (pooled)	J-003845-12	GCUCAACCGUGAAGUUAUA	Thermo
	J-003845-11	CCACAGAGCGAUCACAUUA	Thermo
	J-003845-10	CAGAUGAACUGGAUUGUUA	Thermo
	J-003845-09	GCAGAUAUCAGACGAAUUU	Thermo
ROBO1	S103055472	CACAAGGGCTCTCAAAGTATA	Qiagen
WNT2	S104271694	CAGGAAGGCTGTAAAGCGGTT	Qiagen
CYTH1	S104217185	CGGGACAGAGGTTCCGGATAA	Qiagen
ARNO	S100061299	CACGCTGTTGGTAATCTTATT	Qiagen
CYTH3	S100061257	CAGCATGTTGTGCTCGGACAA	Qiagen
GEP100	S103019408	CTGAAGGGTAGCAGTAATGAA	Qiagen
Target Gene Symbol	**shRNA**	**Sense Sequence 5'to 3'**	**Vendor**
ARF6_#1	TRCN0000048003	GTCAAGTTCAACGTATGGGAT	SIGMA
ARF6_#3	TRCN0000048005	CTCACATGGTTAACCTCTAACT	SIGMA

Supplementary Table 2. Primer sequences for RT-PCR.

Gene		Sequences (5' to 3')
hFZD1	(F)	gtgagccgaccaaggtgtat
	(R)	cagccggacaagaagatgat
hFZD2	(F)	gcgtcttctccgtgctctac
	(R)	ctgttggtgaggcgagtgta
hFZD3	(F)	tgagtgttcgaagctctatgg
	(R)	atcacgcacatgcagaaaag
hFZD4	(F)	ccaacatggctgttgaaatg
	(R)	tcacccaaccatttcctctc
hFZD5	(F)	tgctaccagccgtccttcagt
	(R)	ccatgccgaagaagtagaccag
hFZD6	(F)	attttggtgtccaaggcatc
	(R)	tattgcaggctgtgctatcg
hFZD7	(F)	gtgcagtgttctcccgaact
	(R)	gaacggtaaagagcgtcgag
hFZD8	(F)	tcttgtcgctcacatggttc
	(R)	tgtagagcacggtgaacagg
hFZD9	(F)	cgctggtcttcctactgctc
	(R)	agaagaccccgatcttgacc
hFZD10	(F)	gcggtgaagaccatcctg
	(R)	gcacggtgtacagcacagag
hGAPDH	(F)	accacagtccatgcatcac
	(R)	tccaccaccctgttgctgt
hAxin2	(F)	ctggctttggtgaactgttg
	(R)	agttgctcacagccaagaca
hWNT2	(F)	actctcaggacatgctggct
	(R)	acgaggtcatttttcgttgg
hWNT5a	(F)	ccacatgcagtacatcggag
	(R)	cactctcgtaggagcccttg
hGEP100	(F)	gcctttagcaacgatgtcatc
	(R)	cacatggtcctcattggtctt
CYTH1	(F)	ctgtgaggaaggttatcgg
	(R)	tccagagtagtccagttagg
ARNO	(F)	tgtggtcttggaggtggagtc
	(R)	ggctgctgctgcttctgg
CYTH3	(F)	ggagaagcagcaggaagg
	(R)	tctaactcagcaccacagc

CHAPTER 3

ARF6 IS AN ACTIONABLE NODE THAT ORCHESTRATES ONCOGENIC GNAQ SIGNALING IN UVEAL MELANOMA

Summary

Activating mutations in Gαq proteins, which form the α subunit of certain heterotrimeric G proteins, drive uveal melanoma oncogenesis by triggering multiple downstream signaling pathways, including PLC/PKC, Rho/Rac, and YAP. Here we show that the small GTPase ARF6 acts as a proximal node of oncogenic Gαq signaling to induce all of these downstream pathways as well as β-catenin signaling. ARF6 activates these diverse pathways through a common mechanism - the trafficking of GNAQ and β-catenin from the plasma membrane to cytoplasmic vesicles and the nucleus, respectively. Blocking ARF6 with a novel small molecule reduces uveal melanoma cell proliferation and tumorigenesis in a mouse model, confirming the functional relevance of this pathway and suggesting a new therapeutic strategy for Gα-mediated diseases.

Introduction

Mutations that confer constitutive activity to G protein-coupled receptors (GPCRs) or Gα proteins have been identified in numerous diseases, including human

cancers[1-4], McCune-Albright syndrome[5], and Sturge-Weber syndrome[6,7]. One such disease is uveal melanoma in which over 80% of tumors harbor an oncogenic activating mutation in either of two Gα q class (Gαq) proteins: GNAQ and GNA11[8,9].

Uveal melanoma is the most common primary ocular malignancy and there are no effective treatments for metastatic forms of this disease. The discovery of oncogenic *GNAQ* and *GNA11* mutations in uveal melanoma has led to the identification of multiple downstream signaling pathways that could be targeted for therapeutic purposes[10]. These signaling pathways include phospholipase C-β (PLC-β)/protein kinase C (PKC) and Rac1/RhoA, which lead to the activation of ERK, p38, JNK, and YAP and subsequent AP-1- and YAP/TEAD-mediated transcription[11-15]. However, it has been unclear how activating mutations in Gαq proteins exert their control over these divergent downstream pathways and whether activated Gαq proteins govern additional oncogenic pathways.

The small GTPase ADP-ribosylation factor 6 (ARF6)[16] is an attractive candidate for being an effector of Gαq signaling. ARF6 is activated by a variety of different ARF-guanine nucleotide exchange factors (ARF-GEFs), depending on the stimulating factor or cell type. Heterologous expression studies in HEK293T cells have suggested that activated Gαq proteins associate with various ARF-GEFs and ARF6, which leads to the activation of ARF6[17,18]. Other studies have shown the crucial role ARF6 plays in invasion, metastasis, and proliferation of several different types of cancers[19-24]. ARF6 is a critical mediator of endocytosis and the recycling of multiple membrane receptors, including GPCRs and cadherin-catenin complexes[25-28]. We recently demonstrated that in human cutaneous melanoma cells, WNT5A-stimulation of the GPCR FZD4 activates

ARF6, which promotes the trafficking of β-catenin from its N-cadherin-bound membrane form to the nucleus where it stimulates TCF-mediated transcription[19].

Here, we show that oncogenic GNAQ interacts with the ARF-GEF GEP100 to activate ARF6, which then functions as an immediate downstream effector to increase PLC/PKC, Rac1/RhoA, ERK/p38/JNK, YAP, and β-catenin signaling. Importantly, the ARF6-mediated increase in Gαq signaling is correlated with the trafficking of GNAQ from the plasma membrane to cytoplasmic vesicles, suggesting that the intracellular location of mutant Gαq proteins may play an important role in oncogenic signaling. Consistent with a nodal signaling role for ARF6, blocking ARF6 activation reduces tumor establishment and growth in a xenograft model of uveal melanoma. These results provide a mechanistic framework for studying other cancers harboring activating Gα protein mutations and suggest that targeting a single immediate effector of Gαq offers a new therapeutic approach for inhibiting multiple oncogenic pathways.

Results

We investigated whether ARF6 might also be important in cancers harboring somatic activating mutations of Gαq subunits based on the reported role of ARF6 in several cancers[19-24] and studies showing that Gαq proteins can activate or signal through ARF6[17,18,29]. We first examined ARF6 protein levels in human uveal melanomas, known to often carry activating mutations of *GNAQ* or *GNA11*. ARF6 protein levels were approximately 3-fold higher in uveal melanomas than in non-tumor ocular tissues (Figure 3.1a). We next tested whether GNAQ in Mel92.1 and Mel202 uveal melanoma cells was required for ARF6 activation. Mel202 and Mel92.1 cells carry $GNAQ^{Q209L}$, the most

common activating mutation in GNAQ[8]. The levels of ARF6-GTP were measured following *GNAQ* knockdown using two different siRNAs. Each knockdown reduced ARF-GTP levels by greater than 50% compared to a negative control siRNA that lacks homology to any known mammalian gene (Figure 3.1b). Consistent with these results, HEK293T cells transfected with vectors expressing $GNAQ^{Q209L}$ exhibited elevated levels of ARF6-GTP whereas those cells expressing wild type GNAQ did not (Supplementary Figure 3.1). Interestingly, uveal melanoma cells that carry GNAQ mutations do not express WNT5A, while tumor cells that possess wild type GNAQ and GNA11 express high levels of WNT5A, which is necessary for ARF6 activation in those cells (Supplementary Figure 3.2). Knockdown of *GNAQ* in cultured uveal melanoma cells has been shown to inhibit cell growth[8]. To determine if this inhibition is ARF6 dependent, we compared growth parameters between uveal melanoma cells transfected with siRNAs directed against *ARF6* or *GNAQ*. Knockdown of *ARF6* or *GNAQ* in both Mel92.1 and Mel202 cells caused similar reductions in cell proliferation and anchorage-independent colony growth (Figure 3.1c and 3.1d). These results demonstrate a central role for ARF6 in oncogenic GNAQ-mediated cell proliferation.

Signaling pathways stimulated by oncogenic GNAQ include those mediated by PLC-PKC and Rac/Rho[11,13,14,30]. Knockdown of either *ARF6* or *GNAQ* in uveal melanoma cells resulted in a significant reduction in PLC activity ranging from 24% to 80% inhibition when using a phosphoinositide turnover assay (Figure 3.2a). Consistent with this reduction in PLC activity, the level of phosphorylated myristoylated alanine-rich C kinase substrate (p-MARCKS), a substrate of PKC, was decreased by *ARF6* knockdown (Figure 3.2b and Supplementary Figure 3.3a). Knockdown of *ARF6* or

GNAQ also significantly reduced the levels of Rac1-GTP/RhoA-GTP and their downstream readouts, phosphorylated ERK, p38, JNK, and c-jun (Figures 3.2c-3.2e and Supplementary Figures 3.3b-3.3g). The reduction of c-jun phosphorylation resulted in decreased AP-1 transcriptional activity (Figure 3.2f).

Oncogenic GNAQ enhances nuclear YAP activation through Rac1/RhoA, implicating YAP as a potential therapeutic target for uveal melanoma[13,14]. Blocking *ARF6* or *GNAQ* inhibited by 60% the nuclear localization of YAP in uveal melanoma cells, as detected by immunocytofluorescence and subcellular fractionation/immunoblotting (Figures 3.2g, 3.2h, and Supplementary Figure 3.3h). mRNA levels of the YAP target genes *CYR61* and *CTGF* were also reduced in Mel92.1 and Mel202 cells in which ARF6 was knocked down (Figure 3.2i).

The finding that ARF6 is an effector of oncogenic GNAQ that activates multiple signaling pathways suggested that constitutively active ARF6 ($ARF6^{Q67L}$) would also activate these same pathways. Overexpression of $ARF6^{Q67L}$ or $GNAQ^{Q209L}$ in HEK293T cells induced the PLC-PKC and Rac1/RhoA-MAPK pathways, including the activation of ERK, p38, JNK, and c-jun and the increase in AP-1 transcriptional activity, YAP nuclear accumulation, and YAP-mediated transcription (Supplementary Figures 3.4b-3.4f). These results show that ARF6 is both necessary and sufficient to mediate oncogenic GNAQ activity and thus serves as a critical signaling node.

Activating mutations in β-catenin are found in many human cancers[31]. Our previous work showed that in a model of cutaneous melanoma, WNT5A-activated ARF6 promotes the relocalization of β-catenin from the membrane to the nucleus to induce β-catenin-mediated transcription and cancer cell invasion and metastasis[19]. We therefore

examined whether the oncogenic GNAQ-activated ARF6 also increased the translocation of β-catenin from the membrane to the nucleus in uveal melanoma cells. Knocking down *GNAQ* or *ARF6* in uveal melanoma cells resulted in an increase in the membrane pool of β-catenin and a corresponding decrease in the cytosolic and nuclear pools, as shown by both immunocytofluorescence and subcellular fractionation analyses (Figures 3.3a and 3.3b). These treatments also significantly reduced luciferase activity in a 7TFP-mediated luciferase reporter assay (a measure of β-catenin-mediated transcription) (Figure 3.3c). Knockdown of *GNAQ* and *ARF6* did not alter total β-catenin protein levels (Supplementary Figure 3.5a), suggesting that the mechanism that controls β-catenin intracellular localization by $GNAQ^{Q209L}$-activated ARF6 is independent of the mechanism of β-catenin stabilization by WNTs. In HEK293T cells, ectopic expression of $ARF6^{Q67L}$ or $GNAQ^{Q209L}$ decreased the membrane pool of β-catenin and concomitantly increased the cytosolic and nuclear pools of β-catenin (Supplementary Figure 3.5b). These same active forms of ARF6 or GNAQ also increased the activity of a β-catenin responsive luciferase reporter (Supplementary Figure 3.5c). Together, these results provide the first demonstration that an oncogenic Gαq protein induces β-catenin signaling and that it does so through the activation of its effector ARF6, which promotes the relocalization of β-catenin from the plasma membrane to the nucleus.

β-catenin signaling can increase cell proliferation in some cancer cells[31,32]. To determine whether β-catenin signaling in uveal melanoma cells influences cell proliferation, we exposed Mel92.1 and Mel202 cells to two different inhibitors of β-catenin signaling XAV-939 and IWR-1-endo[33,34]. After 72 hours of treatment, both XAV939 and IWR-1-endo inhibited cell proliferation in a concentration-dependent

manner with a GI_{50} (50% growth inhibition) of around 3 μM and 10 μM, respectively, in both cell lines (Supplementary Figure 3.5d). These results suggest that $GNAQ^{Q209L}$-ARF6-mediated β-catenin signaling plays a role in uveal melanoma cell proliferation.

We next sought to identify the ARF-GEF responsible for oncogenic GNAQ-mediated ARF6 activation. Both ARNO and GEP100 are known ARF6-GEFs in endothelial cells and in multiple cancer cells[19,21,23,35], and both ARF-GEFs are expressed in human uveal melanoma tissues (Supplementary Figure 3.6a). Knockdown of *GEP100* (Supplementary Figure 3.6c), but not *ARNO* (Supplementary Figure 3.6b), reduced ARF6-GTP levels by 60% in uveal melanoma cells. Knockdown of *GEP100* resulted in 50% inhibition of cell proliferation and 80% inhibition in anchorage-independent colony growth (Supplementary Figures 3.6d and 3.6e), mimicking the cellular phenotypes of ARF6 knockdown. Similar to the silencing of ARF6 and GNAQ, knockdown of *GEP100* also inhibited PLC-PKC, Rac1/RhoA, MAPK, YAP, and β-catenin signaling, as evidenced by decreased activation of the downstream effectors and reduced nuclear localization and transcriptional activity of YAP and β-catenin (Supplementary Figures 3.7 and 3.8). We hypothesized that oncogenic GNAQ and GEP100 might form a complex that activates ARF6 in uveal melanoma cells, because such complexes have been shown to occur following ectopic expression of Gαq and GEP100 in HEK293T cells[17,18]. Immunoprecipitation of oncogenic $GNAQ^{Q209L}$ from uveal melanoma cells co-precipitated GEP100 (Supplementary Figure 3.6f), suggesting the existence of a $GNAQ^{Q209L}$-GEP100 complex.

ARF6 has a known role in endocytosis of GPCRs[25,27], and GPCRs and Gα proteins are known to traffic between the plasma membrane and early endosomes[36-42]. To

examine whether ARF6 might control activated GNAQ signaling through a similar protein trafficking mechanism, we knocked down *ARF6* in Mel92.1 and Mel202 cells and assessed intracellular localization of $GNAQ^{Q209L}$ using both immunocytofluorescence and cell fractionation analysis. Upon ARF6 silencing, there was an increase in $GNAQ^{Q209L}$ localized to the plasma membrane with a concomitant reduction of $GNAQ^{Q209L}$ in the cytosol and cytoplasmic vesicles (Figure 3.4). *GEP100* knockdown likewise exhibited a shift of $GNAQ^{Q209L}$ localization from the cytosol and cytoplasmic vesicles to the plasma membrane (Supplementary Figure 3.9). These results suggest that activated ARF6 directs $GNAQ^{Q209L}$ to the cytoplasmic vesicles leading to an increase in signaling of downstream oncogenic pathways.

Our finding that ARF6 acts as an immediate downstream effector of $GNAQ^{Q209L}$ that controls all of the currently recognized signaling pathways governed by oncogenic Gαq compelled us to investigate whether chemical inhibitors of ARF6 activation might provide an effective pharmacologic treatment of uveal melanoma. To our knowledge, no direct inhibitors of ARF6 have been published or are commercially available. Therefore, ARF-GEF inhibitors, such as SecinH3, have been used as surrogates for ARF6 inhibition in past studies[19,43]. However, ARNO, a target for SecinH3 inhibition, promotes epidermal growth factor receptor activation independent of its ARF-GEF activity[44], so inhibiting ARF-GEFs rather than ARF6 directly could lead to off-target effects. Therefore, it is imperative to find direct ARF6 inhibitors that can reduce these unintended consequences. To identify such inhibitors, a high throughput screen (HTS) based on a fluorometric biochemical assay was devised to identify chemically tractable, reversible, allosteric inhibitors that target ARF6 directly (Figure 3.5a and Supplementary Figures 3.10a-

3.10c). The requirement for an allosteric, non-nucleotide-competitive mode of action was dictated by intracellular concentrations of GTP, which are approximately 100 µM. A comparative evaluation of more than 20 chemical series and singleton HTS hits from the DiverSet collection[45] of approximately 50,000 compounds (ChemBridge) identified the pyrazolopyrimidinone compound NAV-2729 (Figure 3.5b and Supplementary Figures 3.11) as the most promising ARF6 chemical probe candidate. This compound was selected for further evaluation based on the following properties: i) low micromolar potency with IC_{50} values of 1.0 µM and 3.4 µM determined using fluorometric and orthogonal radiometric ARF6 nucleotide exchange assays, respectively (Figure 3.5c); ii) direct inhibition of ARF6 as evidenced by nearly equipotent inhibitory effects towards spontaneous and ARF-GEF-catalyzed ARF6 nucleotide exchange (Figure 3.5d); iii) a non-nucleotide competitive mechanism supported by the observation that GTP does not affect the ability of the inhibitor to stimulate release of a fluorogenic nucleotide from its complex with ARF6 (Figure 3.5e and Supplementary Figure 3.10d); iv) high selectivity as evidenced by the lack of inhibitory effects for other small GTPases such as RhoA, Rac1, H-Ras, and Cdc42 at concentrations up to 50 µM (Supplementary Figures 3.10e-3.10h); v) reversible inhibition (Figure 3.5f); and vi) overall chemical tractability including apparent lack of commonly recognized reactive and "frequent hitter" functionalities[46].

The proposed direct inhibitory mechanism of NAV-2729 agrees well with the results of molecular docking studies using a structural homology model of the ARF6/ARF-GEF complex (Figure 3.5g). The model predicts association of NAV-2729 with ARF6 in its GEF-binding area, which does not overlap with the nucleotide-binding

pocket. A hydrogen bond between the inhibitor carbonyl group and ε-amino group of ARF6 Lys58 residue, as well as the interaction of its nitrophenyl moiety with a hydrophobic pocket formed by aromatic side chains of ARF6 residues Phe47, Trp62, Trp74, and Tyr77 make major contributions to the inhibitor binding energy (Supplementary Figure 3.10i). Most importantly, NAV-2729 exhibited a spectrum of biological activities in uveal melanoma cells that are predicted for an ARF6 inhibitor. Treatment of Mel92.1 and Mel202 cells with NAV-2729 inhibited ARF6 activation (Figure 3.5h) and mimicked ARF6 and GEP100 knockdown by driving GNAQ from the cytoplasmic vesicles to the plasma membrane (Figures 3.5i and 3.5j) and reducing anchorage-independent colony growth (Figure 3.5k).

The finding that the activation state of ARF6 regulates multiple oncogenic GNAQ signaling pathways by controlling the intracellular localization of $GNAQ^{Q209L}$ suggested that ARF6 may be a viable therapeutic target for GNAQ-mediated tumorigenesis. We tested this hypothesis in an orthotopic xenograft mouse model of uveal melanoma. Stable uveal melanoma cells expressing either short hairpin RNAs (shRNA) directed against ARF6 or a nonspecific control sequence were generated by lentiviral infection of Mel202 cells. These cells were injected into the posterior vitreous chamber of the eyes of immunocompromised nude mice. Tumor incidence and size were markedly decreased in mice injected with Mel202 cells expressing ARF6 shRNA compared to mice injected with cell expressing control shRNA (Figures 3.6a and 3.6b). Systemic treatment by intraperitoneal injection of the direct ARF6 inhibitor NAV-2729 also significantly reduced uveal melanoma tumor establishment and growth in an orthotopic xenograft mouse model (Figures 3.6c and 3.6d). No gross signs of toxicity were seen in these

studies or in other studies in which the drug was used at these same concentrations. Collectively, these results suggest that the pharmacological inhibition of ARF6 may represent an effective therapeutic approach to the treatment of uveal melanoma and possibly other cancers driven by activating Gα mutations.

Discussion

Activated oncogenes such as Gα proteins or members of the RAS superfamily of GTPases act through central signaling nodes that subsequently trigger multiple molecular events that together induce cancer initiation and invasion[4,47]. Previous studies have shown that activating mutations in the Gαq proteins GNAQ or GNA11 promote PLC/PCK and Rac/Rho signaling, leading to both the activation of ERK, p38, JNK, and YAP and subsequent AP-1- and YAP/TEAD-mediated transcription[11-14]. In the present study, we have expanded the number of signaling pathways that are known to be regulated by an activated Gαq protein to include an ARF6-β-catenin pathway in which activated ARF6 promotes the release and subsequent translocation of membrane-bound β-catenin to the nucleus where it induces transcription. To our knowledge, this is the first report that β-catenin trafficking can be controlled by an activated Gαq protein. By employing biochemical and cellular assays and a newly identified small molecule inhibitor, we also show that a $GNAQ^{Q209L}$-GEP100 complex activates ARF6, which functions as an immediate downstream effector to induce the PLC/PKC and Rho/Rac signaling pathways that lead to AP-1 and YAP/TEAD-mediated transcription (Figure 3.6e). Thus, the activation of ARF6 controls all of the currently known oncogenic pathways mediated by Gαq activating mutations.

Our data suggest that activated ARF6 controls GNAQ and β-catenin signaling by regulating protein trafficking between intracellular compartments. Oncogenic GNAQ forms a protein complex with GEP100, which activates ARF6 to promote the redistribution of cell surface GNAQ to cytoplasmic vesicles. GNAQ signaling appears to primarily occur in these vesicles, because knockdown of ARF6 or GEP100 or chemical inhibition of ARF6 induces the relocalization of GNAQ from the cytoplasm to the plasma membrane with a concomitant decrease in signaling of all GNAQ-mediated pathways. Although signaling from G proteins such as Gα and RAS proteins have traditionally been thought to occur only at the plasma membrane, more recent studies have challenged this view, suggesting that signaling can also derive from cytoplasmic vesicles[36-42,48-51]. Our data agree with these recent studies but unexpectedly suggest that most of the signaling from active GNAQ in uveal melanoma emanates from cytoplasmic vesicles rather than the plasma membrane. These results, coupled with previous work suggesting that maximal oncogenic H-RAS signaling requires endocytosis and endocytic recycling[52], suggest that the intracellular location of an oncogene may determine its level of activity and that blocking the trafficking of an oncogene to its primary signaling center may effectively diminish its activity. In the case of GNAQ and H-RAS, the primary signaling center appears to be in cytoplasmic vesicles. The activation of ARF6 by oncogenic GNAQ also leads to the release of β-catenin from the plasma membrane and its subsequent transportation to the nucleus where it induces gene transcription and helps to promote uveal melanoma cell proliferation. This result is consistent with our previous study in cutaneous melanoma, which demonstrated a similar relocalization of β-catenin

and increased β-catenin-mediated transcription following stimulation of the FZD4/LRP6 co-receptor complex with WNT5A[19].

Our discovery that ARF6 is an immediate downstream effector of the $GNAQ^{Q209L}$-GEP100 complex suggests that targeting ARF6 with a single small molecule may inhibit all of the currently known Gαq-mediated oncogenic signaling pathways. The necessity and sufficiency of ARF6 activation in orchestrating activated Gαq oncogenic signaling also reveals a strategy to blunt cancer initiation and progression, not just tumor invasion and metastasis. We provide evidence that ARF6 is an actionable node suitable for further development as a therapeutic target by identifying a novel, direct inhibitor of ARF6 that reduces tumor establishment and growth in a xenograft model of uveal melanoma.

Uveal melanoma is a devastating cancer and serves as the prototype for activated Gα protein-mediated cancers. Current treatment relies on surgery and radiation for localized disease, but there is no effective systemic therapy for advanced disease[53]. The identification of ARF6 as a signaling partner of GNAQ offers a target for new treatment regimens that has implications extending beyond Gαq proteins and uveal melanoma to other cancers harboring activated Gα oncogenes, such as pancreatic and biliary cancers[3]. Directly targeting certain oncogenes, e.g., activated RAS GTPase, has been challenging[54,55], although recent advances have been made[56,57]. Approaches that individually inhibit each arm of an activated oncogenic pathway have been adopted but are inefficient, spurring interest in combination trials as an alternate approach[58]. By illuminating how a specific activated Gα oncogene orchestrates multiple divergent downstream signaling arms through a single effector, our work suggests that targeting

such primary nodal points in the signaling pathways of other GTPases could provide an effective method for combatting oncogenesis and tumor establishment.

Materials and Methods

Cell lines, proliferation assay, and anchorage-independent colony growth

Uveal melanoma cells were maintained in RPMI 1640 supplemented with 10% fetal bovine serum (FBS). LOX and HEK293T cells were purchased from ATCC and maintained in DMEM supplemented with 10% FBS. Cell proliferation assays were performed using CyQUANT (Invitrogen) according to the manufacturer's instructions. 5×10^3 uveal melanoma cells were plated into each of three or four wells of a 96-well plate and fluorescence was measured 4 h later after cell attachment to obtain baseline measurements and at 72 h as endpoint measurements. Anchorage-independent colony growth was quantified by the CytoSelect 96-Well Cell Transformation Assay (Cell Biolabs) as per manufacturer's instructions. After 12-15 days, relative colony size/number was confirmed by microscopic examination and measured by adding CyQUANT reagent to the cultures and measuring fluorescence using a plate reader at excitation/emission wavelengths of 485/530 nm.

RNA interference, plasmids, transfections, lentiviral transduction, qRT-PCR, and chemicals

siRNA duplexes (20 nmol) were transfected into uveal melanoma cells using Lipofectamine RNAiMAX (Invitrogen). Plasmids for wild type GNAQ and GNAQ^{Q209L} were obtained from Missouri S&T cDNA Resource Center. The coding regions of both

constructs were re-cloned into pcDNA3.1 vector for MYC epitope-tagging at the N-terminal. For ectopic expression in HEK293T, cells were seeded in 10-cm plates and transfected with the respective plasmids using Lipofectamine LTX (Invitrogen). Lentiviruses containing control and *ARF6* shRNA expression constructs were purchased from Sigma and were used to infect Mel202 uveal melanoma cells. Infected cells were selected using 1 μg/ml of puromycin (Invitrogen) for 5 days. qRT-PCR was performed with the Applied Biosystems 7900HT and QuantiTect SYBR Green PCR kit (Qiagen) with the primers listed in Table S1. IWR-1-endo and XAV-939 were purchased from Calbiochem.

ARF6/RhoA/Rac1 pull-downs, immunoblots, immunoprecipitation,
cell fractionation, PLC assay, luciferase assay,
and immunocytofluorescence staining

ARF6-GTP pull-downs were performed with Arf6 Activation Assay Kit (Cell Biolabs) and RhoA/Rac1-GTP pull-downs were prepared with Rac1 Activation Assay Kit/RhoA Activation Assay Kit (Millipore) according to the manufacturer's instructions.

For immunoblotting and immunoprecipitation, cell lysates were prepared in 25 mM HEPES (pH 7.5), 150 mM NaCl, 1% NP-40, 10 mM $MgCl_2$, 1 mM EDTA, and 2% glycerol, plus phosphatase and protease inhibitors. Immunoprecipitation was performed as previously described[19]. For immunoblotting, primary antibodies were diluted in 5% NFDM or 5% BSA in PBS or TBS plus 0.1% Tween 20 and incubated overnight at 4℃. Plasma membrane or total membrane fraction was isolated with Plasma Membrane Protein Extraction Kit (Abcam) and cytosolic/nuclear fractions were prepared with NE-PER Nuclear and Cytoplasmic Extraction Reagents (Thermo Scientific) according to the

manufacturer's instructions. Antibodies against ARF6 (Millipore), GNAQ (Abcam), GEP100 (Sigma), ARNO (Abnova), β-tubulin, MYC (Santa Cruz Biotechnology), Rac1, β-catenin (BD Biosciences), β-actin, GAPDH, HA, RhoA, MARCKS, p-MARCKS, ERK, p-ERK, p38, p-p38, JNK, p-JNK, c-jun, p-c-jun, YAP, Na K-ATPase, and Lamin A/C (Cell Signaling Technology) were used for immunoblotting and/or immunoprecipitation. Quantification for all immunoblots was by scanning densitometry whereby changes were normalized to loading control, input, and/or total particular protein level, and represents an amalgamation of all independent experimental replicates. Geometric means and 95% confidence intervals were calculated to determine statistically significant changes in protein levels.

β-catenin- and AP-1-mediated transcriptional activities in uveal melanoma cells were assayed using lentivirally transduced cells that stably express the TOPflash-based 7TFP luciferase reporter (Addgene)[59] or AP-1 luciferase reporter (Qiagen). 20-40 μg of cell lysates were assayed for firefly luciferase with the Luciferase Assay System (Promega). Luciferase assays for β-catenin, AP-1, and YAP in HEK293T were performed following the transfection of TOPflash, AP-1, or TEAD4 firefly luciferase reporter plasmids (Addgene) and renilla plasmid for a normalized control. Dual luciferases were detected with Dual-Luciferase Reporter Assay System (Promega) according to the manufacturer's instructions.

PLC activity was determined using phosphoinositide turnover assay as previously described[11]. Briefly, 1×10^6 siRNA-transfected Mel92.1 and Mel202 uveal melanoma cells were seeded into each well of a 6-well plate and 2×10^5 HEK293T cells ectopically expressing specific genes following plasmid transfection were plated on each well of a

24-well plate. Cells were incubated with 3 µCi or 1 µCi/well of myo-[^{3}H]-inositol (Perkin Elmer) for 24 h. 10 mM LiCl was added for 20 min to stop the phosphoinositide turnover. 5% TCA was used for cell lysis and the supernatants were applied to an anion-exchange column (Bio-Rad, AG1-X8). Radioactivity in eluted samples was determined with a Beckman scintillation counter.

3×10^6 Mel92.1 and Mel202 uveal melanoma cells were plated on 100 mm dishes and transfected using Lipofectamine RNAiMAX (Invitrogen) with siRNAs against ARF6, GEP100, or a control sequence (Qiagen) for 48 h. Transfectants were replated and retransfected for an additional 24 h in complete medium at a density of 10^5 cells/well in 8-well chambered coverglasses coated with 2% 225-bloom Gelatin (EM sciences) in ddH2O. After 24 h, monolayers were fixed for 20 min in 10% Neutral Buffered Formalin and then washed 3 times in 1× TBS. Antibodies against YAP (1A12) (Cell Signaling), β-catenin (BD Biosciences), and GNAQ (Abcam) were diluted 1/400, 1/100, and 1/250, respectively, in 1× TBS containing 1% BSA and 0.1% Saponin and applied to cells overnight at 4˚C. Wells were rinsed 4 times in 1× TBS, and 10 µg/ml Alexafluor 488-conjugated anti-Mouse or anti-Rabbit IgG diluted in 1% BSA /0.1% Saponin was applied for 1 h at room temperature in a darkened box. Unbound secondary antibody was removed by 4 washes in 1× TBS, and DAPI anti-Fade medium was applied to the drained wells. Fields were randomly selected via the DAPI channel at 1200× with oil immersion. Z-stacked images (4 × 0.5 µm slices/field) were taken on an Olympus FV1000 confocal microscope at the University of Utah's Cell Imaging core facility. The same procedure was also performed on untransfected Mel92.1 and Mel202 that were treated either with 5

μM NAV-2729/0.1% DMSO or 0.1% DMSO alone (control) for 1 h before being fixed and imaged as described above.

Human uveal melanoma patient samples

Primary human uveal melanoma samples were collected at the time of enucleation as previously described[60]. All samples were confirmed to be uveal melanomas by pathologic evaluation. Human ocular non-tumor samples were purchased from the Lions Eye Bank at the University of Utah.

Orthotopic xenograft mouse model of uveal melanoma

All animal studies were performed in accordance with a protocol approved by the University of Utah Institutional Animal Care and Use Committee. Athymic nude mice were purchased from Jackson Laboratories for this study. Mice were anesthetized with an intraperitoneal injection of a mixture of ketamine and xylazine. The eye was viewed under a dissecting microscope, and a sterile 30-gauge needle was used to puncture the posterior chamber of eye. 10^5 cells in 5 μl were injected into the eye with a Hamilton syringe. For systemic treatment of NAV-2729, the compound was administered by intraperitoneal injection at a dosage of 30 mg/kg every day over a period of 5 weeks starting on the day of cell injection. After 5 weeks of tumor growth, mice were euthanized with CO_2, and eyes were collected, fixed, embedded, sectioned, stained with H&E, and examined histologically for primary tumors by a pathologist who was blinded to the treatment regimen.

Recombinant Protein Expression and Purification

All recombinant proteins for the ARF6 assay development were produced as N-terminally His-tagged fusions in *E. coli* cultures and purified to apparent homogeneity as described previously[61], including the truncated form of ARF6 (14-175), which does not require membranes or lipid vesicles for full activity, as well as the Sec7 domain-containing fragments of GEP100 and ARNO that encompass residues 391-602 and 50-255, respectively. The recombinant ARF6 purified in 50 mM Tris-HCl, pH 7.8, 2 mM $MgCl_2$, 10% glycerol, 2 mM β-mercaptoethanol, and approximately 150 mM imidazole was routinely converted into GDP-bound form by 2-h incubation in the presence of GDP in 10-fold molar excess relative to ARF6 and 5 mM EDTA. Upon addition of $MgCl_2$ to 20 mM to terminate nucleotide exchange, two rounds of ultrafiltration, using Amicon Ultra-15-10K centrifugal filter units, were performed to remove free nucleotide and replace buffer system with 50 mM Tris-HCl, pH 7.5, 2 mM $MgCl_2$, 10% glycerol, and 2 mM β-mercaptoethanol.

Fluorometric Nucleotide Exchange Assay

Our fluorometric nucleotide exchange assay for ARF6 and other small GTPases exploits fluorogenic nucleotide probe, GTP labeled with BODIPY FL, for monitoring GDP-to-GTP exchange at the nucleotide-binding site of ARF6. Intrinsic fluorescence of GTP-BODIPY is intramolecularly quenched in the unbound state but is significantly increased upon its binding to the target protein such as ARF6 or other small GTPases[62]. The fluorometric ARF6 nucleotide exchange assay used for high-throughput screening and routine inhibition assays was carried out in 96-well format using 100-µl aliquots of 50 mM Tris-HCl, pH 7.5, 1 mM $MgCl_2$, 0.01% Triton X-100, 2 mM β-mercaptoethanol,

1% DMSO, 50 nM GTPBODIPY FL, 25 nM ARNO or GEP100, and 200 nM ARF6•GDP (unless indicated otherwise). Replacement of ARF6-bound GDP by GTP-BODIPY FL was monitored by measuring increases in fluorescence intensity during a 30-60 min time course using a plate reader at the excitation and emission wavelengths of 490 nm and 520 nm, respectively. The high-throughput screening was performed at the University of Utah Drug Screening Resource using DiverSet library of compounds (ChemBridge) at 10 µM concentrations. The selectivity tests were conducted in the same format using small GTPases at 200 nM concentrations. All members of the selectivity panel, namely, RhoA, Rac1, Cdc24, and H-Ras that represent bacterially expressed N-terminally His-tagged full-length recombinant proteins were purchased from Cytoskeleton, Inc. GTP-BODIPY FL was provided by Life Technologies. For the determination of signal-to-background ratio (S:B) and Z'-factor, the assay was performed using a 96-well plate with half of the wells supplemented with 10 µM GDP to estimate background fluorescence (B), which is equivalent to mean negative control value (µn), and another half with DMSO control to determine signal intensity (S), which is equivalent to mean positive control value (µp). Z' factor value was calculated using the following formula: $Z'=1 - 3(\sigma p + \sigma n)/(\mu p - \mu n)$, which also includes standard deviations for the positive and negative controls (σp and σn, respectively).

Radiometric Nucleotide Exchange Assay

The confirmation of HTS hits using a radiometric assay for ARF6 nucleotide exchange was carried out using 100-µl aliquots of same assay mix specified above for the fluorometric technique with the exception that 50 nM [^{35}S]-GTPγS (2 µCi/ml) was included to replace GTPBODIPY FL. Upon incubation for 30 min in the presence of test

articles, 200 µl of ice-cold assay buffer supplemented with 10 mM $MgCl_2$ was added to stop the reaction followed by a rapid vacuum filtration of the samples using a nitrocellulose-bottomed 96-well plate, three washes of the membrane with the above stop solution, and scintillation counting to quantify GTPγS bound to ARF6.

Synthetic Methods

All solvents and reagents were purchased from commercial sources and used without further purification unless otherwise noted. Reactions were monitored by TLC (thin layer chromatography) using 0.25 mm silica gel 60 F254 plates purchased from EMD chemicals. Purification was performed with Teledyne ISCO Combi*Flash R*f. ^{1}H NMR and ^{13}C spectra were recorded on a Varian Mercury 400 MHz instrument. Proton chemical shifts are expressed in parts per million (ppm) relative to TMS and calibrated using residual undeuterated solvent as internal reference. High-resolution mass spectra (HRMS) were recorded on Finnigan LTQ-FT, Thermo Electron Corporation. Compound purity was determined by an Agilent HP1050 instrument with a 4.6 mm × 150 mm Xterra C18 3.5 µm column. The flow rate was 1.2 mL/min, and the injection volume was 10 µl. HPLC conditions were as follows: mobile phase A, HPLC grade water (0.01% TFA); mobile phase B, HPLC grade acetonitrile (0.01% TFA); UV detector, 254 nm; 95% A/5% B to 0% A/100% B in 10 min, 100% B in 10−11 min, 100% B to 95% A/5% B in 11−13 min, 95% A/5% B in 13−15 min. The final compound was ≥95% pure by HPLC. Synthesis of 2-benzyl-3-(4-chlorophenyl)-5-(4-nitrophenyl)-4H-pyrazolo[1,5-a]pyrimidin-7-one (NAV-2729) involves refluxing 3-benzyl-4-(4-chlorophenyl)-1*H*-pyrazol-5-amine and ethyl 3-(4-nitrophenyl)-3-oxo-propanoate in acetic acid for 16 h. To a suspension of 3-benzyl-4-(4-chlorophenyl)-1*H*-pyrazol-5-amine (3.0 g, 10.6 mmol) in

acetic acid (50 mL) was added ethyl 3-(4-nitrophenyl)-3-oxo-propanoate (2.5 g, 10.6 mmol) at room temperature. The reaction mixture was heated at 120 ℃, 16 h. At the end of this period, the mixture was cooled to room temperature and the precipitate was collected, filtrated, and washed with acetic acid. The filter cake was triturated with 20% ethyl acetate in hexanes to provide NAV-2729 (3.40 g, 70%). TLC (CH_2Cl_2:MeOH, 95:5 v/v): RF = 0.46;1H-NMR (400 MHz, DMSO-*d*6) (Figure S6J) δ 12.32 (s, 1H), 8.35 (d, *J*=8.5 Hz, 2H), 8.00 (d, *J*= 7.8 Hz, 2H), 7.50-7.34 (m, 4H), 7.28-7.00 (m, 5H), 6.10 (s, 1H), 4.00 (s, 2H); 13C- NMR (400 MHz, DMSO-*d6*) (Figure S6K) δ 32.5, 96.4, 123.4, 126.1, 128.2, 128.4, 129.3, 129.7, 131.7, 131.8, 138.5, 148.6, 155.6; HRMS (Figure S6L) (FT-ESI) (*m*/*z*): [M + H] + calculated for C25H18ClN4O3 457.1061, found 457.1078; HPLC (Figure S6M) purity, 96.9% (*t*R = 8.54 min).

Molecular Modeling

Molecular modeling was performed using program package ICM-Pro (MolSoft, LLS, San Diego, CA) that includes modules for homology modeling, docking, and virtual ligand screening. Homology model of N-terminally truncated ARF6 (Δ13) structure was built using ARF1 (Δ17) template extracted from a crystal structure of ternary ARF1 (Δ17)-GDP ARNO complex with inhibitor brefeldin A (Protein Data Bank ID 1S9D) [61]. Then ARF1 structure in the ternary complex was replaced with the homology model of ARF6 and brefeldin A (BFA) was removed from the complex. Inhibitor NAV-2729 was docked into a binding site at the interface between ARF6 and ARNO. The preliminary model of ARF6-ARNO complex with NAV-2729 was refined using a binding site side chain optimization procedure available with ICM-Pro program.

Statistical Analyses

Statistical analyses were performed using GraphPad Prism 6.0f. When two groups were being compared and the data appeared to be normally distributed, the Student's t test was used. When multiple groups were being compared and the data were normally distributed, one-way ANOVA with Dunnett's multiple comparisons test was performed, given that each treatment group was being compared to a single control group. When the data did not appear to be normally distributed, the Mann-Whitney U test was used. For statistical analyses of immunoblots, the density of each band was normalized to an internal control protein and then the ratio of the normalized density of the band from the experimental treatment to the normalized density of the paired control treatment band was obtained. Because these values are ratios, geometric means and 95% confidence intervals were calculated and the ratios were plotted on a logarithmic scale to determine significance.

References

1. Marinissen, M.J. & Gutkind, J.S. G-protein-coupled receptors and signaling networks: emerging paradigms. *Trends in Pharmacological Sciences* **22**, 368-376 (2001).

2. Dorsam, R.T. & Gutkind, J.S. G-protein-coupled receptors and cancer. *Nature Reviews. Cancer* **7**, 79-94 (2007).

3. O'Hayre, M., *et al.* The emerging mutational landscape of G proteins and G-protein-coupled receptors in cancer. *Nat Rev Cancer* **13**, 412-424 (2013).

4. O'Hayre, M., Degese, M.S. & Gutkind, J.S. Novel insights into G protein and G protein-coupled receptor signaling in cancer. *Current Opinion in Cell Biology* **27**, 126-135 (2014).

5. Weinstein, L.S., *et al.* Activating mutations of the stimulatory G protein in the McCune-Albright syndrome. *N Engl J Med* **325**, 1688-1695 (1991).

6. Shirley, M.D., *et al.* Sturge-Weber syndrome and port-wine stains caused by somatic mutation in GNAQ. *N Engl J Med* **368**, 1971-1979 (2013).

7. Nakashima, M., *et al.* The somatic GNAQ mutation c.548G>A (p.R183Q) is consistently found in Sturge-Weber syndrome. *Journal of Human Genetics* **59**, 691-693 (2014).

8. Van Raamsdonk, C.D., *et al.* Frequent somatic mutations of GNAQ in uveal melanoma and blue naevi. *Nature* **457**, 599-602 (2009).

9. Van Raamsdonk, C.D., *et al.* Mutations in GNA11 in uveal melanoma. *N Engl J Med* **363**, 2191-2199 (2010).

10. Shoushtari, A.N. & Carvajal, R.D. GNAQ and GNA11 mutations in uveal melanoma. *Melanoma Res* **24**, 525-534 (2014).

11. Vaque, J.P., *et al.* A genome-wide RNAi screen reveals a Trio-regulated Rho GTPase circuitry transducing mitogenic signals initiated by G protein-coupled receptors. *Mol Cell* **49**, 94-108 (2013).

12. Wu, X., Zhu, M., Fletcher, J.A., Giobbie-Hurder, A. & Hodi, F.S. The protein kinase C inhibitor enzastaurin exhibits antitumor activity against uveal melanoma. *PLoS One* **7**, e29622 (2012).

13. Feng, X., *et al.* Hippo-independent activation of YAP by the GNAQ uveal melanoma oncogene through a Trio-regulated Rho GTPase signaling circuitry. *Cancer Cell* **25**, 831-845 (2014).

14. Yu, F.X., *et al.* Mutant Gq/11 promote uveal melanoma tumorigenesis by activating YAP. *Cancer Cell* **25**, 822-830 (2014).

15. Khalili, J.S., *et al.* Combination small molecule MEK and PI3K inhibition enhances uveal melanoma cell death in a mutant GNAQ- and GNA11-dependent manner. *Clinical Cancer Research : An Official Journal of The American Association for Cancer Research* **18**, 4345-4355 (2012).

16. Kahn, R.A. & Gilman, A.G. Purification of a protein cofactor required for ADP-ribosylation of the stimulatory regulatory component of adenylate cyclase by cholera toxin. *The Journal of Biological Chemistry* **259**, 6228-6234 (1984).

17. Giguere, P., *et al.* ARF6 activation by Galpha q signaling: Galpha q forms molecular complexes with ARNO and ARF6. *Cell Signal* **18**, 1988-1994 (2006).

18. Laroche, G., Giguere, P.M., Dupre, E., Dupuis, G. & Parent, J.L. The N-terminal coiled-coil domain of the cytohesin/ARNO family of guanine nucleotide

exchange factors interacts with Galphaq. *Molecular and Cellular Biochemistry* **306**, 141-152 (2007).

19. Grossmann, A.H., *et al.* The small GTPase ARF6 stimulates beta-catenin transcriptional activity during WNT5A-mediated melanoma invasion and metastasis. *Science Signaling* **6**, ra14 (2013).

20. Hu, B., *et al.* ADP-ribosylation factor 6 regulates glioma cell invasion through the IQ-domain GTPase-activating protein 1-Rac1-mediated pathway. *Cancer Research* **69**, 794-801 (2009).

21. Hu, Z., *et al.* GEP100/Arf6 is required for epidermal growth factor-induced ERK/Rac1 signaling and cell migration in human hepatoma HepG2 cells. *PLoS One* **7**, e38777 (2012).

22. Li, M., *et al.* Adenosine diphosphate-ribosylation factor 6 is required for epidermal growth factor-induced glioblastoma cell proliferation. *Cancer* **115**, 4959-4972 (2009).

23. Morishige, M., *et al.* GEP100 links epidermal growth factor receptor signalling to Arf6 activation to induce breast cancer invasion. *Nature Cell Biology* **10**, 85-92 (2008).

24. Muralidharan-Chari, V., *et al.* ADP-ribosylation factor 6 regulates tumorigenic and invasive properties in vivo. *Cancer Research* **69**, 2201-2209 (2009).

25. Chen, W., *et al.* Dishevelled 2 recruits beta-arrestin 2 to mediate Wnt5A-stimulated endocytosis of Frizzled 4. *Science* **301**, 1391-1394 (2003).

26. D'Souza-Schorey, C., Li, G., Colombo, M.I. & Stahl, P.D. A regulatory role for ARF6 in receptor-mediated endocytosis. *Science* **267**, 1175-1178 (1995).

27. Hunzicker-Dunn, M., Gurevich, V.V., Casanova, J.E. & Mukherjee, S. ARF6: a newly appreciated player in G protein-coupled receptor desensitization. *FEBS Letters* **521**, 3-8 (2002).

28. Palacios, F., Price, L., Schweitzer, J., Collard, J.G. & D'Souza-Schorey, C. An essential role for ARF6-regulated membrane traffic in adherens junction turnover and epithelial cell migration. *The EMBO Journal* **20**, 4973-4986 (2001).

29. Bose, A., *et al.* G(alpha)11 signaling through ARF6 regulates F-actin mobilization and GLUT4 glucose transporter translocation to the plasma membrane. *Mol Cell Biol* **21**, 5262-5275 (2001).

30. Wu, X., Li, J., Zhu, M., Fletcher, J.A. & Hodi, F.S. Protein kinase C inhibitor AEB071 targets ocular melanoma harboring GNAQ mutations via effects on the

PKC/Erk1/2 and PKC/NF-kappaB pathways. *Mol Cancer Ther* **11**, 1905-1914 (2012).

31. Clevers, H. Wnt/beta-catenin signaling in development and disease. *Cell* **127**, 469-480 (2006).

32. Reya, T. & Clevers, H. Wnt signalling in stem cells and cancer. *Nature* **434**, 843-850 (2005).

33. Huang, S.M., *et al.* Tankyrase inhibition stabilizes axin and antagonizes Wnt signalling. *Nature* **461**, 614-620 (2009).

34. Chen, B., *et al.* Small molecule-mediated disruption of Wnt-dependent signaling in tissue regeneration and cancer. *Nature Chemical Biology* **5**, 100-107 (2009).

35. Zhu, W., *et al.* Interleukin receptor activates a MYD88-ARNO-ARF6 cascade to disrupt vascular stability. *Nature* **492**, 252-255 (2012).

36. Calebiro, D., *et al.* Persistent cAMP-signals triggered by internalized G-protein-coupled receptors. *PLoS Biology* **7**, e1000172 (2009).

37. Ferrandon, S., *et al.* Sustained cyclic AMP production by parathyroid hormone receptor endocytosis. *Nature Chemical Biology* **5**, 734-742 (2009).

38. Hynes, T.R., Mervine, S.M., Yost, E.A., Sabo, J.L. & Berlot, C.H. Live cell imaging of Gs and the beta2-adrenergic receptor demonstrates that both alphas and beta1gamma7 internalize upon stimulation and exhibit similar trafficking patterns that differ from that of the beta2-adrenergic receptor. *J Biol Chem* **279**, 44101-44112 (2004).

39. Irannejad, R., *et al.* Conformational biosensors reveal GPCR signalling from endosomes. *Nature* **495**, 534-538 (2013).

40. Scarselli, M. & Donaldson, J.G. Constitutive internalization of G protein-coupled receptors and G proteins via clathrin-independent endocytosis. *J Biol Chem* **284**, 3577-3585 (2009).

41. Van Dyke, R.W. Heterotrimeric G protein subunits are located on rat liver endosomes. *BMC Physiology* **4**, 1 (2004).

42. Zheng, B., *et al.* Regulation of epidermal growth factor receptor degradation by heterotrimeric Galphas protein. *Mol Biol Cell* **15**, 5538-5550 (2004).

43. Hafner, M., *et al.* Inhibition of cytohesins by SecinH3 leads to hepatic insulin resistance. *Nature* **444**, 941-944 (2006).

44. Bill, A., *et al.* Cytohesins are cytoplasmic ErbB receptor activators. *Cell* **143**, 201-211 (2010).

45. Chuprina, A., Lukin, O., Demoiseaux, R., Buzko, A. & Shivanyuk, A. Drug- and lead-likeness, target class, and molecular diversity analysis of 7.9 million commercially available organic compounds provided by 29 suppliers. *J Chem Inf Model* **50**, 470-479 (2010).

46. Baell, J.B. & Holloway, G.A. New substructure filters for removal of pan assay interference compounds (PAINS) from screening libraries and for their exclusion in bioassays. *J Med Chem* **53**, 2719-2740 (2010).

47. Pylayeva-Gupta, Y., Grabocka, E. & Bar-Sagi, D. RAS oncogenes: weaving a tumorigenic web. *Nature Reviews. Cancer* **11**, 761-774 (2011).

48. Irannejad, R. & von Zastrow, M. GPCR signaling along the endocytic pathway. *Curr Opin Cell Biol* **27**, 109-116 (2014).

49. Fehrenbacher, N., Bar-Sagi, D. & Philips, M. Ras/MAPK signaling from endomembranes. *Molecular Oncology* **3**, 297-307 (2009).

50. Hancock, J.F. Ras proteins: different signals from different locations. *Nat Rev Mol Cell Biol* **4**, 373-384 (2003).

51. Vilardaga, J.P., Jean-Alphonse, F.G. & Gardella, T.J. Endosomal generation of cAMP in GPCR signaling. *Nature Chemical Biology* **10**, 700-706 (2014).

52. Roy, S., Wyse, B. & Hancock, J.F. H-Ras signaling and K-Ras signaling are differentially dependent on endocytosis. *Mol Cell Biol* **22**, 5128-5140 (2002).

53. Harbour, J.W. The genetics of uveal melanoma: an emerging framework for targeted therapy. *Pigment Cell Melanoma Res* **25**, 171-181 (2012).

54. Spiegel, J., Cromm, P.M., Zimmermann, G., Grossmann, T.N. & Waldmann, H. Small-molecule modulation of Ras signaling. *Nature Chemical Biology* **10**, 613-622 (2014).

55. Stephen, A.G., Esposito, D., Bagni, R.K. & McCormick, F. Dragging ras back in the ring. *Cancer Cell* **25**, 272-281 (2014).

56. Ostrem, J.M., Peters, U., Sos, M.L., Wells, J.A. & Shokat, K.M. K-Ras(G12C) inhibitors allosterically control GTP affinity and effector interactions. *Nature* **503**, 548-551 (2013).

57. Lim, S.M., *et al.* Therapeutic targeting of oncogenic K-Ras by a covalent catalytic site inhibitor. *Angew Chem Int Ed Engl* **53**, 199-204 (2014).

58. Thompson, H. US National Cancer Institute's new Ras project targets an old foe. *Nat Med* **19**, 949-950 (2013).

59. Fuerer, C. & Nusse, R. Lentiviral vectors to probe and manipulate the Wnt signaling pathway. *PLoS One* **5**, e9370 (2010).

60. Onken, M.D., *et al.* Loss of heterozygosity of chromosome 3 detected with single nucleotide polymorphisms is superior to monosomy 3 for predicting metastasis in uveal melanoma. *Clinical Cancer Research : An Official Journal of The American Association for Cancer Research* **13**, 2923-2927 (2007).

61. Renault, L., Guibert, B. & Cherfils, J. Structural snapshots of the mechanism and inhibition of a guanine nucleotide exchange factor. *Nature* **426**, 525-530 (2003).

62. McEwen, D.P., Gee, K.R., Kang, H.C. & Neubig, R.R. Fluorescent BODIPY-GTP analogs: real-time measurement of nucleotide binding to G proteins. *Anal Biochem* **291**, 109-117 (2001).

Figure 3.1 ARF6 is activated by oncogenic GNAQ and is required for uveal melanoma cell proliferation. (**a**) ARF6 protein levels in uveal melanomas as assessed by immunoblotting and densitometry; data represented as mean ± SD; Welch's unpaired two-tailed *t* test, **p < 0.01. (**b**) ARF6-GTP levels in uveal melanoma cells transfected with control (Ctrl), GNAQ#1, or GNAQ#2 siRNAs as assessed by immunoblotting and densitometry. The graph shows individual data points normalized to control along with geometric means and 95% confidence intervals (95% CI). 95% CIs that do not cross the dotted line at y=1 represent significant differences relative to the control at α=0.05. (**c**) Uveal melanoma cell proliferation following transfection with Ctrl, ARF6#1, ARF6#2, or GNAQ siRNAs as assessed by DNA content using CyQUANT and a fluorescence microplate reader. FU: Fluorescence Units. (**d**) Anchorage-independent colony growth of cells transfected as in panel c. Percentage of cells normalized to control. Scale bar: 250 µm. Data in panels c and d are represented as mean ± SD, *n=3* experiments. One-way ANOVA, Dunnett's multiple comparisons test, ***p < 0.001.

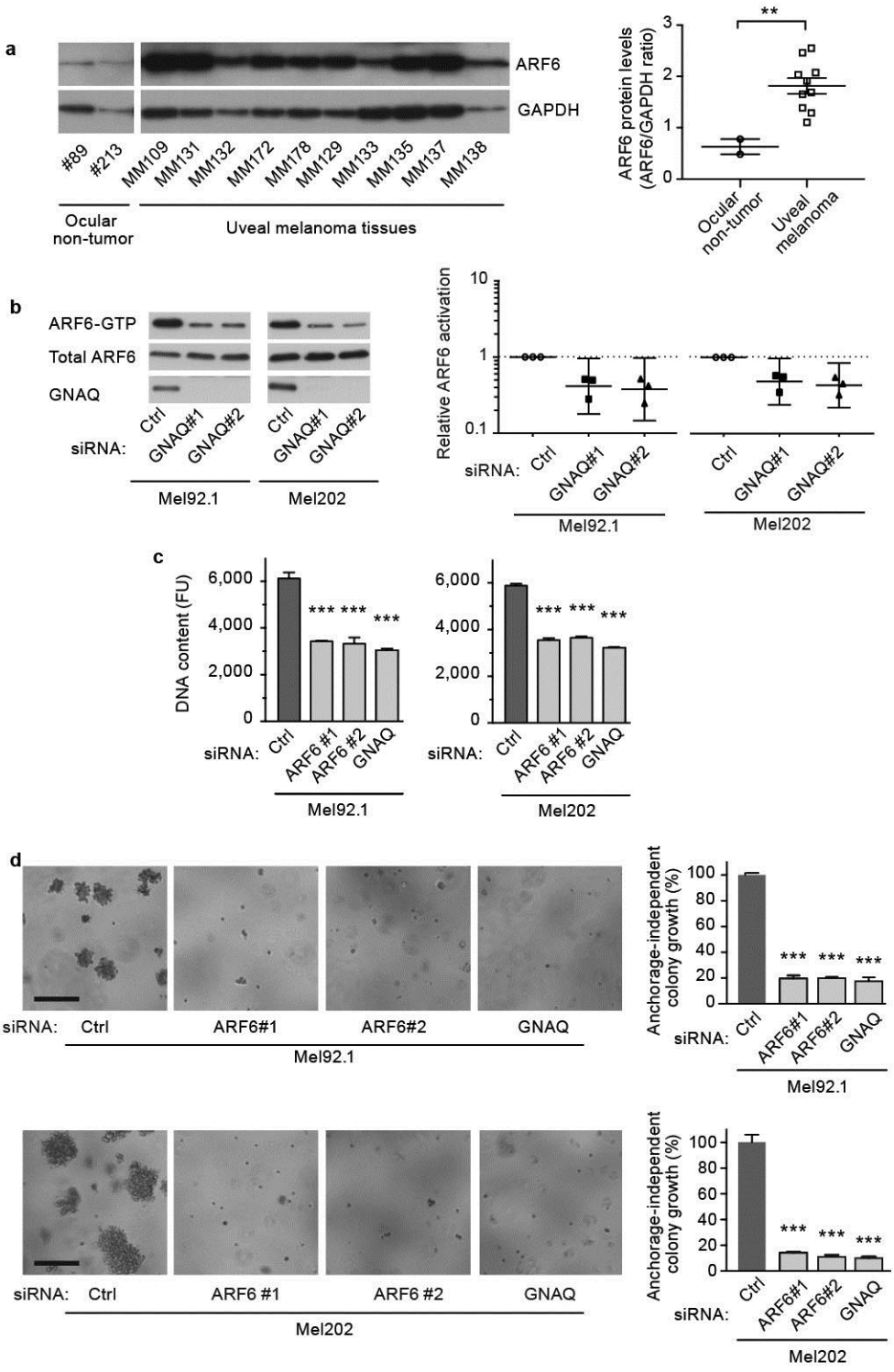
a
ARF6
GAPDH
#89
#213
MM109
MM131
MM132
MM172
MM178
MM129
MM133
MM135
MM137
MM138
Ocular non-tumor
Uveal melanoma tissues
ARF6 protein levels (ARF6/GAPDH ratio)
**
Ocular non-tumor
Uveal melanoma
b
ARF6-GTP
Total ARF6
GNAQ
siRNA:
Ctrl
GNAQ#1
GNAQ#2
Mel92.1
Mel202
Relative ARF6 activation
c
DNA content (FU)
***
ARF6 #1
ARF6 #2
GNAQ
d
Anchorage-independent colony growth (%)
ARF6#1
ARF6#2

Figure 3.2 ARF6 is necessary for oncogenic GNAQ-induced PLC/PKC, Rac/Rho, MAPK, and YAP activation. (**a**) Phosphoinositide turnover assay in uveal melanoma cells transfected with control (Ctrl), ARF6#1, ARF6#2, or GNAQ siRNAs. (**b-e**) Levels of p-MARCKS/MARCKS (**b**), Rac1-GTP/total Rac1 (**c**), RhoA-GTP/total RhoA (**d**), p-ERK/ERK, p-p38/p38, p-JNK/JNK, and p-c-jun/c-jun (**e**) as assessed by immunoblotting from cells transfected as in panel a. (**f**) AP-1-mediated luciferase activities in uveal melanoma cells transfected with Ctrl, ARF6#1, ARF6#2, or GNAQ siRNAs. (**g-i**) Examination of YAP activation in uveal melanoma cells following treatment with ARF6 or GNAQ siRNAs as illustrated by immunocytofluorescence (**g**), subcellular fractionation (**h**), and target gene expression (**i**) assays. Scale bar: 30 µm. Data are represented as mean $\pm$ SD, *n=3* experiments. One-way ANOVA, Dunnett's multiple comparisons test, ***p < 0.001.

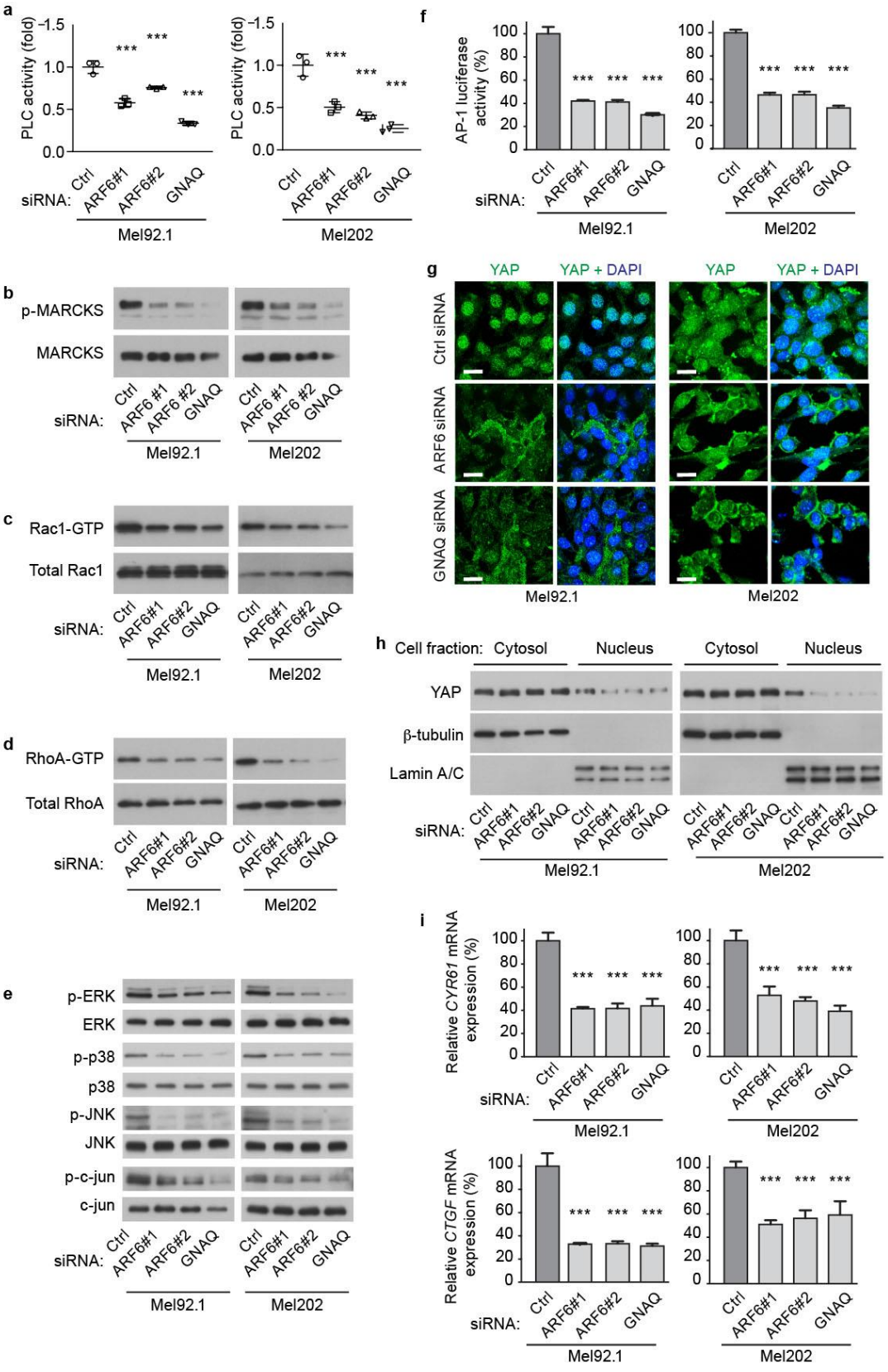
a
PLC activity (fold)
siRNA: Ctrl ARF6#1 ARF6#2 GNAQ
Mel92.1
Mel202
b
p-MARCKS
MARCKS
c
Rac1-GTP
Total Rac1
d
RhoA-GTP
Total RhoA
e
p-ERK
ERK
p-p38
p38
p-JNK
JNK
p-c-jun
c-jun
f
AP-1 luciferase activity (%)
g
YAP
YAP + DAPI
Ctrl siRNA
ARF6 siRNA
GNAQ siRNA
h
Cell fraction: Cytosol Nucleus
YAP
β-tubulin
Lamin A/C
i
Relative CYR61 mRNA expression (%)
Relative CTGF mRNA expression (%)

Figure 3.3 GNAQ and ARF6 control the subcellular localization and transactivation of β-catenin in uveal melanoma cells. (**a**) Immunocytofluorescent staining for β-catenin intracellular localization (green) and (**b**) subcellular fractionation (membrane, cytosol, and nucleus) in Mel92.1 and Mel202 uveal melanoma cells transfected with control (Ctrl), ARF6#1, ARF6#2, or GNAQ siRNAs. Scale bar: 30 μm. Individual data points that have been normalized to the control are shown along with geometric means and 95% confidence intervals (CIs). 95% CIs that do not cross the dotted line at y=1 represent significant differences relative to the control at α=0.05. (**c**) β-catenin-mediated luciferase activities in uveal melanoma cells transfected with Ctrl, ARF6#1, ARF6#2, or GNAQ siRNAs. Data are represented as mean $\pm$ SD, *n=3* experiments. One-way ANOVA, Dunnett's multiple comparisons test, ***$p < 0.001$.

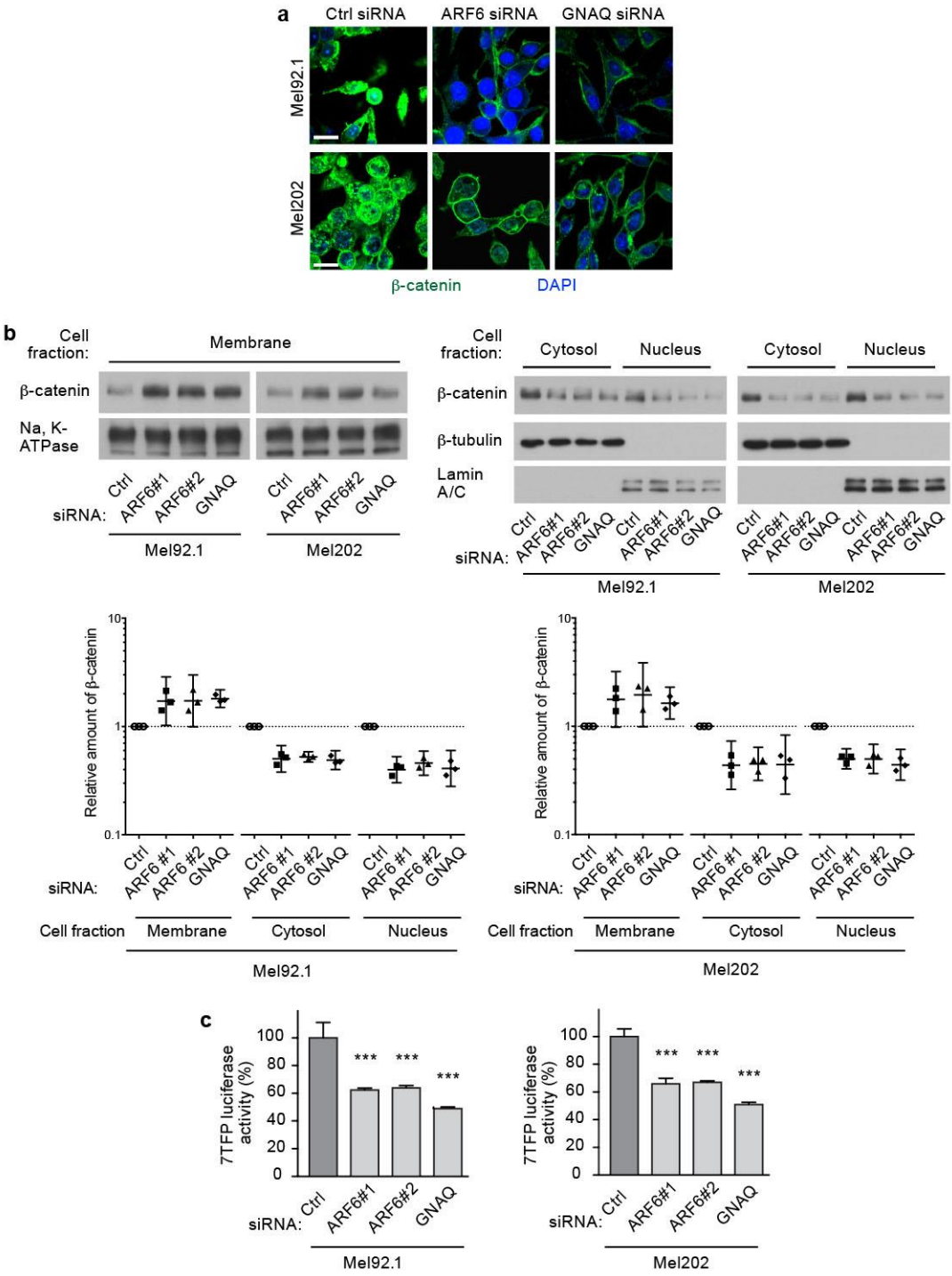
a
Ctrl siRNA
ARF6 siRNA
GNAQ siRNA
Mel92.1
Mel202
β-catenin
DAPI
b
Cell fraction:
Membrane
β-catenin
Na, K-ATPase
siRNA:
Ctrl
ARF6#1
ARF6#2
GNAQ
Mel92.1
Mel202
Cytosol
Nucleus
β-tubulin
Lamin A/C
Relative amount of β-catenin
Cell fraction
c
7TFP luciferase activity (%)
***

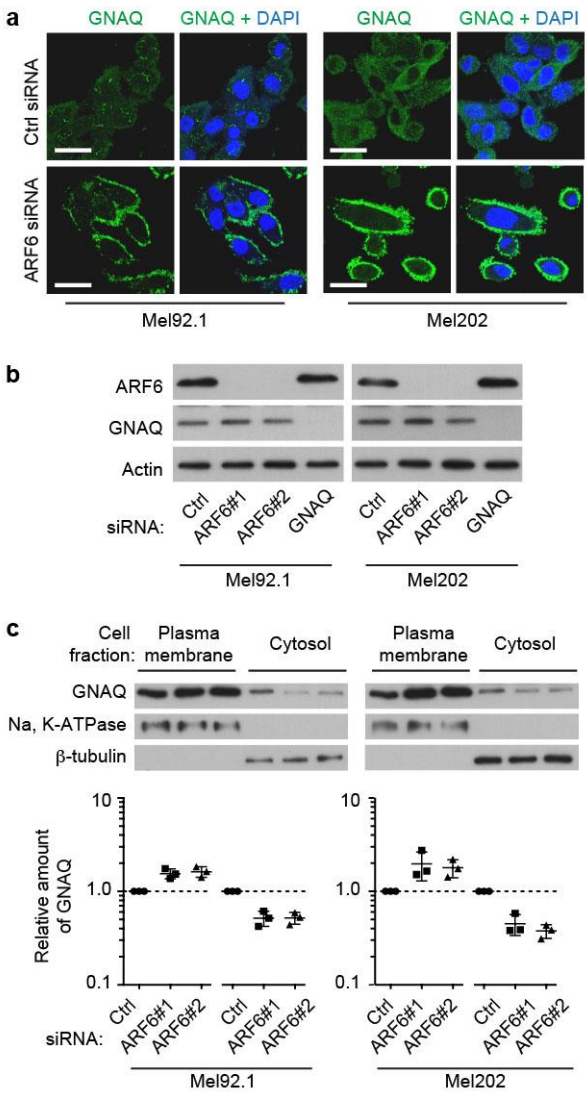

Figure 3.4 ARF6 controls GNAQ trafficking between the plasma membrane and cytoplasmic vesicles/cytosol. (**a**) Immunocytofluorescent assays to assess GNAQ intracellular localization (green) following treatment of Mel92.1 and Mel202 cells with control (Ctrl) or ARF6 siRNA. Cells were counterstained with DAPI. Scale bar: 30 µm. (**b**) Immunoblots illustrating specific knockdown of ARF6 using the two ARF6 siRNAs used in subcellular fractionation studies shown in panel c. (**c**) Subcellular fractionation of GNAQ in Mel92.1 and Mel202 cells following treatment with two independent ARF6 siRNAs and Ctrl siRNA. Individual data points that have been normalized to the control are shown along with geometric means and 95% confidence intervals (CIs). 95% CIs that do not cross the dotted line at y=1 represent significant differences relative to the control at α=0.05.

Figure 3.5 Discovery, confirmation, and assessment of NAV-2729. (**a**) Principle of high-throughput assay. (**b**) Structure and IC_{50} of NAV-2729. (**c** and **d**) Evaluation of NAV-2729 inhibitory potency on fluorometric and radiometric nucleotide exchange assays (**c**) and on ARNO-mediated or GEP100-mediated ARF6 nucleotide exchange assays (**d**). (**e**) Assay for the effect of GTP on NAV-2729-stimulated dissociation of GTP-BODIPY. (**f**) Test for reversibility of NAV-2729 inhibition. (**g**) Model of ARF6-ARNO complex showing where NAV-2729 interacts with the complex. (**h**) Immunoblots of ARF-GTP pull-downs following treatment of Mel92.1 and Mel202 cells with NAV-2729 or vehicle (0). (**i**) Immunocytofluorescent assays to assess GNAQ intracellular localization (green) in uveal melanoma cells following NAV-2729 or DMSO (vehicle) treatment. (**j**) Subcellular fractionation of GNAQ in Mel92.1 and Mel202 cells treated with NAV-2729 or DMSO (vehicle). (**k**) Anchorage-independent colony growth in Mel92.1 and Mel202 cells treated with NAV-2729 or DMSO (vehicle). Scale bars: 250 μm. The graph shows the percentage of cells present relative to the control. Data are represented as mean $\pm$ SD, *n=3* experiments. Student's two-tailed t test, ***$p < 0.001$. For panels h and j, individual data points have been normalized to DMSO (vehicle) and are shown along with geometric means and 95% confidence intervals (CIs). 95% CIs that do not cross the dotted line at y=1 represent significant differences relative to the control at α=0.05.

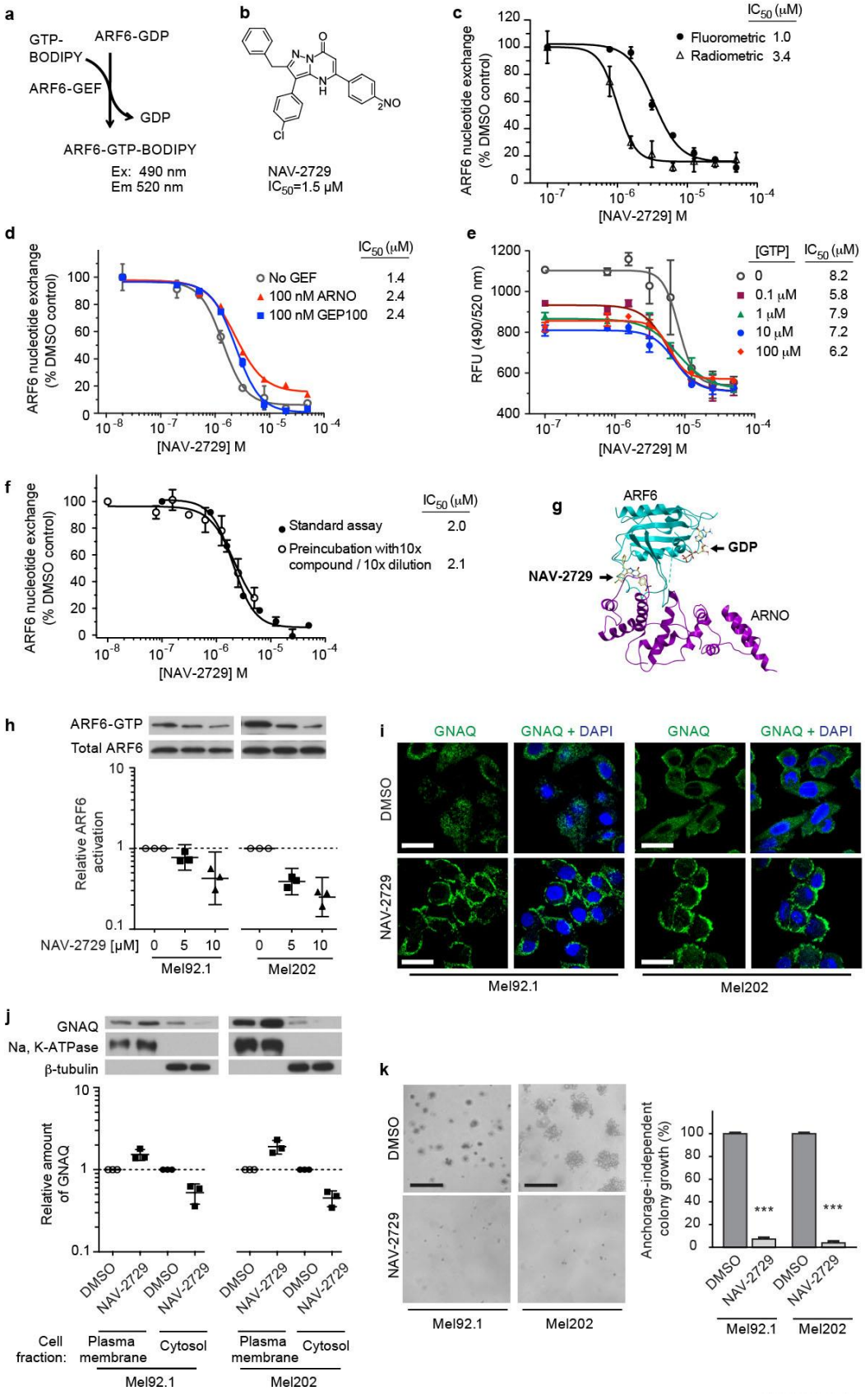
a
GTP-BODIPY
ARF6-GDP
ARF6-GEF
GDP
ARF6-GTP-BODIPY
Ex: 490 nm
Em 520 nm
b
NAV-2729
IC50=1.5 μM
c
IC50 (μM)
Fluorometric 1.0
Radiometric 3.4
ARF6 nucleotide exchange (% DMSO control)
[NAV-2729] M
d
IC50 (μM)
No GEF 1.4
100 nM ARNO 2.4
100 nM GEP100 2.4
ARF6 nucleotide exchange (% DMSO control)
[NAV-2729] M
e
[GTP] IC50 (μM)
0 8.2
0.1 μM 5.8
1 μM 7.9
10 μM 7.2
100 μM 6.2
RFU (490/520 nm)
[NAV-2729] M
f
IC50 (μM)
Standard assay 2.0
Preincubation with10x compound / 10x dilution 2.1
ARF6 nucleotide exchange (% DMSO control)
[NAV-2729] M
g
ARF6
GDP
NAV-2729
ARNO
h
ARF6-GTP
Total ARF6
Relative ARF6 activation
NAV-2729 [μM] 0 5 10 0 5 10
Mel92.1
Mel202
i
GNAQ
GNAQ + DAPI
GNAQ
GNAQ + DAPI
DMSO
NAV-2729
Mel92.1
Mel202
j
GNAQ
Na, K-ATPase
β-tubulin
Relative amount of GNAQ
DMSO NAV-2729 DMSO NAV-2729 DMSO NAV-2729 DMSO NAV-2729
Cell fraction: Plasma membrane Cytosol Plasma membrane Cytosol
Mel92.1
Mel202
k
DMSO
NAV-2729
Mel92.1
Mel202
Anchorage-independent colony growth (%)
***
***
DMSO NAV-2729 DMSO NAV-2729
Mel92.1
Mel202

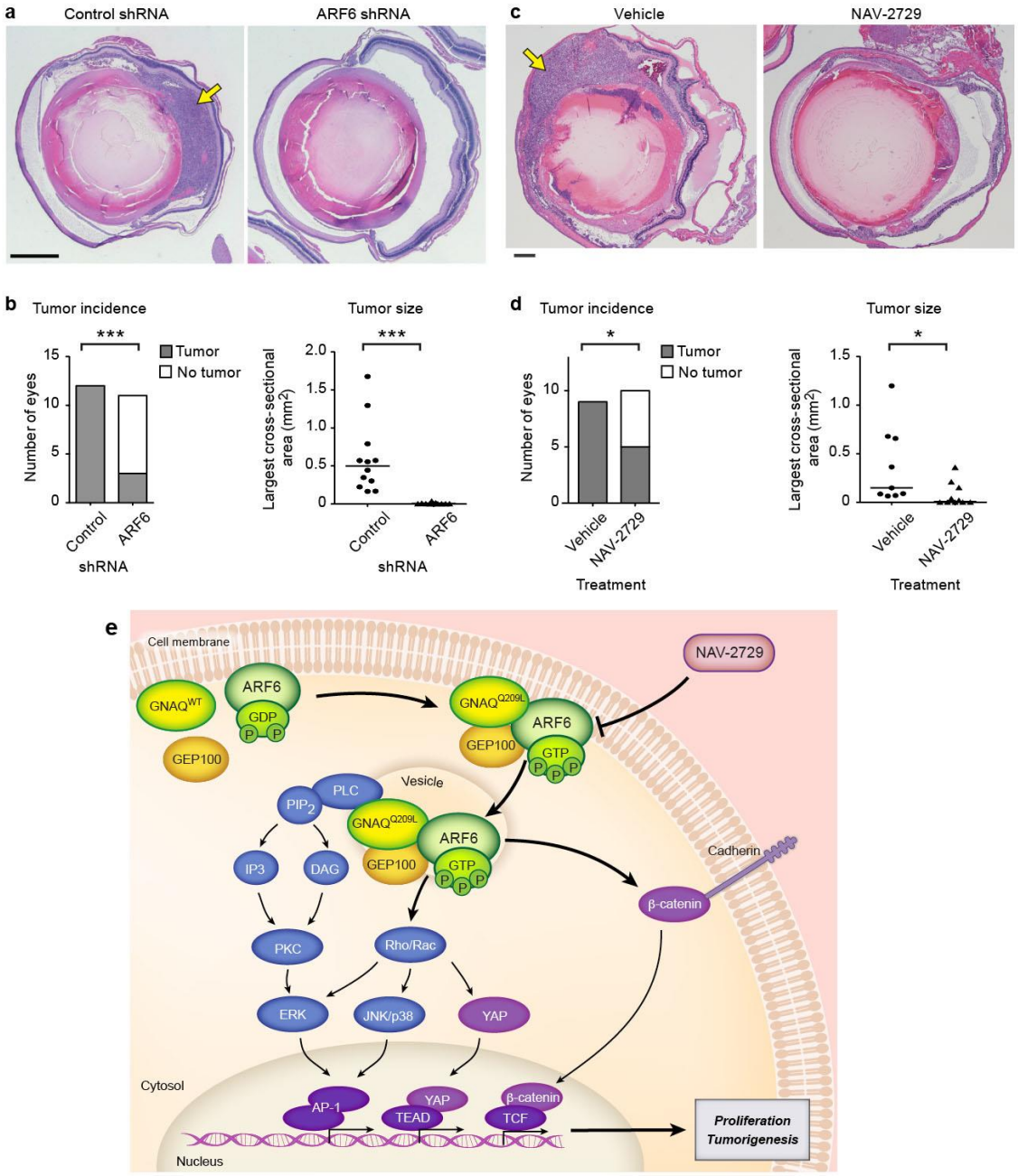

Figure 3.6 Silencing or pharmacological inhibition of ARF6 reduces uveal melanoma tumorigenesis *in vivo*. (**a**) Hematoxylin and eosin (H&E) stained sections from eyes engrafted with Mel202 cells expressing either control or ARF6 shRNAs. Scale bar: 500 µm. (**b** and **d**) *Left*, number of eyes with and without a tumor (Fisher's exact test). *Right*, primary tumor size (median; Mann-Whitney U test). *p < 0.05, ***p < 0.001. (**c**) H&E stained sections from eyes engrafted with Mel202 cells, followed by treatment of mice with either vehicle or NAV-2729. Scale bar: 200 µm. Arrows in panels A and C point to clusters of uveal melanoma cells. (**e**) Proposed oncogenic GNAQ/GEP100/ARF6 signaling pathway.

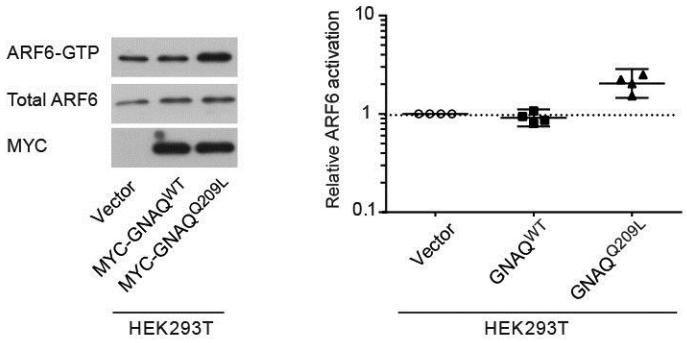

Supplementary Figure 3.1 Oncogenic GNAQ increases ARF6-GTP levels. Immunoblot of ARF6-GTP pull-downs from HEK293T cells that were transfected with MYC-tagged $GNAQ^{Q209L}$, MYC-tagged wild type (WT) GNAQ, or vector. The graph shows individual data points normalized to control along with means and 95% confidence intervals (95% CI). 95% CIs that do not cross the dotted line at y=1 represent significant differences relative to the control at α=0.05.

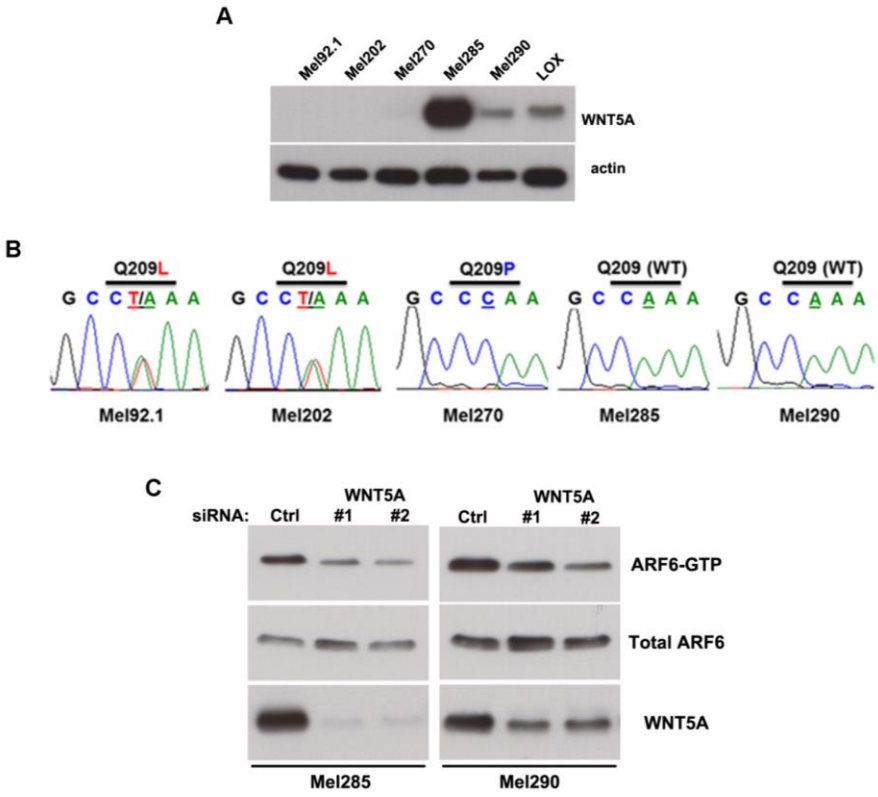

Supplementary Figure 3.2 Wild type GNAQ and GNA11 uveal melanoma cells express WNT5A, which is necessary for ARF6 activation, Related to Figure 1. (A) WNT5A protein levels in uveal melanoma cells that carry GNAQ mutations [Q209L (Mel92.1 and Mel202) and Q209P (Mel270)] and wild type (Mel285 and Mel290). (B) Nucleotide sequencing for confirming GNAQ mutants and GNAQ wild type. LOX is a cutaneous melanoma cell which expresses WNT5A as a positive control. (C) Immunoblot of ARF6-GTP pull-downs from uveal melanoma cells Mel285 and Mel290 transfected with control (Ctrl), WNT5A#1, or WNT5A#2 siRNAs.

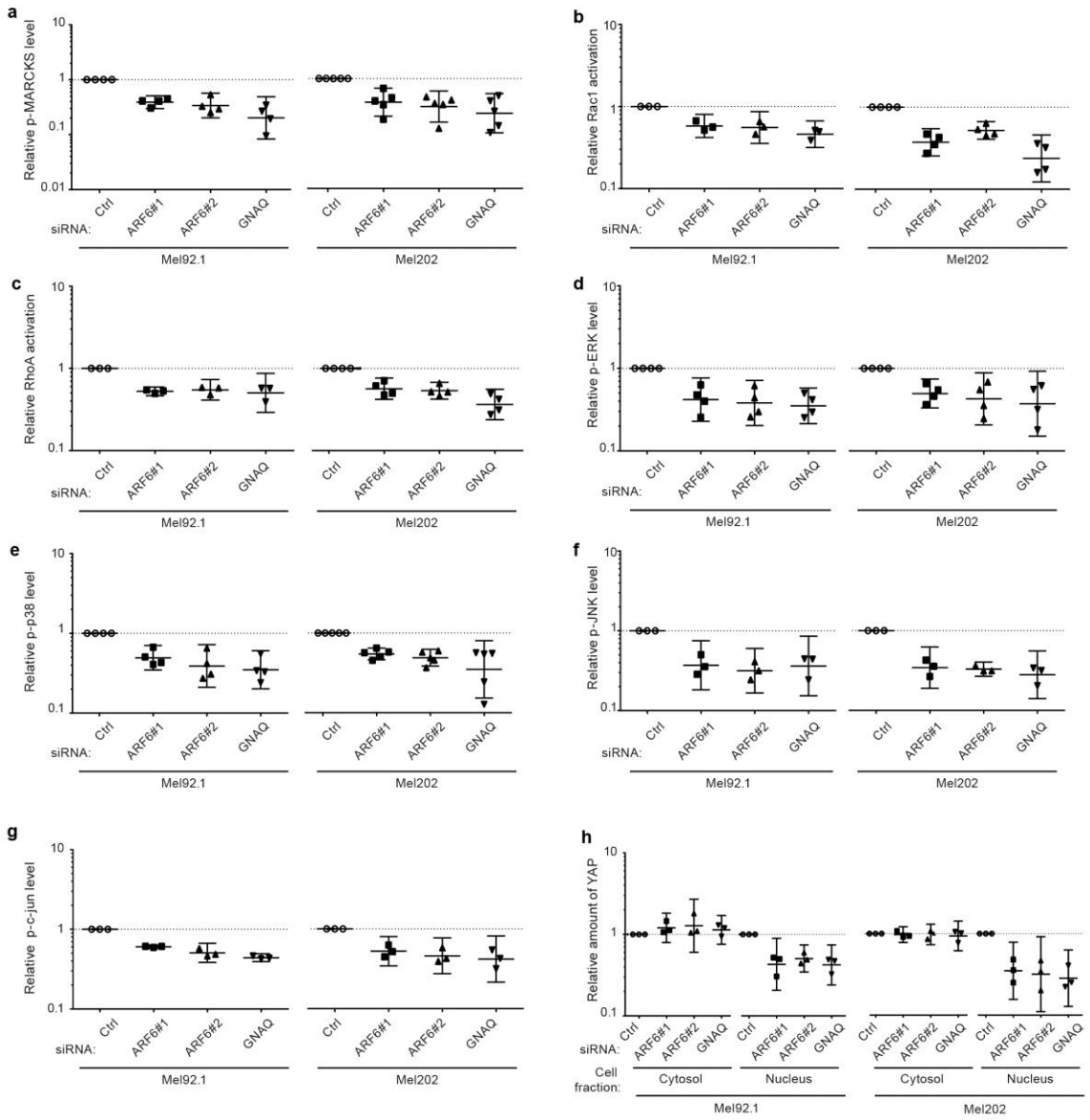

Supplementary Figure 3.3 Quantitation of western blots shown in Figure 2. (**a-h**) Quantitation of the activation of MARCKS (**a**), Rac1 (**b**), RhoA (**c**), ERK (**d**), p38 (**e**), JNK (**f**), c-jun (**g**), and the subcellular localization of YAP (**h**) from the immunoblots shown in Figure 2. The graphs show individual data points normalized to control along with means and 95% confidence intervals (95% CI). 95% CIs that do not cross the dotted line at y=1 represent significant differences relative to the control at α=0.05.

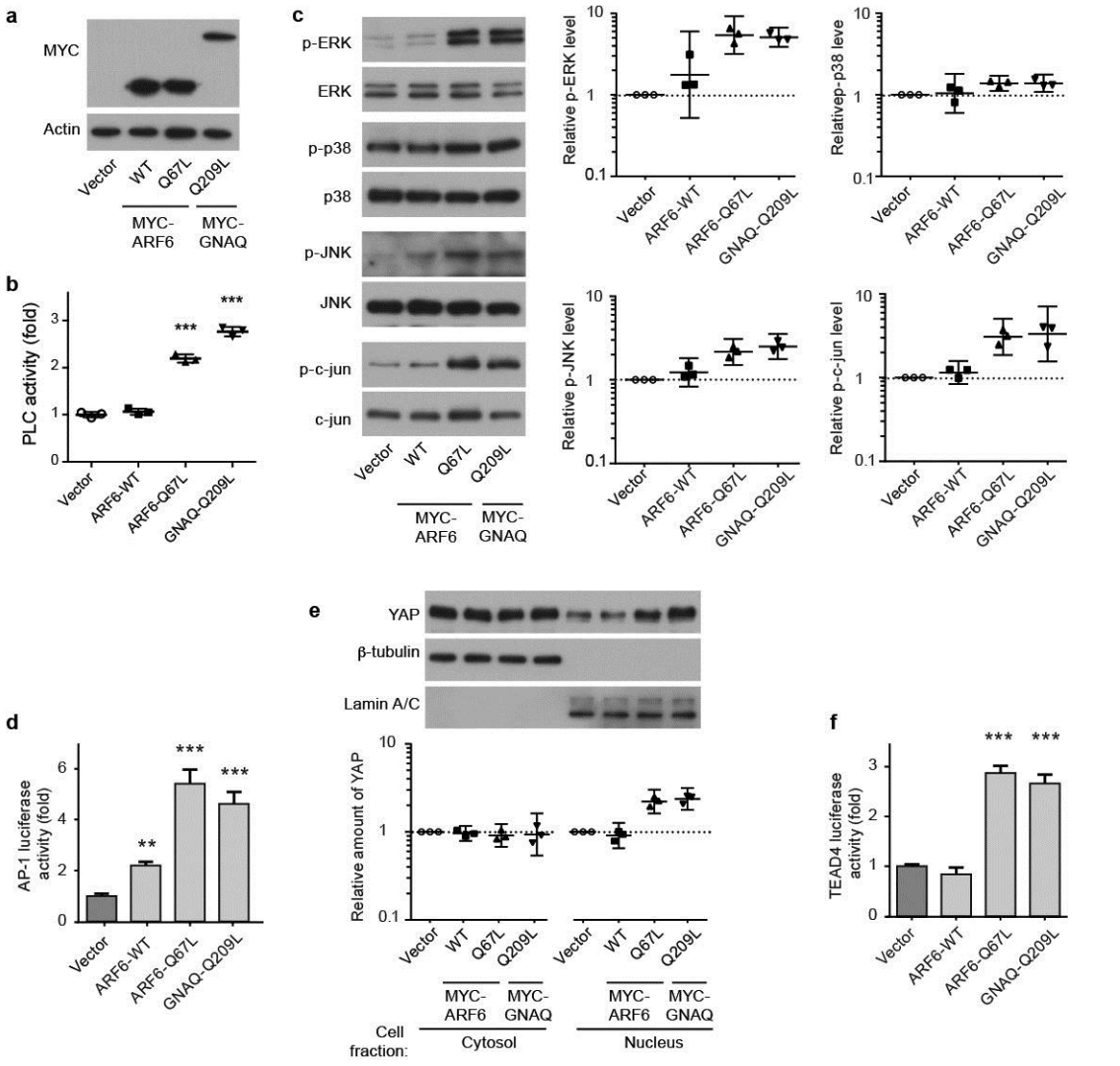

Supplementary Figure 3.4 Ectopic expression of constitutively active ARF6 ($ARF6^{Q67L}$) in HEK293T cells activates downstream oncogenic GNAQ signaling pathways. HEK293T cells were transfected with empty vector, MYC-tagged wild type (WT) ARF6, MYC-tagged $ARF6^{Q67L}$, or MYC-tagged $GNAQ^{Q209L}$. (**a**) Immunoblot showing that MYC-$ARF6^{WT}$, MYC-$ARF6^{Q67L}$, and MYC-$GNAQ^{Q209L}$ are expressed in HEK293T cells. (**b**) PLC activity in a phosphoinositide turnover assay. (**c**) Immunoblots of phosphorylated (p) ERK, p38, JNK, and c-jun. (**d**) Graph illustrating AP-1-mediated transcriptional activity in a luciferase reporter assay. (**e**) Immunoblots and quantitation showing the subcellular fractionation of YAP. (**f**) Graph illustrating YAP-mediated transcriptional activity in a luciferase reporter assay. For panels c and e, the graphs show individual data points normalized to control along with geometric means and 95% confidence intervals (95% CI). 95% CIs that do not cross the dotted line at y=1 represent significant differences relative to the control at α=0.05. For panels b, d, and f, the data are represented as mean $\pm$ SD, *n=3* experiments. One-way ANOVA, Dunnett's multiple comparisons test, **p < 0.01, ***p < 0.001.

Supplementary Figure 3.5 Knockdown of ARF6 or GNAQ does not alter the stability of β-catenin in uveal melanoma cells and ectopic expression of $ARF6^{Q67L}$ or $GNAQ^{Q209L}$ activates β-catenin signaling. (**a**) Immunoblots showing total β-catenin levels in Mel92.1 and Mel202 cells following treatment with ARF6#1, ARF6#2, GNAQ, or control (Ctrl) siRNAs and quantitation of the immunoblots. (**b**) Immunoblots showing the subcellular fractionation of β-catenin following transfection of HEK293T cells with empty vector, MYC-tagged wild type (WT) ARF6, MYC-tagged $ARF6^{Q67L}$, or MYC-tagged $GNAQ^{Q209L}$ and quantitation of the immunoblots. (**c**) β-catenin-mediated transcriptional activity in a luciferase reporter assays following transfection of HEK293T cells with empty vector, MYC-tagged $ARF6^{WT}$, MYC-tagged $ARF6^{Q67L}$, or MYC-tagged $GNAQ^{Q209L}$. (**d**) Mel92.1 and Mel202 cell proliferation assays following inhibition of β-catenin signaling with XAV939 or IWR-1-endo. Dotted horizontal line represents baseline DNA content before the addition of inhibitor. For panels a and b, the graphs show individual data points normalized to control along with geometric means and 95% confidence intervals (95% CI). 95% CIs that do not cross the dotted line at y=1 represent significant differences relative to the control at α=0.05. For panels c and d, the data are represented as mean $\pm$ SD, *n=3* experiments. For panel c, one-way ANOVA, Dunnett's multiple comparisons test was performed, ***$p < 0.001$.

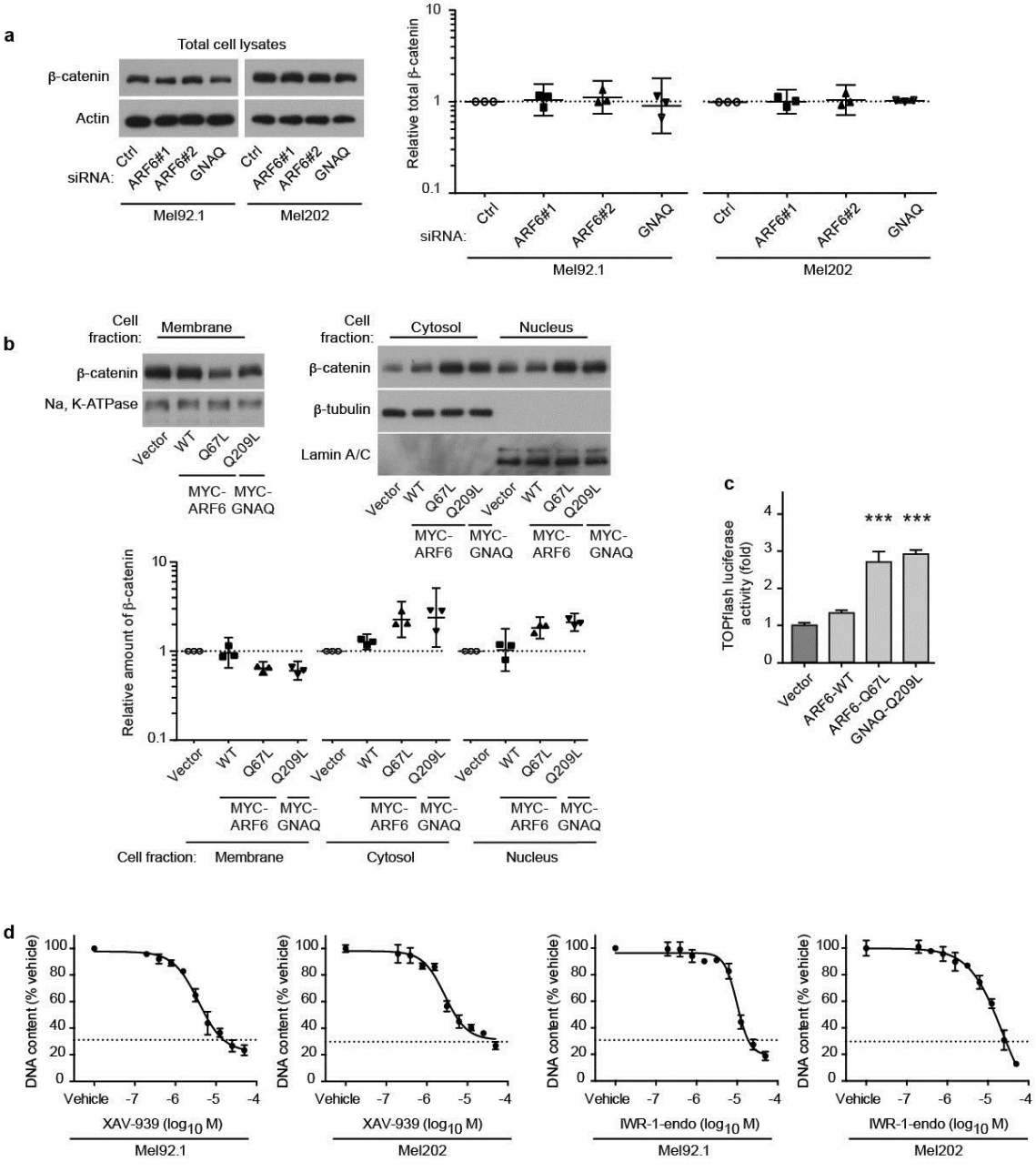
a
Total cell lysates
β-catenin
Actin
siRNA:
Ctrl
ARF6#1
ARF6#2
GNAQ
Mel92.1
Mel202
Relative total β-catenin
10
1
0.1
b
Cell fraction:
Membrane
Cytosol
Nucleus
Na, K-ATPase
β-tubulin
Lamin A/C
Vector
WT
Q67L
Q209L
MYC-ARF6
MYC-GNAQ
Relative amount of β-catenin
Cell fraction:
c
TOPflash luciferase activity (fold)
***
ARF6-WT
ARF6-Q67L
GNAQ-Q209L
d
DNA content (% vehicle)
XAV-939 (log10 M)
IWR-1-endo (log10 M)
Vehicle

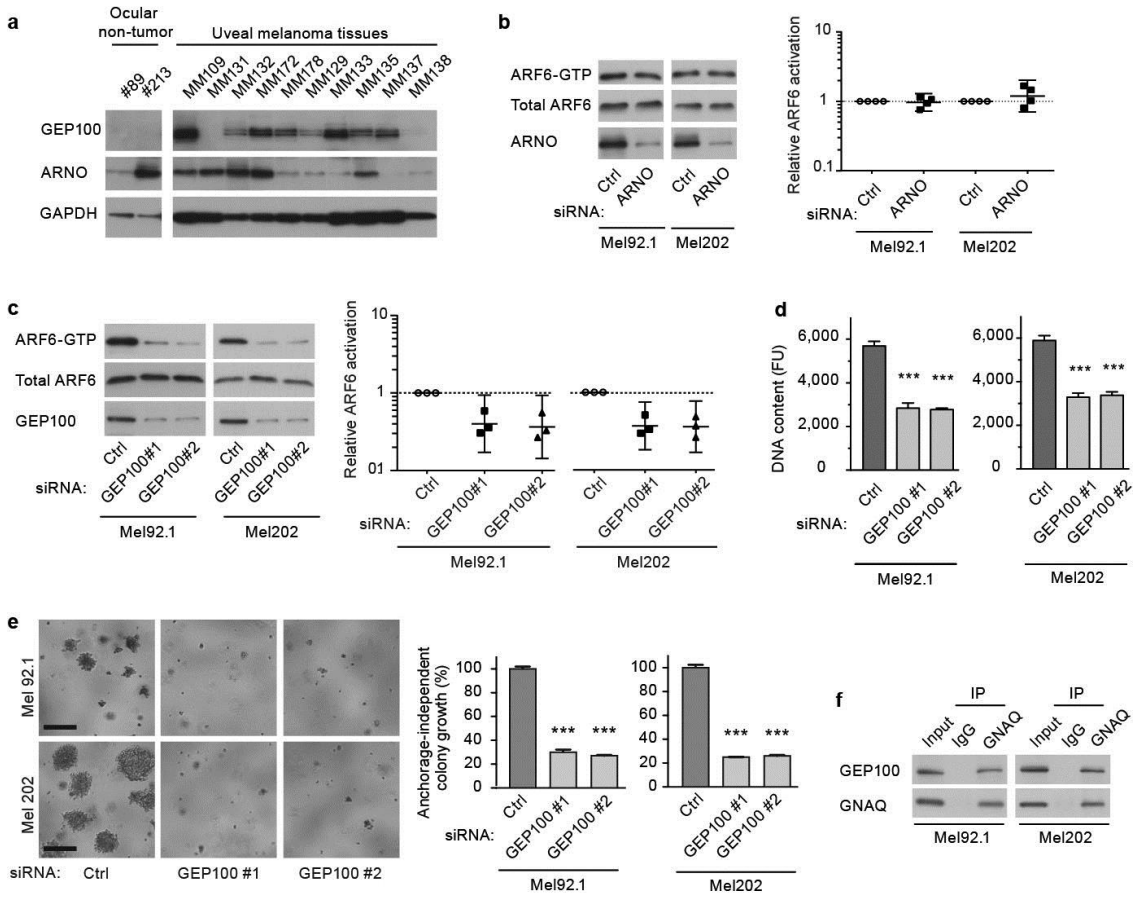

Supplementary Figure 3.6 An oncogenic GNAQ-GEP100 complex activates ARF6 and is necessary for uveal melanoma cell proliferation. (**a**) GEP100 and ARNO are expressed in uveal melanoma tissues. (**b**) ARF6-GTP levels in uveal melanoma cells transfected with control (Ctrl) or ARNO siRNAs as measured by pull-down assays and immunoblotting. (**c**) ARF6-GTP levels in uveal melanoma cells transfected with Ctrl, GEP100#1, or GEP100#2 siRNAs. In panels b and c, individual data points that have been normalized to the control are shown along with geometric means and 95% confidence intervals (CIs). 95% CIs that do not cross the dotted line at y=1 represent significant differences relative to the control at α=0.05. (**d**) Mel92.1 and Mel202 cell proliferation following transfection with Ctrl, GEP100#1, or GEP100#2 siRNAs as assessed by DNA content using CyQUANT and a fluorescence microplate reader. FU = Fluorescence units. (**e**) Anchorage-independent colony growth of cells transfected as in panel d. The graph shows the percentage of cells present relative to the control. Scale bar: 250 µm. (**f**) Immunoblots of co-immunoprecipitated (IP) oncogenic GNAQ and GEP100 in uveal melanoma cell extracts. IgG is negative control. Data in panels d and e are represented as mean $\pm$ SD, *n=3* experiments. One-way ANOVA, Dunnett's multiple comparisons test, ***$p < 0.001$.

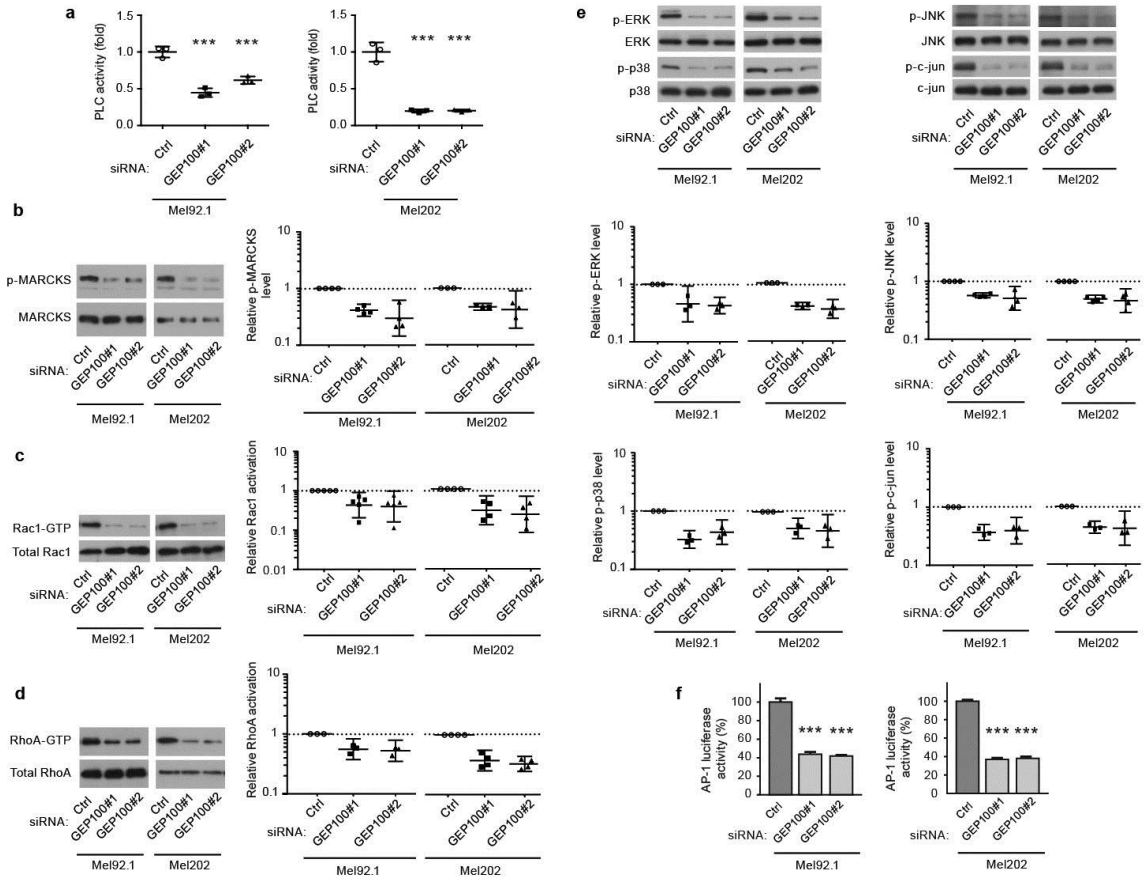

Supplementary Figure 3.7 Silencing of GEP100 inhibits oncogenic GNAQ-induced PLC/PKC and Rho/Rac signaling in uveal melanoma cells. (**a-e**) PLC activity in a phosphoinositide turnover assay (**a**) and activation of MARCKS (**b**), Rac1 (**c**), RhoA (**d**), and ERK, p38, JNK, and c-jun (**e**) as measured by densitometry of immunoblots following treatment of Mel92.1and Mel202 cells with two independent GEP100 siRNAs (GEP100#1 and GEP100#2) or Ctrl siRNA. (**f**) AP-1-mediated transcription in a luciferase activity assay following GEP100 knockdown in Mel92.1 and Mel202 cells using two independent siRNAs. For panels b-e, the graphs show individual data points normalized to control along with geometric means and 95% confidence intervals (95% CI). 95% CIs that do not cross the dotted line at y=1 represent significant differences relative to the control at α=0.05. For panel f, the data are represented as mean $\pm$ SD, *n=3* experiments. One-way ANOVA, Dunnett's multiple comparisons test, ***p < 0.001.

Supplementary Figure 3.8 Silencing of GEP100 inhibits oncogenic GNAQ-induced YAP and β-catenin signaling in uveal melanoma cells. (**a**) Subcellular fractionation assays of YAP and (**b**) YAP target-gene mRNA levels following GEP100 silencing. (**c**) Subcellular fractionation assays of β-catenin and (**d**) β-catenin-mediated transcriptional activity in a luciferase reporter assay following GEP100 knockdown. For panels a and c, the graphs show individual data points normalized to control along with geometric means and 95% confidence intervals (95% CI). 95% CIs that do not cross the dotted line at y=1 represent significant differences relative to the control at α=0.05. For panels b and d, the data are represented as mean $\pm$ SD, *n=3* experiments. One-way ANOVA, Dunnett's multiple comparisons test, ***$p < 0.001$.

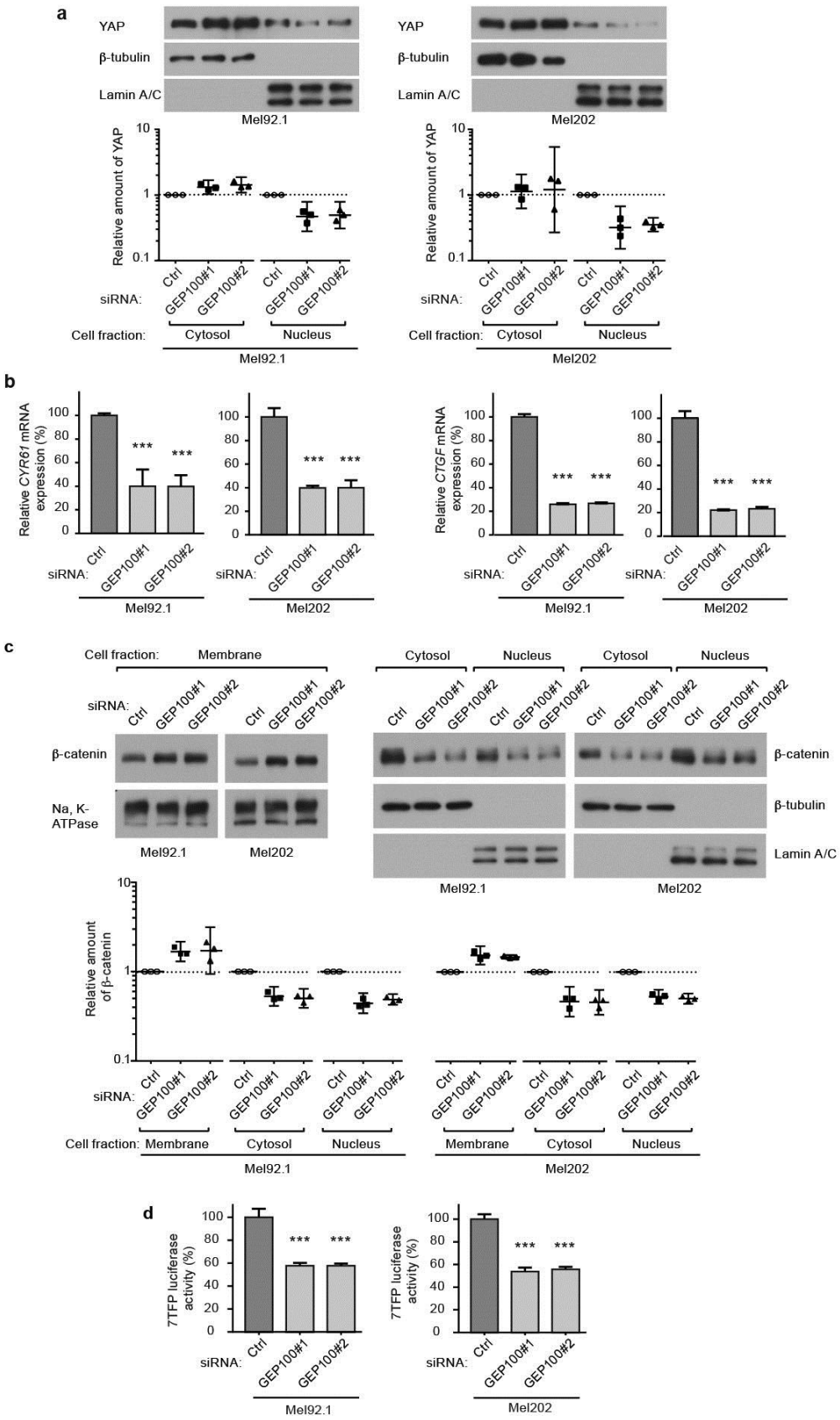
a
YAP
β-tubulin
Lamin A/C
Mel92.1
Mel202
Relative amount of YAP
siRNA:
Ctrl
GEP100#1
GEP100#2
Cell fraction:
Cytosol
Nucleus
b
Relative CYR61 mRNA expression (%)
Relative CTGF mRNA expression (%)
***
c
Cell fraction:
Membrane
Cytosol
Nucleus
β-catenin
Na, K-ATPase
β-tubulin
Lamin A/C
Relative amount of β-catenin
d
7TFP luciferase activity (%)

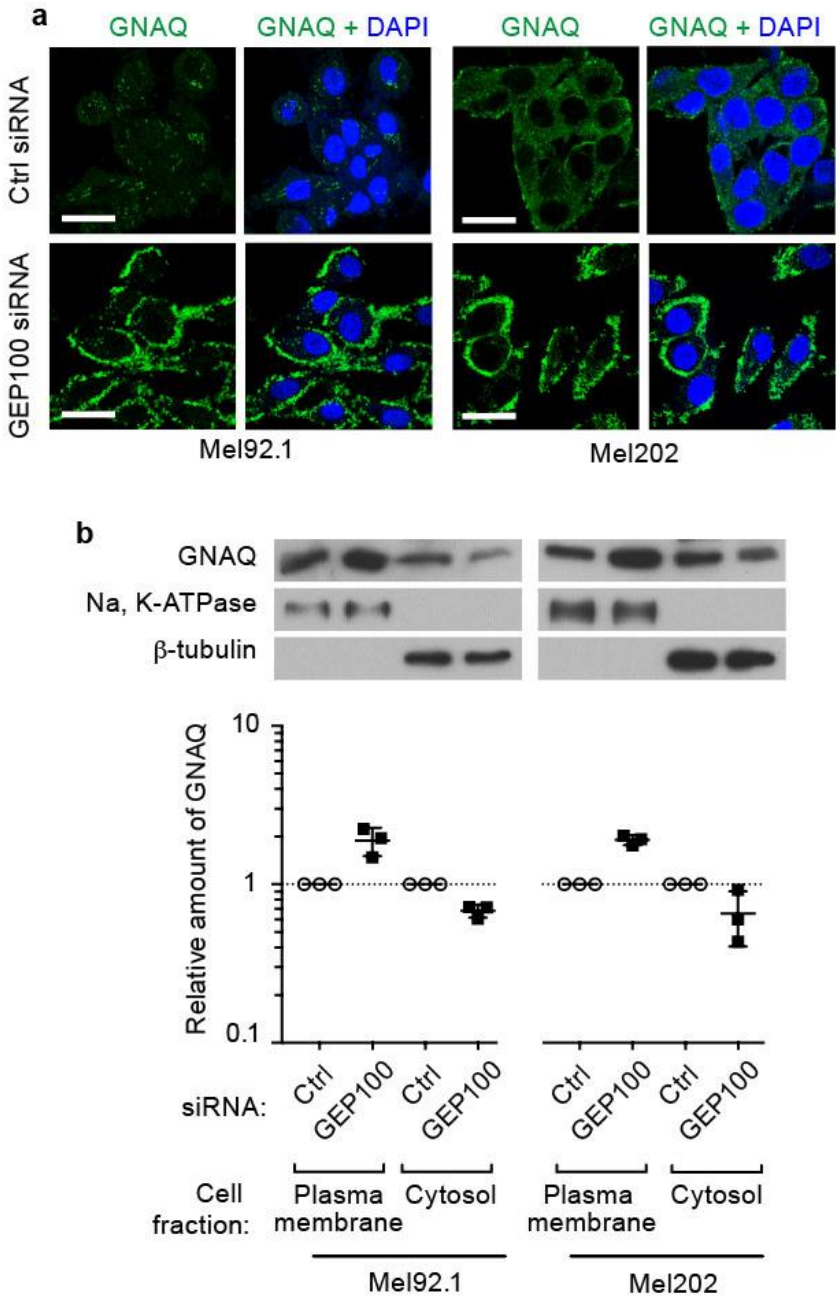

Supplementary Figure 3.9 GEP100 knockdown promotes localization of GNAQ to the plasma membrane. (**a**) Immunocytofluorescent staining and (**b**) subcellular fractionation of GNAQ in Mel92.1 and Mel202 cells that were transfected with GEP100 or control (Ctrl) siRNA. Scale bar: 30 µm. The graph shows individual data points normalized to control along with geometric means and 95% confidence intervals (95% CI). 95% CIs that do not cross the dotted line at y=1 represent significant differences relative to the control at α=0.05.

Supplementary Figure 3.10 Development and validation of a fluorometric ARF6 nucleotide exchange assay. (**a**) Dependence of signal intensity on the presence of ARF6 and an ARF-GEF (ARNO). The arrow indicates the concentration of ARNO selected for the assay protocol. (**b**) Validation assay using GDP as a reference inhibitor. (**c**) Determination of signal-to-background ratio (S:B) and Z'-factor. (**d**) Stimulation of GTP-BODIPY release from its complex with ARF6 by NAV-2729. (**e-h**) Non-inhibitory effects of NAV-2729 for other small GTPases (RhoA, Rac1, H-Ras, and Cdc42). (**i**) Molecular docking model of NAV-2729 binding to ARF6-ARFGEF complex showing the major interactions of ARF6 residues with the inhibitor.

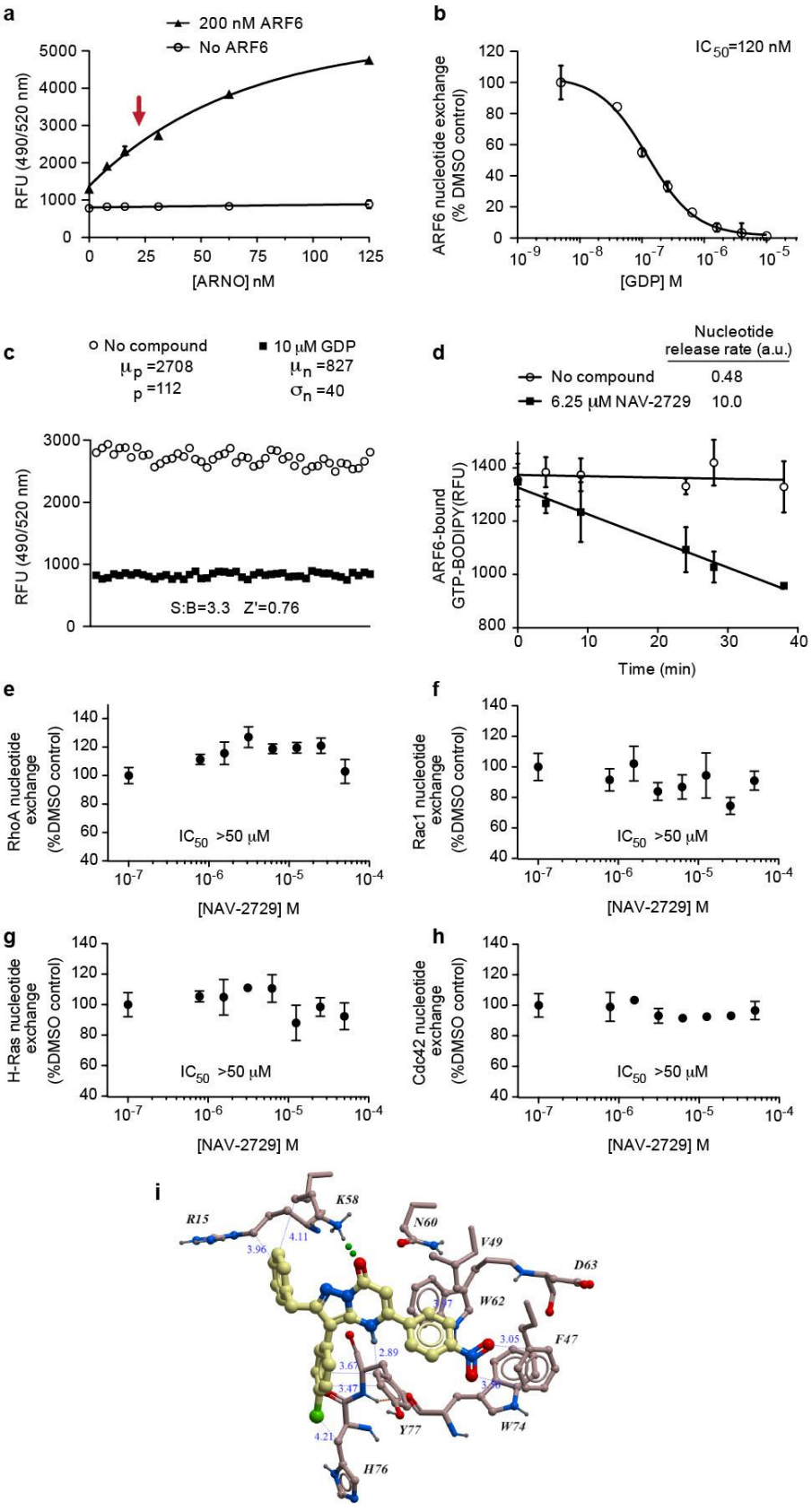
a
200 nM ARF6
No ARF6
RFU (490/520 nm)
[ARNO] nM
b
IC50=120 nM
ARF6 nucleotide exchange (% DMSO control)
[GDP] M
c
No compound
μp =2708
p =112
10 μM GDP
μn =827
σn =40
RFU (490/520 nm)
S:B=3.3 Z'=0.76
d
Nucleotide release rate (a.u.)
No compound 0.48
6.25 μM NAV-2729 10.0
ARF6-bound GTP-BODIPY(RFU)
Time (min)
e
RhoA nucleotide exchange (%DMSO control)
IC50 >50 μM
[NAV-2729] M
f
Rac1 nucleotide exchange (%DMSO control)
IC50 >50 μM
[NAV-2729] M
g
H-Ras nucleotide exchange (%DMSO control)
IC50 >50 μM
[NAV-2729] M
h
Cdc42 nucleotide exchange (%DMSO control)
IC50 >50 μM
[NAV-2729] M
i
K58
R15
N60
V49
D63
W62
F47
Y77
W74
H76

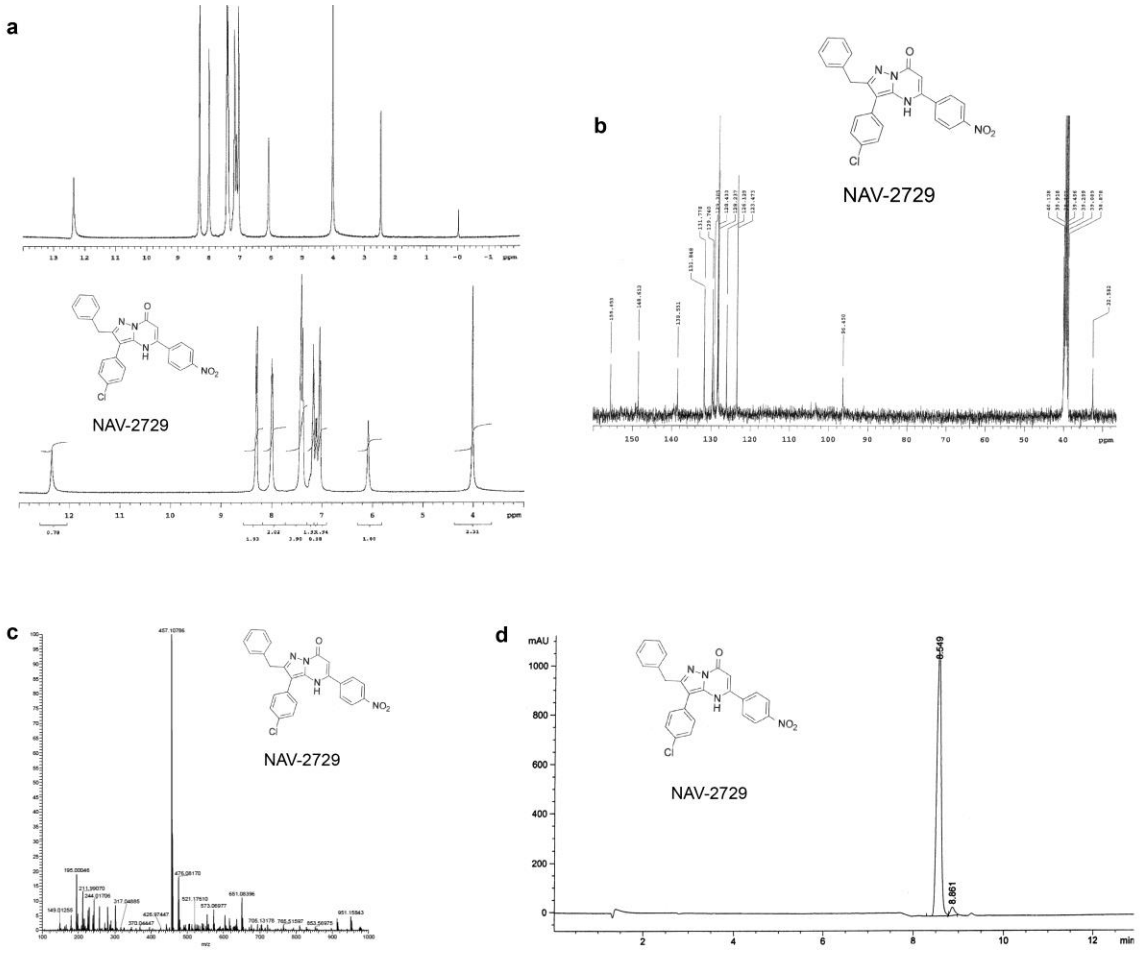

Supplementary Figure 3.11 Characterization of NAV-2729. (**a**) Proton NMR spectra of NAV-2729. (**b**) Carbon-13 spectra of NAV-2729. (**c**) High Resolution Mass Spectra of NAV-2729. (**d**) HPLC of NAV-2729.

CHAPTER 4

CONCLUDING REMARKS

The findings presented in this dissertation make two major contributions to our understanding of the molecular mechanisms that control tumor cell behavior. First, I demonstrate that ARF6 is a convergence point in the integration of competing signals that dictate β-catenin function. WNT5A activates ARF6 to shift the plasma membrane pool of β-catenin into the nucleus where it induces the transcription of genes that promote the invasion and metastasis of cutaneous melanoma, while SLIT2 inactivates ARF6, fortifying the association of β-catenin with N-cadherin at the plasma membrane and inhibiting invasion and metastasis[1]. Consistent with our results, SLIT2-ROBO1 has been shown to inhibit canonical WNT signaling in mammary epithelial cells[2]. Our data show that both WNT5A and SLIT2-ROBO1 control invasion of cutaneous melanoma by modulating ARF6 activity, which regulates β-catenin protein trafficking from the cell surface to nucleus. Although previous studies have primarily described WNT5A as an activator of noncanonical β-catenin signaling[3,4], there are several studies showing that WNT5A can stimulate β-catenin signaling depending on cellular context[4,5]. The results for the role of β-catenin in cutaneous melanoma are discordant. There are studies suggested that β-catenin functions in the suppression of melanoma cell invasion and that

the loss of β-catenin is a prediction marker for a poor survival rate in melanoma patients[6-8]. Other studies have shown that activated β-catenin signaling enhances melanoma metastasis[3,9,10]. However, these studies may overlook the dual functions of β-catenin: 1) its role as a stabilizer of cell-cell interactions and 2) its role as an activator of transcription[11]. During the dynamic invasion process, β-catenin function alternates between the cell surface and the nucleus. Therefore, β-catenin cellular function should be evaluated based on subcellular localization using subcellular specific localized β-catenin. We have shown that pharmacologic inhibition of ARF6 activity fortifies adherens junctions, inhibiting β-catenin trafficking from plasma membrane to the nucleus, invasion, and metastasis of melanoma[1]. As a key molecule for controlling β-catenin signaling induced by WNT5A, ARF6 will be an ideal therapeutic target for blocking invasion and metastasis of cutaneous melanoma. Here, I have explored a previously unknown role for ARF6 in WNT5A-mediated β-catenin function and have shown that this signaling pathway controls invasion and metastasis. Therefore, the study for ARF6 offers a new therapeutic approach in WNT/β-catenin-driven cancers.

The second major contribution of this work involves our understanding of the role of ARF6 in uveal melanoma. Using biochemical tools, cellular assays, and orthotopic xenograft mouse models, I demonstrate that an oncogenic GNAQ-GEP100-ARF6 complex controls multiple signaling pathways to promote the proliferation of uveal melanoma cancer cells and tumorigenesis. I show that ARF6 is an immediate downstream effector of a $GNAQ^{Q209L}$-GEP100 complex that controls the activation of all the currently known GNAQ-mediated oncogenic signaling pathways by regulating the intracellular trafficking of GNAQ. I also show that the GNAQ-GEP100-ARF6 complex

controls β-catenin signaling, thus identifying an additional pathway regulated by oncogenic GNAQ. Previously, several investigations have showed that constitutively active mutants of *GNAI* (encoding Gαi), *GNAS* (encoding Gαs), *GNAQ* (encoding Gαq), *GNAO1* (encoding Gαo), and *GNA12* (encoding Gα12) induce the transformation of cells, which suggests that activating mutations in G proteins have a potential to promote tumorigenesis and enhance proliferation[12]. Recently, intensive genomic research in human cancers has confirmed the mutations of various G proteins in addition to GNAQ/GNA11. For example, mutations in *GNAS* occur in pituitary tumours (28%), thyroid adenomas (5%), colon cancer (4%), pancreatic tumours (12%), hepatocellular carcinoma (2%), and parathyroid cancer (3%)[13]. Similar to activating mutations in GNAQ or GNA11 in uveal melanoma, these major mutations in GNAS mainly occur in two amino acids, R201 or Q227, which result in constitutive activity by decreasing GTPase activity[13]. Interestingly, these activating mutations in *GNAS* are frequently found in a specific tumor type such as pancreatic cancer. *GNAS* mutations are found in 66% of intraductal papillary mucinous neoplasms (IPMNs), which are precursors of pancreatic adenocarcinoma, suggesting that constitutively active *GNAS*-driven signaling pathways contribute to pancreatic neoplasia[14,15]. Although the presence of activating mutations in *GNAS*, *GNAQ*, and *GNA11* in multiple cancers is clear, further study will be required to understand how these activating mutations in G proteins induce tumorigenesis. Based on the previous report that ARF6 is originally found as a cofactor for the cholera toxin-catalyzed ADP ribosylation of GNAS[16], an intriguing hypothesis is that ARF6 acts as a downstream signaling node in GNAS driven-cancers. I further postulate that targeting ARF6 or other similar nodes might not only be efficacious for treating GNAQ, GNA11,

or GNAS-mediated cancers but also for the multiple cancers controlled by other Gα protein mutations. Further experiments will be required to test these crucial hypotheses.

Recently, the results of deep genome sequencing in multiple human cancers have indicated the loss of function for SLIT-ROBO through allelic deletion or hypermethylation in their promoter[17], suggesting that SLIT-ROBO signaling plays important roles in tumorigenesis, cancer progression, and metastasis. Also, the loss of *ROBO1* expression in uveal melanoma helps to identify patients at high risk for metastasis[18]. Based on our findings from cutaneous melanoma, it will be important to identify the key molecular components of the SLIT-ROBO-ARF6 signaling axis and their role in uveal melanoma invasion and metastasis.

Although over 80% of uveal melanomas harbor activating mutations in GNAQ or GNA11[19], the oncogenic driver in uveal melanomas that do not possess GNAQ or GNA11 mutations is unknown. According to our preliminary data, uveal melanoma cells that have GNAQ mutations do not express WNT5A, while tumor cells that possess wild type GNAQ and GNA11 express high levels of WNT5A. Interestingly, WNT5A is necessary for ARF6 activation in wild type GNAQ and GNA11 uveal melanoma cells. Frizzled receptors contain seven transmembrane domains and are classified as GPCRs[20]. Previous studies have shown that the differential effects of Gα proteins either increase or decrease WNT/β-catenin signaling dependent on the subtype of Gα proteins[21]. Specifically, it has been shown that GNAQ signaling contributes to WNT-mediated melanoma invasion and metastasis through frizzled receptors[22,23]. Therefore, I hypothesize that WNT5A, acting through a frizzled receptor and Gα protein/GEF complex, activates ARF6, which then this transduces the downstream oncogenic

signaling pathways in GNAQ and GNA11 wild type uveal melanoma cells. Future studies could test this hypothesis and help define whether there is a common WNT-Gα-ARF6 signaling cascade in both cutaneous and uveal melanoma. This discovery suggests that a more effective therapeutic approach might be to target ARF6 directly, thereby inhibiting WNT/β-catenin signaling as well as all of the known downstream GNAQ-mediated oncogenic pathways with a single inhibitor. To this end, we have begun to identify direct inhibitors of ARF6 and show that one of these, NAV-2729, can inhibit tumor formation and growth in a orthotopic xenograft model of uveal melanoma.

In summary, our work provides the first example of an endogenous canonical WNT5A signaling pathway in a mammalian system and a mechanistic explanation, through ARF6, for how this typically noncanonical WNT stimulates β-catenin-mediated transcription. Previously, WNTs had not been shown to affect junctional β-catenin. We demonstrate that WNT5A draws upon this cadherin-bound pool of β-catenin to boost transcription. Pharmacologic inhibition of ARF6 activation is also effective in opposing this WNT5A/β-catenin pathway and inhibits spontaneous metastasis of melanoma *in vivo*. Thus, targeting ARF6 may be an effective approach for inhibiting WNT-driven cancers. We also show that oncogenic GNAQ, a Gαq protein, induces its multiple signaling pathways through a single actionable node—the small GTPase ARF6. These results not only reveal the mechanism by which a proximal downstream effector of an oncogene can simultaneously influence multiple divergent signaling pathways but also suggest that targeting such nodes could be an efficacious approach for treating cancers driven by oncogenes that have proven recalcitrant to direct inhibition.

References

1. Grossmann, A.H., *et al.* The small GTPase ARF6 stimulates beta-catenin transcriptional activity during WNT5A-mediated melanoma invasion and metastasis. *Science Signaling* **6**, ra14 (2013).

2. Pellon-Cardenas, O., Clancy, J., Uwimpuhwe, H. & D'Souza-Schorey, C. ARF6-regulated endocytosis of growth factor receptors links cadherin-based adhesion to canonical Wnt signaling in epithelia. *Molecular and Cellular Biology* **33**, 2963-2975 (2013).

3. Weeraratna, A.T., *et al.* Wnt5a signaling directly affects cell motility and invasion of metastatic melanoma. *Cancer Cell* **1**, 279-288 (2002).

4. Kikuchi, A., Yamamoto, H., Sato, A. & Matsumoto, S. Wnt5a: its signalling, functions and implication in diseases. *Acta Physiol (Oxf)* **204**, 17-33 (2012).

5. Mikels, A.J. & Nusse, R. Purified Wnt5a protein activates or inhibits beta-catenin-TCF signaling depending on receptor context. *PLoS Biology* **4**, e115 (2006).

6. Kageshita, T., *et al.* Loss of beta-catenin expression associated with disease progression in malignant melanoma. *The British Journal of Dermatology* **145**, 210-216 (2001).

7. Chien, A.J., *et al.* Activated Wnt/beta-catenin signaling in melanoma is associated with decreased proliferation in patient tumors and a murine melanoma model. *Proceedings of the National Academy of Sciences of the United States of America* **106**, 1193-1198 (2009).

8. Arozarena, I., *et al.* In melanoma, beta-catenin is a suppressor of invasion. *Oncogene* **30**, 4531-4543 (2011).

9. Damsky, W.E., *et al.* beta-catenin signaling controls metastasis in Braf-activated Pten-deficient melanomas. *Cancer Cell* **20**, 741-754 (2011).

10. Delmas, V., *et al.* Beta-catenin induces immortalization of melanocytes by suppressing p16INK4a expression and cooperates with N-Ras in melanoma development. *Genes & Development* **21**, 2923-2935 (2007).

11. Nelson, W.J. & Nusse, R. Convergence of Wnt, beta-catenin, and cadherin pathways. *Science* **303**, 1483-1487 (2004).

12. Dorsam, R.T. & Gutkind, J.S. G-protein-coupled receptors and cancer. *Nature Reviews. Cancer* **7**, 79-94 (2007).

13. O'Hayre, M., *et al.* The emerging mutational landscape of G proteins and G-protein-coupled receptors in cancer. *Nature Reviews. Cancer* **13**, 412-424 (2013).

14. Wu, J., *et al.* Recurrent GNAS mutations define an unexpected pathway for pancreatic cyst development. *Science Translational Medicine* **3**, 92ra66 (2011).

15. Furukawa, T., *et al.* Whole-exome sequencing uncovers frequent GNAS mutations in intraductal papillary mucinous neoplasms of the pancreas. *Scientific Reports* **1**, 161 (2011).

16. O'Neal, C.J., Jobling, M.G., Holmes, R.K. & Hol, W.G. Structural basis for the activation of cholera toxin by human ARF6-GTP. *Science* **309**, 1093-1096 (2005).

17. Ballard, M.S. & Hinck, L. A roundabout way to cancer. *Advances in Cancer Research* **114**, 187-235 (2012).

18. Onken, M.D., Worley, L.A., Tuscan, M.D. & Harbour, J.W. An accurate, clinically feasible multi-gene expression assay for predicting metastasis in uveal melanoma. *The Journal of Molecular Diagnostics : JMD* **12**, 461-468 (2010).

19. Field, M.G. & Harbour, J.W. Recent developments in prognostic and predictive testing in uveal melanoma. *Current Opinion in Ophthalmology* **25**, 234-239 (2014).

20. Foord, S.M., *et al.* International Union of Pharmacology. XLVI. G protein-coupled receptor list. *Pharmacological Reviews* **57**, 279-288 (2005).

21. Regard, J.B., *et al.* Wnt/beta-catenin signaling is differentially regulated by Galpha proteins and contributes to fibrous dysplasia. *Proceedings of the National Academy of Sciences of the United States of America* **108**, 20101-20106 (2011).

22. Dissanayake, S.K., *et al.* The Wnt5A/protein kinase C pathway mediates motility in melanoma cells via the inhibition of metastasis suppressors and initiation of an epithelial to mesenchymal transition. *The Journal of Biological Chemistry* **282**, 17259-17271 (2007).

23. Sheldahl, L.C., Park, M., Malbon, C.C. & Moon, R.T. Protein kinase C is differentially stimulated by Wnt and Frizzled homologs in a G-protein-dependent manner. *Current Biology : CB* **9**, 695-698 (1999).